

**EXPERIMENTAL STUDY ON TURBULENT FLOW AROUND A
PAIR OF CYLINDERS PLACED ALONG PLANE OF
SYMMETRY IN A RECTANGULAR OPEN CHANNEL**

Saika Nowshin Nowrin



Department of Water Resources Engineering
Bangladesh University of Engineering and Technology
Dhaka, Bangladesh
December 2020

**EXPERIMENTAL STUDY ON TURBULENT FLOW AROUND A
PAIR OF CYLINDERS PLACED ALONG PLANE OF
SYMMETRY IN A RECTANGULAR OPEN CHANNEL**

by

Saika Nowshin Nowrin

A thesis submitted in partial fulfillment of the requirements for the degree of
MASTER OF SCIENCE IN WATER RESOURCES ENGINEERING



Department of Water Resources Engineering
Bangladesh University of Engineering and Technology
Dhaka, Bangladesh
December 2020

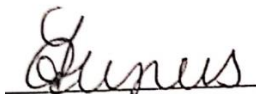
The thesis/project titled “**EXPERIMENTAL STUDY ON TURBULENT FLOW AROUND A PAIR OF CYLINDERS PLACED ALONG PLANE OF SYMMETRY IN A RECTANGULAR OPEN CHANNEL**” submitted by **Saika Nowshin Nowrin**, Roll No.: **0417162031**, Session: **April 2017**, has been accepted as satisfactory in partial fulfillment of the requirement for the degree of **MASTER OF SCIENCE IN WATER RESOURCES ENGINEERING** on **December 19, 2020**.

BOARD OF EXAMINERS



Chairman
(Supervisor)

Dr. A. T. M. Hasan Zobeyer
Professor
Department of Water Resources Engineering,
BUET, Dhaka- 1000



Member
(Ex- officio)

Dr. Anika Yunus
Professor and Head
Department of Water Resources Engineering,
BUET, Dhaka- 1000



Member

Dr. Md. Ataur Rahman
Professor
Department of Water Resources Engineering,
BUET, Dhaka- 1000



Member
(External)

Dr. Mohammad Mamun
Professor
Department of Mechanical Engineering,
BUET, Dhaka- 1000

CANDIDATE'S DECLARATION

It is hereby declared that this thesis/project or any part of it has not been submitted elsewhere for the award of any degree or diploma.

Saika Nowshin Nowrin.

Saika Nowshin Nowrin

Dedicated to My Parents and Sister

Table of Contents

List of Tables and Figures.....	viii
List of Tables and Abbreviations of Technical Symbols and Terms.....	xii
Acknowledgement	xiii
Abstract	xiv
CHAPTER 1 Introduction.....	1
1.1 General	1
1.2 Study Objectives.....	2
1.3 Study Scope, outcomes and Contents.....	2
CHAPTER 2 Literature Review.....	5
2.1 General	5
2.2 Bluff-bodies.....	5
2.3 Turbulent Flow	6
2.4 Instantaneous velocities.....	6
2.4.1 Turbulent Intensity	7
2.4.2 Turbulent Kinetic Energy.....	7
2.4.3 Turbulent Shear Stress	7
2.5 Separation and Wakes	8
2.6 Near wake and Far wake region	8
2.7 Basic Equations	9
2.7.1 Schlichting's Equation	9
2.7.2 Balachandar's Equation	9
2.8 Previous Studies on Flow around Cylinder.....	11
CHAPTER 3 Laboratory Experiment.....	19
3.1 General	19

3.2	Laboratory Equipments	19
3.2.1	Two-dimensional wave flume.....	19
3.2.2	Water reservoir.....	20
3.2.3	Material and dimension of cylinder	20
3.2.4	Acoustic Doppler Velocimeter (ADV)	21
3.2.5	Selection of scale for experimentation.....	22
3.3	Experimental Set-up	22
3.4	Data Acquisition.....	26
3.5	Experimental Procedure	27
3.5.1	Progressive operation for the experiment	27
3.5.2	Uncertainty Analysis.....	30
CHAPTER 4 Experimental Results and Discussion.....		31
4.1	General	31
4.2	Normalized Longitudinal Velocity Variation along POS (Mid-Stream Section).....	31
4.3	Wall Wake Similarity Profile along the POS in Midstream.....	36
4.4	Normalized Longitudinal Velocity Variation along POS (Down-Stream Section).....	37
4.5	Wall Wake Similarity Profile along the POS in Downstream	42
4.6	Turbulence Parameters at Mid-stream	43
4.6.1	Turbulent intensity at mid-stream of 3D c/c spacing.....	43
4.6.2	Kinetic Energy at mid-stream of 3D c/c spacing	48
4.6.3	Turbulent intensity at mid-stream of 6D c/c spacing.....	49
4.6.4	Kinetic Energy at mid-stream of 6D c/c spacing	54
4.6.5	Turbulent intensity at mid-stream of 9D c/c spacing.....	55
4.6.6	Kinetic Energy at mid-stream of 9D c/c spacing	60

4.6.7	Turbulent shear stress at midstream.....	61
4.7	Turbulence Parameters at Downstream.....	63
4.7.1	Turbulent intensity at downstream of 3D c/c spacing.....	63
4.7.2	Kinetic Energy at downstream of 3D c/c spacing.....	68
4.7.3	Turbulent intensity at downstream of 6D c/c spacing.....	69
4.7.4	Kinetic Energy at downstream of 6D c/c spacing.....	74
4.7.1	Turbulent intensity at downstream of 9D c/c spacing.....	75
4.7.2	Kinetic Energy at downstream of 9D c/c spacing.....	80
4.7.3	Turbulent shear stress at downstream.....	81
4.8	Wake Similarity Profile in Term of Near Wake on Horizontal Plane at Mid-Depth.....	83
CHAPTER 5 Conclusions.....		90
5.1	Conclusions.....	90
5.2	Recommendation for Future Works.....	92
References.....		94

List of Figures

Figure 2.1: Wake vortices forming scour hole around a cylindrical shaped bluff-body [14]	6
Figure 2.2: Instantaneous Velocity Graph	7
Figure 2.3: Wake generated behind a cylinder producing boundary wall separation [16].	8
Figure 2.4: Definition sketch for plane wall wake [18]	9
Figure 2.5: Schematic of the test body and coordinate system; (b) photographs of the flow field	11
Figure 2.6: Schematic of Balachander's profile of plane near wake	11
Figure 3.1: Laboratory flume (21.3 m long, 0.76 m wide and 0.74 m deep)	20
Figure 3.2: Concrete cylinders used in experiment	20
Figure 3.3: Acoustic Doppler Velocimeter (ADV)	21
Figure 3.4: Components of Acoustic Doppler Velocimeter	22
Figure 3.5: Plan view of data collection at mid-stream & down-stream	23
Figure 3.6: Plan view of data collection of downstream at depth, $z=h/2$	24
Figure 3.7: Details of Experimental Set-up	24
Figure 3.8: Experimental Set-up	25
Figure 3.9: Wake is generating between two cylinders	27
Figure 3.10: Laboratory set-up of velocity measuring locations	28
Figure 3.11: (a) Plan view of data collection at grid points, (b) Side view of experimental set-up, (c) Frame of ADV, (d) ADV is immersed in water to collect the data at several locations	29
Figure 3.12: Flow visualization	29
Figure 3.13: Changing the position of ADV for different sections	29
Figure 3.14: Data acquisition by WinADV32 software	30
Figure 4.1: Normalized Longitudinal Velocity Profiles along plane of symmetry between two cylinders	33

Figure 4.2: Normalized Longitudinal Depth-Averaged Velocity along a plane of symmetry between two cylinders	34
Figure 4.3: Jet-like longitudinal velocity profiles along with POS between two cylinders	35
Figure 4.4: Wall wake similarity for longitudinal velocity profiles in midstream	37
Figure 4.5: Normalized Longitudinal Velocity Profiles along plane of symmetry at downstream	39
Figure 4.6: Normalized Longitudinal Depth-Averaged Velocity along a plane of symmetry at downstream	40
Figure 4.7: Jet-like longitudinal velocity profiles along with POS at downstream ...	41
Figure 4.8: Wall wake similarity for longitudinal velocity profiles at downstream ..	43
Figure 4.9: (a) Variation of Normalized Turbulent Intensity Profile (b) Variation of Maximum Turbulent Intensity in longitudinal direction along plane of symmetry between two cylinders (3D)	45
Figure 4.10: (a) Variation of Normalized Turbulent Intensity Profile (b) Variation of Maximum Turbulent Intensity in transverse direction along plane of symmetry between two cylinders (3D)	46
Figure 4.11: (a) Variation of Normalized Turbulent Intensity Profile (b) Variation of Maximum Turbulent Intensity in vertical direction along plane of symmetry between two cylinders (3D).....	47
Figure 4.12: (a) Variation of Normalized Kinetic Energy Profile (b) Variation of Maximum Kinetic Energy in vertical direction along plane of symmetry between two cylinders (3D).....	49
Figure 4.13: (a) Variation of Normalized Turbulent Intensity Profile (b) Variation of Maximum Turbulent Intensity in longitudinal direction along plane of symmetry between two cylinders (6D)	50
Figure 4.14: (a) Variation of Normalized Turbulent Intensity Profile (b) Variation of Maximum Turbulent Intensity in transverse direction along plane of symmetry between two cylinders (6D)	52
Figure 4.15: (a) Variation of Normalized Turbulent Intensity Profile (b) Variation of Maximum Turbulent Intensity in vertical direction along plane of symmetry between two cylinders (6D).....	53

Figure 4.16: (a) Variation of Normalized Kinetic Energy Profile (b) Variation of Maximum Kinetic Energy in vertical direction along plane of symmetry between two cylinders (6D).....	55
Figure 4.17: (a) Variation of Normalized Turbulent Intensity Profile (b) Variation of Maximum Turbulent Intensity in longitudinal direction along plane of symmetry between two cylinders (9D)	56
Figure 4.18: (a) Variation of Normalized Turbulent Intensity Profile (b) Variation of Maximum Turbulent Intensity in transverse direction along plane of symmetry between two cylinders (9D)	58
Figure 4.19: (a) Variation of Normalized Turbulent Intensity Profile (b) Variation of Maximum Turbulent Intensity in vertical direction along plane of symmetry between two cylinders (9D).....	59
Figure 4.20: (a) Variation of Normalized Kinetic Energy Profile (b) Variation of Maximum Kinetic Energy in vertical direction along plane of symmetry between two cylinders (9D).....	61
Figure 4. 21: Variation of normalized maximum turbulent shear stress for three cases at midstream section.....	63
Figure 4.22: (a) Variation of Normalized Turbulent Intensity Profile (b) Variation of Maximum Turbulent Intensity in longitudinal direction along plane of symmetry downstream of second cylinder(3D)	64
Figure 4.23: (a) Variation of Normalized Turbulent Intensity Profile (b) Variation of Maximum Turbulent Intensity in transverse direction along plane of symmetry downstream of second cylinders (3D).....	66
Figure 4.24: (a) Variation of Normalized Turbulent Intensity Profile (b) Variation of Maximum Turbulent Intensity in vertical direction along plane of symmetry downstream of second cylinders(3D).....	67
Figure 4.25: (a) Variation of Normalized Kinetic Energy Profile (b) Variation of Maximum Kinetic Energy in vertical direction along plane of symmetry downstream of second cylinders(3D)	69
Figure 4.26: (a) Variation of Normalized Turbulent Intensity Profile (b) Variation of Maximum Turbulent Intensity in longitudinal direction along plane of symmetry downstream of second cylinders (6D).....	70

Figure 4.27: (a) Variation of Normalized Turbulent Intensity Profile (b) Variation of Maximum Turbulent Intensity in transverse direction along plane of symmetry downstream of second cylinders (6D).....	72
Figure 4.28: (a) Variation of Normalized Turbulent Intensity Profile (b) Variation of Maximum Turbulent Intensity in vertical direction along plane of symmetry downstream of second cylinders (6D).....	73
Figure 4.29: (a) Variation of Normalized Kinetic Energy Profile (b) Variation of Maximum Kinetic Energy in vertical direction along plane of symmetry downstream of second cylinders(6D)	75
Figure 4.30: (a) Variation of Normalized Turbulent Intensity Profile (b) Variation of Maximum Turbulent Intensity in longitudinal direction along plane of symmetry downstream of second cylinder (9D)	76
Figure 4.31: (a)Variation of Normalized Turbulent Intensity Profile (b) Variation of Maximum Turbulent Intensity in transverse direction along plane of symmetry downstream of second cylinder (9D)	78
Figure 4.32: (a) Variation of Normalized Turbulent Intensity Profile (b) Variation of Maximum Turbulent Intensity in vertical direction along plane of symmetry downstream of second cylinders (9D).....	79
Figure 4.33: (a) Variation of Normalized Kinetic Energy Profile (b) Variation of Maximum Kinetic Energy in vertical direction along plane of symmetry downstream of second cylinders(9D)	81
Figure 4. 34 Variation of normalized maximum turbulent shear stress for three cases at downstream section	82
Figure 4.35: Normalized Longitudinal Velocity Variation at Mid Depth in Transverse Direction between Two Cylinders	85
Figure 4.36: Plane Wake Similarity of longitudinal velocity at Mid-depth in the transverse direction between two cylinders	86
Figure 4.37: Normalized Longitudinal Velocity Variation at Mid Depth in Transverse Direction at Downstream	88
Figure 4.38: Plane Wake Similarity of longitudinal velocity at Mid-depth in the transverse direction downstream of second cylinder	89

List of Tables

Table 3.1: Calculation of cross sectional mean velocity and Reynolds number.....	25
Table 3.2: Test scenarios of experimental runs.....	26
Table 3.3: Uncertainty estimation of ADV measurements	30

List of Symbols

b = Half-width, or length scale

D= Diameter of cylinder

F= Froude number

h = Height of cylinder

H= Depth of water

KE = Turbulent kinetic energy

R= Reynolds number

U= time averaged velocity along x direction

U_o = cross-sectional mean velocity

U_1 = Velocity defect, $U_\infty - U$ in plane wake

U_{1m} = maximum value of U_1

U_2 =Velocity defect, $U_e - U$ in wall wake

U_∞ = Undisturbed uniform ambient velocity

U_{min} = Minimum value of U

u = Instantaneous longitudinal velocity

u_m = maximum value of u

u_{da} = normalized longitudinal depth-averaged velocity

u', v', w' = Root mean square velocity in x, y and z directions, respectively

$\sqrt{u'w'} = \overline{uw} = \overline{u'w'}$ = Reynolds shear stress on x-z plane

x = Longitudinal direction, or distance from the center of the cylinder

y= Spanwise direction

z = Distance from channel bed

Acknowledgement

The author would like to express her deepest gratitude and indebtedness to her supervisor Dr. A. T. M. Hasan Zobeyer, Professor, Department of Water Resources Engineering, BUET for his kind supervision, constant guidance, encouragement, support and thoughtful discussion throughout the entire research. Without his guidance, it was impossible to complete the thesis work.

The author expresses her gratitude to the members of the Board of Examination Dr. Anika Yunus, Professor and Head, Department of WRE, BUET, Dr. Md. Ataur Rahman, Professor, Department of WRE, BUET and Dr. Mohammad Mamun, Professor, Department of Mechanical Engineering, BUET for their valuable comments and constructive suggestions regarding this thesis work.

The author is also grateful to the Department of Water Resources Engineering, BUET, for giving her the opportunity to use the “Hydraulics and River Engineering Laboratory” for the research and also would like to thank CASR of BUET for financing and approving this thesis (Resolution 5, CASR meeting no 323 held on 28-08-2019)

In this regard, the author remains ever grateful to her beloved parents, sister and husband for being the source of inspiration and mental support during the research.

Finally, the author would like to thank almighty Allah for everything in my entire life.

Author

Saika Nowshin Nowrin

December, 2020

Abstract

Piers for hydraulic structures such as bridges, barrages and regulators are often built in open channels which acts as bluff bodies. Piers causes obstruction to the flow, thereby affecting the flow pattern. The turbulent flow behavior around a pair of cylinders which acts like bluff bodies with varying center to center spacing placed along the plane of symmetry (POS) are investigated in a rectangular flume at a fixed discharge and depth of water in this study. Mean and turbulent flow fields between two cylinders along with wake of downstream (d/s) cylinders were investigated using Acoustic Doppler Velocimeter (ADV). Analysis of longitudinal normalized velocity profiles in-between cylinders reveal that the near wake region is identical at each scenario whereas the far wake region is affected by the downstream cylinder in 3D (D =diameter of cylinder) spacing and has zero interruption from downstream cylinder in 6D and 9D spacing. However, the flow gets affected as it approaches the d/s cylinder for 6D and 9D respectively. Analysis of longitudinal normalized velocity profiles downstream of the second cylinder states that upstream (u/s) cylinder has great influence on the both near and far wake of downstream cylinder. The length of the near wake or the recirculation zone increases with the increase in c/c (center to center) spacing of cylinders. In the far wake region, the rate of flow development to achieve cross sectional mean velocity becomes slower with the increment of c/c spacing. In the near wake of midstream, the recirculation is stronger near the surface than the bottom, whereas the reverse is true for the near wake of downstream of second cylinder. However, in overall, the recirculation in the midstream is stronger than the that in the downstream. Wall wake similarity in the far wake region is investigated and the profiles and observation shows that the results at downstream follow wake similarity up to shorter longitudinal distance for all 3 cases although the number of sections in which follow wake similarity reduces with increased c/c spacing, since the size of the near wake region is becomes larger with increasing c/c spacing of cylinders. The range of magnitude and position of peak of turbulent intensity in longitudinal, transverse and vertical directions are similar in three scenarios in midstream. The longitudinal turbulent intensity and vertical turbulent is almost two-third and half respectively of transverse intensity. The maximum turbulent kinetic energy for all three cases occurs near the end of their respective recirculation zones. The measurement of turbulent

shear stress is relatively chaotic than the turbulent intensities. The maximum of turbulent shear stresses occurs within the recirculation zone for all cases. Wake similarity profile in terms of near wake on a horizontal plane at mid-depth is drawn for test results taken from both upstream pier and downstream pier measurements. The findings confirm Balachandar's equation justifying the validity of this experiment. Therefore, these results will be useful in validation of depth averaged as well as CFD modeling of flow affected by similar obstructions, specially these data will help in simulating flows more precisely around the bridge piers. Furthermore, the obtained data in this experimentation are useful for simulation of the flows around bluff bodies in open channels as it will help in simulating flows more precisely around the bridge piers.

CHAPTER 1

Introduction

1.1 General

In Bangladesh and many other countries, bridges are designed for circular piers which acts like bluff bodies mostly for small and medium rivers. The study of flow generated around surface piercing cylinders in open channels is essential for bridge design as fluid flow around bluff bodies like circular, square and rectangular cross-sections is a fundamental fluid mechanics problem and it has been a popular focus of research for many years [1-3]. In engineering projects, the significance of flow around cylinders has been the topic of numerous experimental and numerical investigations. Circular, square and rectangular shaped cylinders are extensively used in civil, mechanical, naval engineering in such structures as bridges, offshore and onshore platforms, and power lines and also in heat exchangers [4-8]. In spite of the substantial number of studies of flow around bridge-pier-like objects, our knowledge of flow around submerged bluff bodies remains bounded. A bluff body is a body that, as a result of its shape, has separated flow over a substantial part of its surface and fluid does not touch the whole boundary of the object due to boundary layer separation. A wake is generated downstream of the body which is the region of re-circulating disturbed flow occurs immediately behind a moving or stationary blunt body, which is accompanied by flow separation and turbulence. The knowledge of flow around surface piercing cylinder such as bluff bodies is of interest for bridge design and parameterization of numerical models of rivers. Numerous analyses have been done by using RANS and LES equations to simulate different engineering applications for flow over bluff bodies [9-11]. Some research have also been conducted for flow around single circular cylinders where they showed wakes behind a circular cylinder using 2D numerical model which can not produce accurate result due to poor model parameterization. As bridge piers are usually designed for double pile like cylindrical piers so it is significant to assess the flow around double pile like pier in laboratory scale for improved bridge design parameters and validation of numerical models.

1.2 Study Objectives

In this research, laboratory experimentation will be performed to investigate the turbulent flow structures and behavior around a pair of surface piercing cylinders with equal height and diameter placed along the plane of symmetry (POS) in a rectangular open channel with varying spacing.

Specific objectives of this study can be set as follows:

- (i) To investigate the variation of the velocity profiles along plane of symmetry and hence the plane wake similarity of the profiles will be assessed.
- (ii) To investigate the variation of the turbulence parameters along plane of symmetry.
- (iii) To perform plane wake analysis on the horizontal plane at mid-depth.

1.3 Study Scope, outcomes and Contents

Some research have been conducted for flow around a single circular cylinder where they showed that modeling wakes behind a circular cylinder using 2D numerical model cannot produce accurate results due to poor model parameterization. Therefore, the flow around double pile like cylindrical pier needs to be assessed in laboratory scale for improved bridge design and validation of numerical models. Moreover, in Bangladesh and some other countries, for medium and small rivers, bridge piers are usually designed as double pile like pier structures. But no study has been so far been reported to investigate the flow and turbulence characteristics around such a pier of cylinders. Therefore, in this study, experiments will be performed to investigate the turbulent flow structures around a pair of surface piercing cylinders placed along plane of symmetry in a rectangular open channel with different spacing.

The prospective outcome of this study will provide an improved understanding of the complex three-dimensional flow and turbulence in the shallow turbulent near and far wake regions generated by a pair of cylinders which in turn will help us improve the design parameters of double pile like bridge piers. It will also help in simulating flows more accurately around these bridge piers.

Laboratory experiments are carried out in a wide rectangular flume with different cylindrical spacing. All the theories, analysis, estimations, experimental investigations are presented in following chapters.

In Chapter 2, the details of bluff bodies, turbulent instantaneous velocity and turbulent parameters, wakes and boundary layer separation, near and far wakes, plane wake, the modified governing equations are described. Both experimental and numerical studies about wake generated behind the obstacles are detailed out here.

In Chapter 3, the details of laboratory experiment are described. Four experimental investigations were carried out. At first description of two-dimensional wave flume, water reservoir, material and dimension of the cylinder used in the experiment, water level and discharges are described. Some information and data processing procedure of 3D turbulent instantaneous velocity measurement device Acoustic Doppler Velocimeter (ADV) with a frequency of 30 Hz, which is used in this experiment, have been explained. Then the plan view of each experiment with their measurements are presented and explained in this chapter. The details of the experimental setup, experimental conditions, data acquisition and procedure system etc. are presented in this chapter.

The analysis of experimentally measured data objectives is presented in Chapter 4. The analyses are done for each objective under three sets of observation at both mid-stream and down-stream sections are presented with relevant explanations. Based on experimentally measured data, normalized longitudinal velocity profile variation and variation of depth averaged velocity along the plane of symmetry and hence the wall wake similarity profiles along plane of symmetry have been developed. Variation of turbulent parameters such as kinetic energy, turbulent intensity and shear stress along plane of symmetry have been assessed. Wake similarity profiles in terms of near wake have been investigated as well.

Finally, an overview of the main conclusions of this study and recommendations for further study are presented in Chapter 5.

CHAPTER 2

LITERATURE REVIEW

2.1 General

Turbulent flows around bluff bodies have received considerable research attention due to their practical importance in a wide range of environmental and fluid engineering applications. Structures which are constructed in a river become submerged when the flow depth is higher than the height of the structure. For example, a well foundation of a bridge pier gets submerged when it receives a high flood during its construction. Also, the bridge piers act as submerged piers when an overdesign flood discharge that flows over the bridge deck passes the bridge site. Sometimes a structure constructed along the river banks for the bank protection behaves as if it were a submerged structure during high floods. Additionally, in coastal and offshore engineering, submerged finite structures are often exposed to the flow tides or currents [12]. As the foundations of the structures get heavily undermined by the erosive action of the flowing stream, the scour at submerged structures or obstacles is of interest in the present study.

The presence of a bluff body which acts like obstacles in a fluid flow gives rise to an extended affected flow zone downstream of the body itself generates wake vortices behind the obstacle, which has distinctive characteristics as compared with the plane boundary layer flow.

2.2 Bluff-bodies

In classical hydrodynamics, an obstacle liable for the wake is commonly termed a bluff body. Vertical bluff bodies are of various kinds, for instance, bridge piers, abutments, piles, and so on in case of real-life situations. For these cases, the wake flows developed downstream of the bluff bodies, owing to an approach fully developed boundary layer flow with an effect from the bottom wall surface are therefore called wall-wake flow. The deficit of flow velocity along with an enhanced turbulence level in wall-wake flow is necessary to ascertain a situation that may likely involved in removal of bed sediment forming an erosion hole shown in figure 2.1 [13].

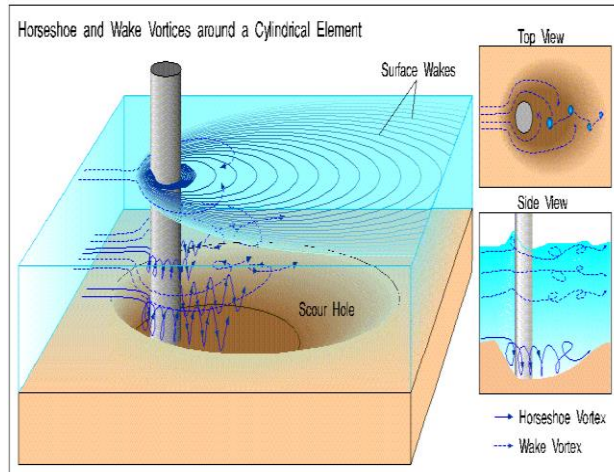


Figure 2.1: Wake vortices forming scour hole around a cylindrical shaped bluff-body [14]

2.3 Turbulent Flow

Real flows are usually classified into two classes such as laminar flow and turbulent flow. As almost all geophysical flows are turbulent, one of the most important topics in hydraulics and fluid mechanics is a clarification of the structure of turbulence. Turbulent flow occurs at higher velocities, low viscosity and at higher characteristics linear dimensions with a Reynolds number greater than 12500. The flow is characterized by the irregular movement of particles of the fluid. The movement of fluid particle is chaotic. In turbulent flow the speed of the fluid at a point is continuously undergoing changes in both magnitude and direction.

2.4 Instantaneous velocities

Instantaneous velocity is the velocity of an object in motion at a specific point in time. This is determined similarly to average velocity, but we narrow the period of time so that it approaches zero. Instantaneous velocities can be split in to time averaged and a fluctuating component. For example, $U_{\text{instantaneous}}$ can be split into a time averaged u and a fluctuating u' components shown in figure 2.2.

$$U_{\text{instantaneous}} = u + u' \quad [2.1]$$

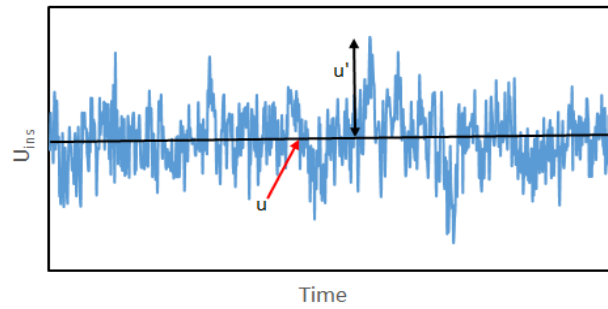


Figure 2.2: Instantaneous Velocity Graph

2.4.1 Turbulent Intensity

Turbulent intensity can be termed as the standard deviation of fluctuation of instantaneous flow velocity over the mean average flow velocity of a flowing fluid. It symbolizes the intensity of fluctuation of flow velocity.

2.4.2 Turbulent Kinetic Energy

Turbulent kinetic energy can be defined as the mean kinetic energy per unit mass which is due to the effect of eddy formation in Turbulent flow. It can be characterized by measuring the root-mean-square (RMS) velocity fluctuations. Generally, the TKE is defined to be the half of the summation of the variances (squared value of standard deviations) of the velocity components.

2.4.3 Turbulent Shear Stress

Turbulent shear stresses represent correlations between velocity components parallel to and perpendicular to the background flow, correlations that would vanish if the turbulence were isotropic.

ADV provides the time averaged velocities and turbulence quantities in all three directions as shown below

Time averaged velocities: u, v, w

Turbulent intensities: $\sqrt{u'^2}, \sqrt{v'^2}, \sqrt{w'^2}$

Turbulent kinetic energy: $KE = \frac{u'^2 + v'^2 + w'^2}{2}$

Turbulent shear stresses: $\overline{u'v'}, \overline{v'w'}, \overline{w'u'}$ [2.2]

2.5 Separation and Wakes

Wake is the region of disturbed flow (often turbulent) downstream of a solid body moving through a fluid, caused by the flow of the fluid around the body [15]. The pressure inside the wake region remains low as the flow separates and a net pressure force (pressure drag) is produced. When flow is passing over an obstacle or bluff body, velocity profiles are changing along its surface, as a result the flow is separating from its substantial part creating a recirculating disturbed flow immediately behind the obstacle or at the downstream shown in figure 2.3. This recirculation zone is accompanied by turbulence.

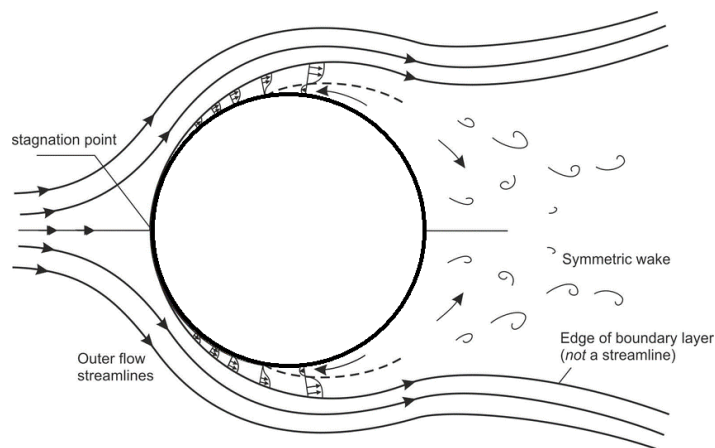


Figure 2.3: Wake generated behind a cylinder producing boundary wall separation [16].

2.6 Near wake and Far wake region

The nearest re-circulating region of wake occurs behind the bluff body or cylinder is called near wake. The region which is at a great distance from the near wake zone is called far wake. Both appear at the downstream. The near- and far-wake flow zones are the two most significant flow zones in bluff body hydrodynamics. They continue up to a certain distance downstream of a wall-mounted bluff body based on the flow condition as well as the size and shape of the body. Beyond the far-wake flow zone, the effects of the wake die down and the flow recovers the uninterrupted upstream profiles. Figure 2.4 shows definition sketch for plane wake where, U = Time-averaged velocity along x directions, U_2 = Velocity defect, $U_\infty - U$ in wall wake, U_∞

U_∞ = Undisturbed uniform ambient velocity, U_{2m} = maximum value of U_2 , b = Half-width, or length scale and h = Cylinder height.

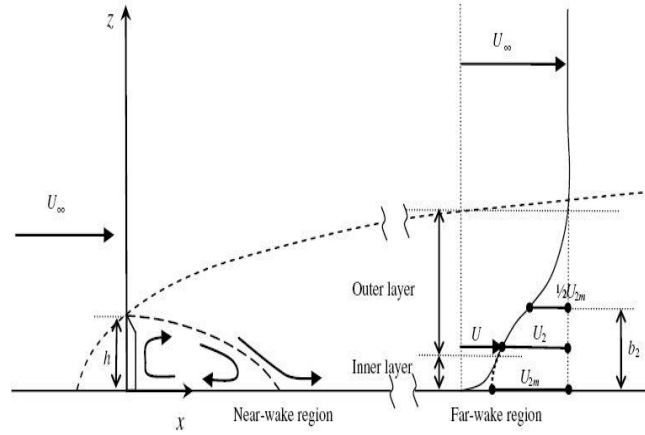


Figure 2.4: Definition sketch for plane wall wake [18]

2.7 Basic Equations

2.7.1 Schlichting's Equation

When a uniform approach flow separates at the top edge of a 2D obstacle forming a recirculation region behind it and becomes reattached to the wall after a certain distance then the disturbed flow far downstream appears to possess the characteristics of a wake in the outer region, while the inner region is affected by the wall. Such a wake can be called a plane wall wake [18].

Schlichting[19] developed an equation to analysis the velocity distribution in far wake region of plane turbulent wakes are similar and this similarity equation is known as the plane wake equation shown at Eqn. [1].

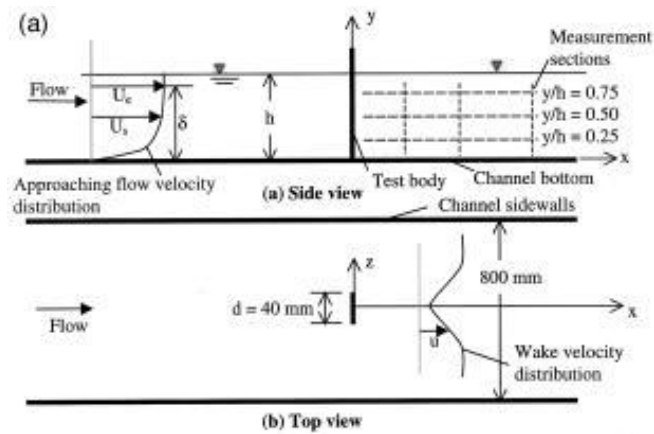
$$\frac{U_1}{U_{1m}} = (1 - 0.293\lambda^{\frac{3}{2}})^2 \quad [2.3]$$

Where, $U_1 = U_\infty - U$ is the velocity defect, U_∞ = undisturbed ambient velocity, U_{1m} = maximum value of U_1 , $\lambda = \frac{z}{b_1}$, and $b_1 = y$ where, $U_1 = 0.5U_{1m}$. U_{1m} and b_1 are considered velocity and length scales for the plane wake.

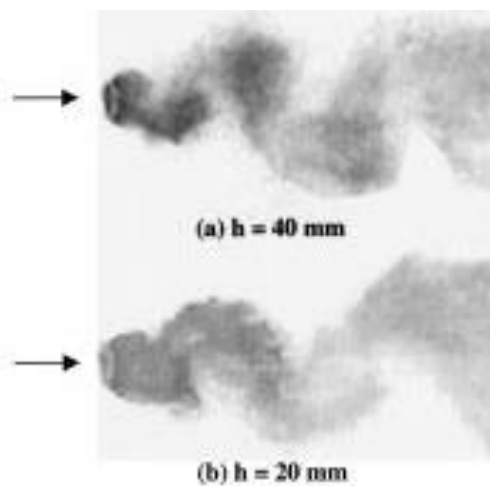
2.7.2 Balachandar's Equation

Balachander, et al [20] conducted a study on the measurement of both velocity and concentration in the near region of shallow turbulent wakes in a rectangular open

channel flume of 0.6 m deep, 0.8 m wide, and 10 m long. A contraction and several stilling arrangements used to reduce any large-scale turbulence in the flow preceded the straight section of the channel. Two tests were carried out at flow depths $h=20$ and 40 mm. In each test, measurements were carried out at three axial stations (2.5, 5, and 10 plate widths) downstream of the bluff body. At each axial station, the velocity measurements were obtained at distances of $h/4$ where h = depth of water, $h/2$, and $3h/4$ from the channel bed and spanning the entire cross section of the wake shown in figure 2.5. The velocity measurements were carried out using a single-component fiber-optic probe laser-Doppler anemometer. The test body was located 4m downstream of the contraction.



(a)



(b)

Figure 2.5: Schematic of the test body and coordinate system; (b) photographs of the flow field

Additionally, developed an improved fourth order polynomial equation of plane wake equation for the near wake velocity profile. It was assumed that $\frac{U-U_{min}}{U_{1m}}=0$ at $\frac{y}{b}=0$; the gradient of $\frac{U-U_{min}}{U_{1m}}=0$ at $\frac{y}{b}=0$; $\frac{U-U_{min}}{U_{1m}}=0.5$ at $\frac{y}{b}=1$; $\frac{U-U_{min}}{U_{1m}}=1$ at $\frac{y}{b}=2.25$; and $\frac{U-U_{min}}{U_{1m}}=0$ at $\frac{y}{b} \geq 2.25$ resulting in;

$$\frac{U-U_{min}}{U_{1m}} = 0.8616\left(\frac{z}{b}\right)^2 - 0.4148\left(\frac{z}{b}\right)^3 + 0.0532\left(\frac{z}{b}\right)^4 \quad [2.4]$$

Where, U = Time averaged velocity along x direction, $U_1 = U - U_{min}$, U_{min} = Minimum value of U , U_{1m} = Maximum value of U_1 , z = distance from the channel bed and $b=y$ where, $U_1=0.5U_{1m}$. Schematic of Balachander's profile is shown in figure 2.6.

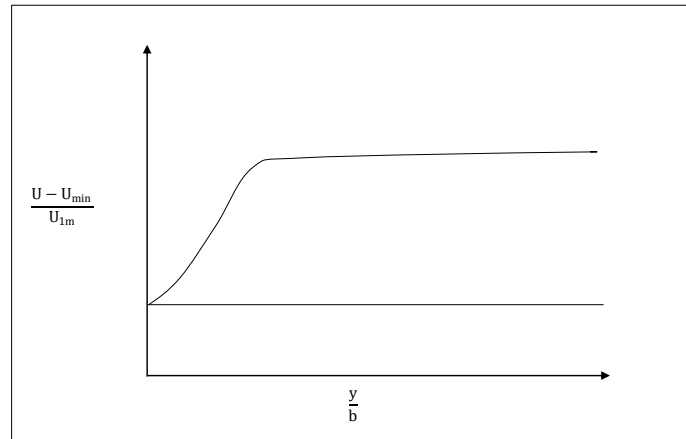


Figure 2.6: Schematic of Balachander's profile of plane near wake

2.8 Previous Studies on Flow around Cylinder

Flow passing a vertical bluff body or cylinder has been a key topic of study among hydraulicians owing to its significance in several theoretical analyses and practical applications.

Lloyd, et al shows that in a deep uniform flow incident on a two-dimensional (2D) cylinder with its axis vertical, vortex shedding (VS) occurs with strong three-dimensional (3D) components where Shallow wakes are generated behind obstacles where the incident velocity has a boundary layer type profile [21]. Ingram, et al. [22]

observed that bed friction effects become important in shallow wakes. Therefore, they proposed a stability parameter. Chen, et al [23] observed in shallow flows around a surface piercing cylinder that vortex street-like instabilities occur. It was further argued that vortex street type instabilities in shallow wakes are similar to a Karman vortex street but there are also differences between these two. A Karman vortex street occurs for a Reynolds number (R_D) range of 100 to 200 in deep wakes, where the height of the cylinder $h \geq 10D$. However, in shallow wakes a vortex street occurs at $R_D \sim 10^4$ to 10^5 . They also found that the Karman vortex street in deep wakes has well defined streamlines, whereas the vortex street that occurs in shallow wakes has fuzzy streamlines.

Sforza, et al. [24] have studied the 2D and 3D turbulent wall wakes and found that the bulk flow properties and the applicability of theoretical models depend on the obstacle geometry in wind tunnel. It was further observed that the decay of the mean velocity defect of air in the wake is rapid in the 3D wake compared to the 2D wake, but there was almost no wake growth in the near wake region. They characterized wake regions behind a 3D obstacle on a flat plate as recirculation region, where the effects of the vortices induced by the obstacle dominate over the effects of viscous diffusion. The velocity profiles are then characterized by zero or slightly negative velocities directly behind the obstacle changing to considerably larger than the free stream velocity near the exposed edges of the obstacle.

Shamloo, et al. [25] investigated studied shallow wakes behind hemispherical objects with different levels of submergence in a smooth bed open channel. They resolved the complexity of the 3D wakes produced by submerged objects by considering a wall wake in the vertical plane and a plane turbulent wake in the horizontal plane. They also analyzed velocity profiles in the downstream plane of symmetry for moderate to deeply submerged hemispheres using the concept of plane wall wake following Rajaratnam, et al. [18]. They found good wall wake similarity in the outer region but the inner region profiles were similar to the logarithmic profile only in the far-wake region. It was further investigated that the longitudinal velocity profiles in the transverse direction were similar and described well by the plane wake

equation. From results the moderate to deeply submerged hemispheres did not exhibit good similarity with the plane wake equation because the data were quite random.

Most research has focused on wakes behind circular cylinders in wind tunnels, where the flow is deep and the aspect ratio (flow depth, H compared to cylinder diameter, D) is high (e.g. Roshko 1961, Antonia 1991). In a pressurized wind tunnel at a high Reynolds numbers transition in which the drag coefficient increases and becomes constant and a definite vortex shedding occurs. But unfortunately, high Reynolds number is not generally available and the time available for this experiment was too short to investigate some points.

Chen, et al. [23] observed the shallow far wake behavior that has been investigated with a special variable porosity wake device that reduces the wake velocity deficit and completely suppresses the VS instabilities in the near-field. The shallow plane wake is observed to "stabilize" for large downstream distances, x/H , in the sense that the growth and maintenance of the large-scale structures in the wake flow become suppressed and the wake collapses into a more ordered flow. This wake stabilization is controlled by two factors: first, the usual evolution in a turbulent wake that reduces the velocity deficit while increasing the wake parameter S , and secondly, the exponential loss of the momentum deficit fluxes in the wake due to bottom friction.

Balachander, et al. [20] conducted a study on noninvasive measurement of both velocity and concentration in the near region of shallow turbulent wakes using a laser-Doppler anemometer and a video-imaging technique and the wake was generated by a flat plate placed normal to the flow. From the results found through the experiments, the approaching flow boundary layer thickness was comparable to the depth of flow and bed friction effects were large. Both velocity and concentration data were obtained at three axial stations across the wake.

Investigations carried out at the near wake region of a circular cylinder by different researchers [28-30] where they studied the topology of the vortex field. Their studies indicated that the formation of a large-scale Karman-type vortex involves

upward fluid ejection through its center, which eventually leads to a horizontal vortex producing significant distortion of the free surface. Akilli, et al. [28] also studied vortex formation and their interactions with the channel bed in shallow flows. They observed that the streamline topology illustrating the structure of wake vortices changes with elevation.

A study of turbulent flow in the near wake region of four different finite cylinders was investigated by Paul, et al. [31]. Details of velocity measurements around and in the near-wake of the cylinder models was conducted by a particle image velocimetry technique. The contours as well as profiles of the mean velocities and turbulence intensities were obtained to document the salient features of the flow field. Reconstruction of the fluctuating velocity components were also used to investigate the role of large-scale structures.

Near wake region of a circular cylinder in shallow water placed vertically is investigated by Ahmed, et al. [32] using a combination of visualization marker and a technique of high-image-density particle image velocimetry. The formation of vortex involves upward ejection of fluid through its center, which eventual leads to a horizontal vortex that induces significant distortion of the free surface. The relationship between patterns of streamline topology and vortices is established for successive phases of the oscillation cycle by using global, instantaneous imaging, and in horizontal planes at and above the bed. The sequence of phase-referenced state shows that it is possible to identify topological characteristics, including the location of a specific point that is consistent at elevations on and above the bed. The degree of concentration of vortices is major at progressive elevations above the bed and large-scale vortex successively decreases.

Wake created by short submerged horizontal cylinders to model the submerged pipelines in rivers studied by Smith, et al. [33]. Arya, et al. [34] studied the atmospheric flow and dispersion in wakes downstream of 3D models of low hills. Jirka studied large scale flow structures and mixing processes in shallow flows [35]. Katopodis encouraged physical modeling studies of shallow flows around fish habitat structures

to overcome the limitations of numerical modeling in describing the small-scale aspects [36].

Notable works have been carried out where the experimental study was performed on flow around cylindrical objects of equal diameter and at four different heights under similar flow conditions. Sadeque, et al. [37] investigated different types of flow components and their locations were inspected using a set of flow visualization tests. Submergence of a cylinder produces stronger three-dimensional flows in the downstream wake and provides valuable knowledge of hydraulics of flow around submerged structures cylinders.

Sadeque, et al. [38] studied patterns of flow in the shallow turbulent near-wakes behind bed-mounted cylinders to investigate wall wake which is well described by the plane wake equation. Wall wake similarity was also observed for turbulent kinetic energy and primary Reynolds stress for moderate to deeply submerged cylinders. Wake analyses in the horizontal plane revealed that similarity of mean velocity profiles across the flow exist in the near-wake region at all elevations for slightly submerged and surface piercing cylinders for moderate and deeply submerged condition. Result shows for slightly submerged and surface piercing cylinders similarity was observed in the near-wake region between the non-dimensional velocity profiles across the wake and the plane wake equation and also states that the velocity profiles could be improve if a modified transverse length scale was used for experimenting the described wake flows.

Hydraulic modeling has been carried out by Sadeque, et al. [39] using River2D which is a numerical tool with depth averaged flow approximation that can be used for fish habitat modeling. Due to unavailability of reliable experimental measurements the competency of hydraulic modeling of shallow near-wake flows could not be verified. The experimental study of shallow wakes in open channel flows provided detailed velocity measurements in the wake of submerged and surface piercing cylinders. For The generated wake velocities for similar channel properties and approach flow conditions by hydraulic model (River2D) are compared with depth averaged

experimental results and observed that the deviation of wake velocity on the downstream plane of symmetry remains less ($\sim 10\%$) for $x \leq 2D$, but increases at $x=3D-10D$. Results were under predicting the velocity profiles in the wakes of deeply submerged and moderately submerged cylinders and the rate of decay of velocity defect was significantly slower in the numerical model than observed in experiments.

Merrick, et al. [40] encountered some difficulties when simulating supercritical Reynolds number flow over curved surfaces of a building in a low speed boundary layer wind tunnel (BLWT). Surface roughness on the facade of the cylinder can affect the location of the separation point and the extent of the wake on the leeward face, upon which the wind-induced responses are dependent. This study attempts to control the flow around a circular cylinder through the implementation of artificial surface roughness across the exterior of the cylinder.

Simulation model was analyzed by Zhang, et al. [41] to evaluate the applicability of the standard $k-\epsilon$ turbulence model in engineering practice in the subcritical to supercritical flow regimes. Two-dimensional numerical simulations of flow around a circular cylinder had been performed using Unsteady Reynolds-Averaged Navier Stokes (URANS) equations with the standard $k-\epsilon$ turbulence model. Solution verification had been studied by evaluating grid and time step size convergence. By comparing the values of these quantities of adjacent grid or time step size resolutions, convergence study has been performed. Solution validation is obtained by comparing the converged results with published numerical and experimental data and it can be observed that the standard $k-\epsilon$ model with enhanced wall treatment appears to be applicable for higher Reynolds number turbulence flow.

Numerically investigations were carried out by Yuce, et al. [42] where the flow field around cylinders of the same characteristic length under identical flow conditions ranging from laminar to turbulent was analyzed. Two-dimensional simulation analyses were performed using the shear stress transport $k-\omega$ turbulence closure model and commercial software. Cylinder shape was found to significantly affect the flow field. Under the same initial flow conditions, wake downstream of the square cylinder was

found to be much more turbulent than that of the circular one and Re increased so the turbulence of the wake flow increased and its length downstream of the cylinders increased.

A study carried out by Khaple, et al. [43] The present study attempts to quantify the effect of the mutual interference of front pier and bridge pier on local scour at the bridge pier. Interference of the piers depends on the shape of the piers, spacings, flow velocity, relative diameters of the piers, sediment size, and oblique distance between the piers and flow oblique angle. It was observed that the maximum scour in the downstream pier is lower than that around the upstream pier. However, the hydrodynamics study along POS between two piers to understand the behavior and effect of turbulent structure more accurately remained unexplored.

Numerical simulations of flow past four square-arranged cylinders are carried out by Gao, et al. [44] at different spacing ratios and Reynolds numbers. The effects of spacing ratio and Reynolds number on the wake flow characteristics are investigated, such as the instantaneous vortices contours, force coefficients, and vortex shedding frequencies. The results show that the flow characteristics behind the four-cylinder cases are significantly affected by the spacing ratios and Reynolds numbers.

Dey, et al. [13] studied on the time-averaged turbulent flow characteristics in a wall-wake flow downstream of a wall-mounted vertical cylinder (free surface piercing) are analyzed from the viewpoint of self-similarity in their vertical profiles. Results show that the values of the maximum deficit Reynolds shear stress of all the quantities diminish with the downstream distance, signifying the recovery of their uninterrupted upstream profiles.

Bose, et al. [45] developed the nonlinear momentum equation for turbulent far-wake flow downstream of a cylinder which is derived from the Reynolds averaged Navier–Stokes equations and solved by iteration and generalized similarity solution.

Both turbulent and laminar far-wake flow cases are analyzed and solutions broadly extend the earlier findings [18].

Dey, et al. [46] investigated the characteristics of turbulent kinetic energy (TKE) fluxes and budget, conditional Reynolds shear stress (RSS) and Reynolds stress anisotropy in the near-wake and far-wake flows downstream of a wall-mounted circular cylinder placed vertically on a rough wall. Result shows that all the profiles of TKE fluxes and budget, conditional RSS and turbulence anisotropy, regain their uninterrupted upstream profiles with an increase in downstream distance.

Therefore, appreciable amount of works needs to be done on understanding the flow around circular cylinder as it is still is one of the challenges in fluid mechanics. Moreover, it is of great interest for practical applications, such as wind loads on cylindrical structures. For the two-dimensional problem in a uniform flow, research since the beginning of this century has produced a good if still incomplete insight into the phenomena. For more general but also for more significant conditions a large amount of work remains to be done. However, the hydrodynamics study along POS between two piers to understand the behavior of flow and effect of turbulent structure more accurately remained unexplored by investigating the three-dimensional turbulence parameters which is the aim of this study.

CHAPTER 3

LABORATORY EXPERIMENT

3.1 General

The experiments are performed in the 21.3m long tilting flume of Hydraulics and River Engineering Laboratory of the Department of Water Resources Engineering, Bangladesh University of Engineering and Technology. A set of experiments are carried out with fixed water depth and discharge varying center to center spacing of cylindrical objects to investigate the flow around the cylinder for several different fixed locations and different vertical depths. An Acoustic Doppler Velocimeter (ADV) was used to obtain the instantaneous velocity field at different locations around a pair of cylinders with a sampling frequency of 30 Hz and duration of one to two minutes.

The experimental setup and procedure of conducting the experimental works are described in this chapter.

3.2 Laboratory Equipments

3.2.1 Two-dimensional wave flume

The experiment has been conducted in a 21.3 m long, 0.76 m wide and 0.74 m deep rectangular tilting flume in the Hydraulics and River Engineering Laboratory as shown in Figure 3.1. The side walls of the flume are vertical, and made of clear glass for visual inspection. The bottom of wave flume is made of steel. Flume bed has been kept horizontal and it is supported on an elevated steel truss. Water was supplied by external pipes and water depth was kept to desired level in the flume. For avoiding any unnecessary leakage in the flume, necessary steps were taken.



Figure 3.1: Laboratory flume (21.3 m long, 0.76 m wide and 0.74 m deep)

3.2.2 Water reservoir

Water reservoir used in the flume is a steel structure. Water is stored in the reservoir during the time of conducting the experiment. In the reservoir, the water supply can be controlled by the existing facilities in the reservoir.

3.2.3 Material and dimension of cylinder

Two concrete cylinders are used for this experimental study of equal height, $h=0.30\text{m}$ and diameter, $D=0.15\text{m}$. For providing a smooth flow, cylinders are covered with plastic sheets as in practical scenario, the surface of a pier becomes smoother over the time due to moss generation caused by continuous flow of water and by covering the cylinders the rough edges of the concrete cylinders could not affect the flow significantly.



Figure 3.2: Concrete cylinders used in experiment

3.2.4 Acoustic Doppler Velocimeter (ADV)

Velocimeters belong to a special class of high-resolution 3D instruments used to study rapid velocity fluctuations in the laboratory or in the ocean. These instruments have three or more focused beams to measure with high sampling rates in a small point. Acoustic Doppler velocimeter is designed to record instantaneous velocity components at a single-point with a relatively high frequency shown figure 3.3. Measurements are performed by measuring the velocity of particles in a remote sampling volume based upon the Doppler shift effect.

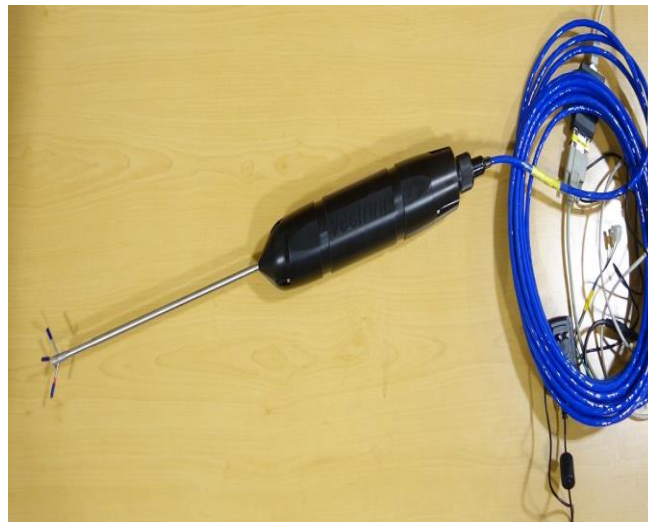


Figure 3.3: Acoustic Doppler Velocimeter (ADV)

Working principle of Acoustic Doppler Velocimeters is process by sending out a short acoustic pulse from the transmit element. When the pulse travels through the focus point for the receiver beams, the echo is recorded in each of the acoustic receiver elements shown in figure 3.4. The echo is then processed to find the Doppler shift, the scaling is adjusted with the measured speed of sound in the liquid velocity vector is recorded or transmitted to a PC at a rapid rate. WinADV32-Version 1.83, public domain software developed for ADV data processing by the USBR (Wahl 2000), was used to convert the raw ADV data recorded in binary format to ASCII format. ADV reading does not vary significantly for different time duration. The fluctuation of reading for different time duration is observed at two decimal places.

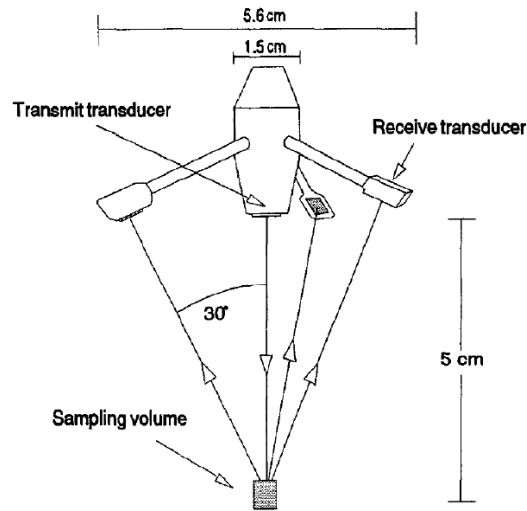


Figure 3.4: Components of Acoustic Doppler Velocimeter

3.2.5 Selection of scale for experimentation

Design of physical model is an iterative process because it is quite difficult to fulfill all scale conditions to the governing processes to obtain complete similitude between the model and prototype. Available space, pump capacity in the laboratory was considered in selecting scale factors to develop model scale depending on available laboratory facilities. In addition, model scale has been selected based on previous study done by Sadeque M. A. F, Rajaratnam N, Loewen M.R, 2009 where the aspect ratio was kept low at $h/D = 2$ to study the shallow wake where h =height of cylinder and D =diameter of cylinder. Greater than this aspect ratio might increase the effect of side walls.

3.3 Experimental Set-up

In 21.3 m long horizontal rectangular flume, two cylinders of equal height $H=0.30$ m and diameter $D=0.15$ m is placed vertically on the bed along the centerline in the middle part of the flume. Three different positions of cylinders are chosen to collect the data by changing the center to center spacing to $3D$, $6D$ and $9D$ respectively. Instantaneous velocity at different points along the plane of symmetry and around the cylinder is measured by using ADV for 2 min with a frequency of 30 Hz. Schematic plan view of each data collection point is given in Figure 3.5 for both mid-stream analysis and downstream analysis for all three test scenarios.

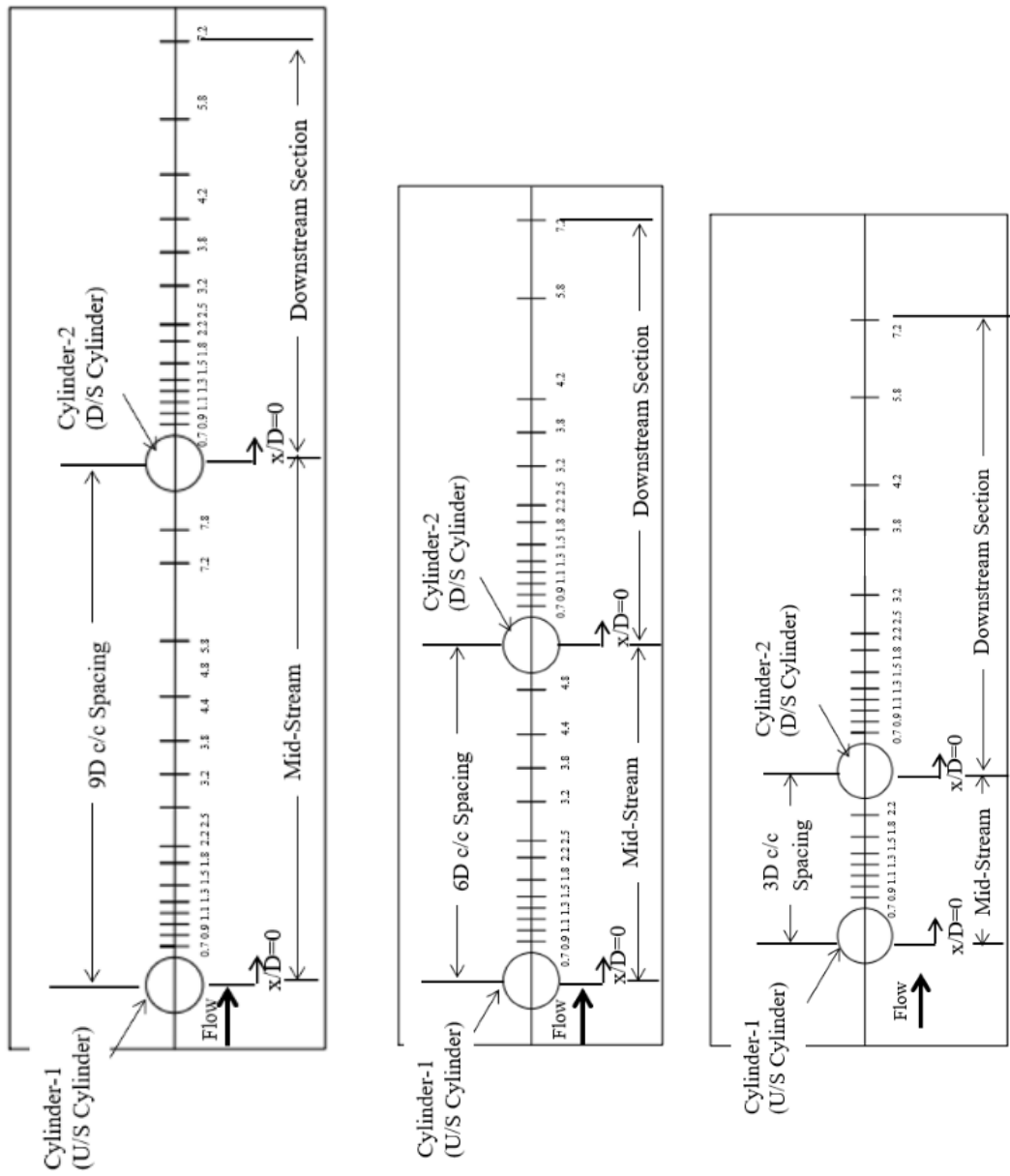


Figure 3.5: Plan view of data collection at mid-stream & down-stream

However, for mid-depth analysis the bed of the flume was divided into certain grids of 0.5D measurement and pier arrangements were kept same for other three case studies. A schematic plan view of 3D spacing is given under this case study in figure 3.6 for upstream and downstream piers. Similarly, the analysis is observed for 6D and 9D spacing as well.

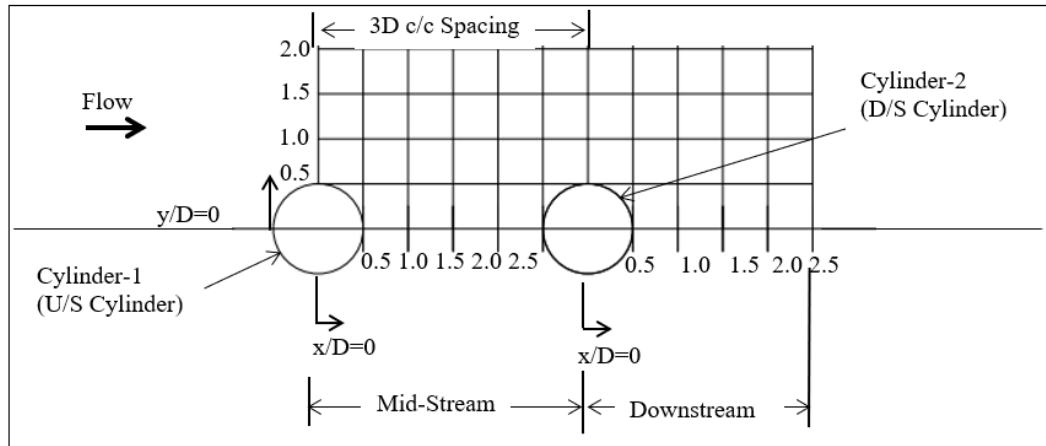


Figure 3.6: Plan view of data collection of downstream at depth, $z = \frac{h}{2}$

Schematic of the experimental set up is shown in figure 3.7.

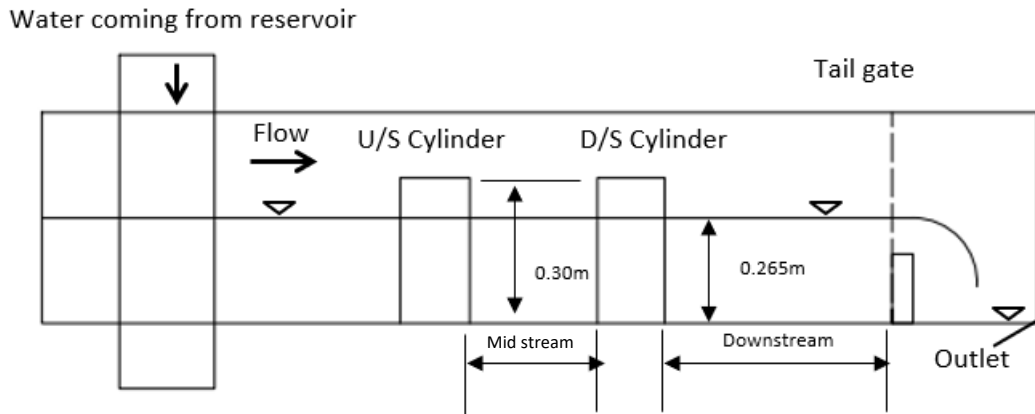


Figure 3.7: Details of Experimental Set-up

3.4 Measurement Techniques and Test Scenarios

The depth of water was kept 0.26m and discharge rate was 250m³/hr during the experimental run. The cross sectional mean velocity of the flow in the flume was 0.34m. For first test scenario the center to center spacing was 3 times of the diameter

of cylinder D which is 0.45m having a discharge of 250m³/hr. Laboratory set up shown in figure 3.8

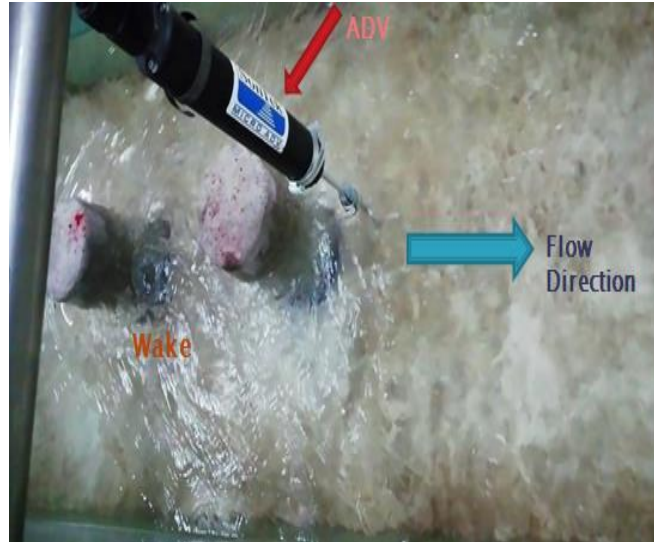


Figure 3.8: Experimental Set-up

For second experimental run, moving the second cylinder to a new position by changing the center to center spacing to six times of diameter of cylinder which is 0.90m whereas the other parameters; water depth and discharge remaining same. Similarly, center to center distance was kept 9 times of the diameter which is 1.35m by moving the second cylinder at same water depth and discharge for the third run. Calculation of cross sectional mean velocity and Reynolds number is listed in table 3.1 and test scenarios of each experimental run is listed in table 3.2.

Table 3.1: Calculation of cross sectional mean velocity and Reynolds number

Discharge, Q (m ³ /hr)	Width of flume (m)	Water depth, H (m)	Cross sectional mean velocity (m/s)	Kinematic viscosity of water, ν (m ² s ⁻¹)	Froud number (F)	Reynolds number (R)
250	0.76	0.26	0.34	1*10 ⁻⁶	0.21	88400

Table 3.2: Test scenarios of experimental runs

Run No.	Diameter of cylinder, D (m)	Height of cylinder h (m)	Discharge Q (m ³ /hr)	Water depth, H (m)	Center to center distance of cylinder (m)	Cross sectional mean velocity (m/s)
1	0.15	0.30	250	0.26	3D=0.45	0.34
2	0.15	0.30	250	0.26	6D=0.90	0.34
3	0.15	0.30	250	0.26	9D=1.35	0.34

Data was collected at fixed stations along the plane of symmetry for ten vertical depths at upstream, in between two cylinders and at downstream section.

3.4 Data Acquisition

To understand the flow behavior around the cylindrical objects, the 3D turbulent velocity data have been collected at described fixed locations using ADV along centerline. For a downward looking ADV the measuring volume is 5 cm below the acoustic transmitter, and the entire probe head needs to be immersed in water. The bottom most point of velocity measurement was 0.5 cm above the bed to ensure strong back scattering of sound from the sampling volume. At each selective section, data of turbulent velocity have been collected for two-minute duration. Red dye color is injected to visualize the flow behavior and direction. Still photographs and video recordings are taken during each run. Wake generation is observed and showed in figure 3.9.



Figure 3.9: Wake is generating between two cylinders

To perform plane wake analysis on horizontal plane at the mid depth the experimental set up is done by dividing the bed of flume into several grids. Water level was maintained at 0.26 m and the discharge was $250\text{m}^3/\text{hr}$. ADV measured the turbulent instantaneous velocity at indicated fixed location at the mid depth. Investigations were done at upstream and downstream section by placing two cylinders at 3D, 6D and 9D c/c spacing.

3.5 Experimental Procedure

First the experimental set up was done as per requirement set by the objectives of the experimental study. The flexibility needed in such experimental, setup to carry out further studies in future was also kept in mind. For conducting the experiment following procedure was followed. To run the experiment and collecting data required not only a great deal of physical work but also a careful observation.

3.5.1 Progressive operation for the experiment

The first step is the fixation of the discharge. Supply pipe line has valve for the regulation of the discharge into the flume. Sufficient depth of water in the downstream reservoir should be present before starting the pump. ADV was placed carefully into the water so that it remains completely vertical and immersed. ADV was directly connected with the PC of Laboratory. Velocity was measured at fixed ten vertical

points on each segment. The ADV was attached with a movable frame for a trouble-free utilization while changing the positions along the centerline for each section. Water level was measured using a measuring tape to maintain the height of water equal for the test runs. To avoid unnecessary movement of cylinders if occur caused by the flow of water, weights were kept above the cylinders. Red dye color was injected into the sides of the cylinder to check the presence of recirculating flow or wake vortices. The turbulent instantaneous velocity data is collected by the software WinADV32-Version 1.83. Same procedure was repeated during observation for all the test runs. Some photographs were taken during the experimental runs is given in Figure 3.10 to Figure 3.14.



Figure 3.10: Laboratory set-up of velocity measuring locations



(a)



(b)



(c)



(d)

Figure 3.11: (a) Plan view of data collection at grid points, (b) Side view of experimental set-up, (c) Frame of ADV, (d) ADV is immersed in water to collect the data at several locations



Figure 3.12: Flow visualization



Figure 3.13: Changing the position of ADV for different sections

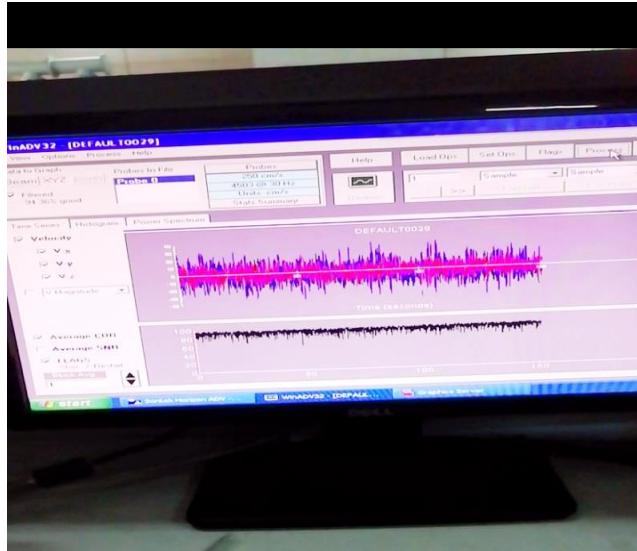


Figure 3.14: Data acquisition by WinADV32 software

3.5.2 Uncertainty Analysis

A detailed analysis of uncertainty and repeatability of ADV data was observed. Uncertainty estimates 95% of confidence limit obtained from 12 sets of ADV data sampled at 30 Hz for a duration of two minutes at three vertical depths $z = 0.5$ cm, $z = 9.5$ cm, $z = 19.5$ cm listed in table 3.3. Each measurement was collected on a different day after resuming the experiment to avoid random error of experimental set-up. The test indicated that the standard deviations were 0.4 to 2.27% for longitudinal mean velocity. 6.4% for near-bed kinetic energy and 9.58% for near-bed Reynolds stress.

Table 3.3: Uncertainty estimation of ADV measurements

z (cm)	U (cm/s)	V (cm/s)	W (cm/s)	u' (cm/s)	v' (cm/s)	w' (cm/s)	KE (cm^2/s^2)	\overline{uw} (cm^2/s^2)
0.5	± 0.38	± 0.33	± 0.06	± 0.19	± 0.07	± 0.02	± 0.86	± 0.05
9.5	± 0.25	± 0.05	± 0.08	± 0.16	± 0.03	± 0.06	± 0.61	± 0.41
19.5	± 0.26	± 0.12	± 0.29	± 0.06	± 0.06	± 0.04	± 0.28	± 0.03

CHAPTER 4

EXPERIMENTAL RESULTS AND DISCUSSION

4.1 General

In this study, a down-looking ADV was used to measure velocity and turbulence around pairs of circular cylinders placed along the plane of symmetry of the rectangular flume with three different spacing of 3D, 6D and 9D. Data were collected along the plane of symmetry with different longitudinal and vertical spacing as described in Chapter 3. The aim is to understand the mean (time-averaged) flow characteristics in terms of variation of longitudinal velocity profiles, size of recirculation zone, velocity development process, near and far wake behavior; and turbulence characteristics in terms of turbulent intensity, turbulent kinetic energy and turbulent shear stress caused by the pair of cylinders. Moreover, data were collected at mid-depth with longitudinal and lateral spacing of 0.5D in the left half of the plane of symmetry to understand the lateral variation of longitudinal velocity and plane wake characteristics of these profiles. The data were collected for a fixed water level of 0.26 m and a fixed discharge of 250m³/hr. For the purpose of these analyses, six sets of observations were carried out with three sets along plane of symmetry and three sets at mid depth on the left half of plane of symmetry. Details of data collections and experimental set up related details are all described in Chapter Three.

4.2 Normalized Longitudinal Velocity Variation along Plane of Symmetry (Mid-Stream Section)

To assess the longitudinal variation of mean turbulent flow characteristics, point velocity was measured by ADV at ten different depths of verticals for the selected points along the POS of the flume. The cylinders were placed at 3D, 6D and 9D c/c spacing for three different cases whereas the depth of water and discharge were unchanged. Normalized profiles of $\frac{u}{U_0}$ vs $\frac{z}{H}$ at midstream are plotted in Figure 4.1 for 3D, 6D and 9D c/c spacing. The corresponding depth averaged velocity is plotted in Figure 4.2. For midstream analysis, x indicates the longitudinal distance from the center of the upstream pier along the POS. For the 3D c/c spacing, the velocity profiles

show that near the bed and near the surface the velocities are negative from $\frac{x}{D}=0.7$ to 2.2. Near $\frac{z}{H}=0.2$ the profiles become slightly positive for $\frac{x}{D}=1.8$ and 2.2. The corresponding depth averaged values of the profiles show that the recirculation zone occupies almost the whole space between the two cylinders for 3D c/c spacing.

For the 6D and 9D spacing, the velocity profiles are almost completely negative for $\frac{x}{D}=0.7$ to 1.5. Based on the depth averaged velocity, the recirculation zone is confined up to $\frac{x}{D}=1.65$ as obtained from interpolation. Thereafter, the profiles become positive and there is a rapid increase in velocity between $\frac{x}{D}=1.5$ to 2.5. This can also be found in terms of depth averaged velocity as shown in Figure 4.2 where the $\frac{u_{da}}{U_o}$ increases from -0.1 at $\frac{x}{D}=1.5$ to 0.47 at $\frac{x}{D}=2.5$ for 6D case and then the rate of increase slows down and the maximum $\frac{u_{da}}{U_o}=0.67$ occurs at $\frac{x}{D}=4.5$. Finally, the velocity dips as the flow approaches the downstream cylinder. For 9D case, $\frac{u_{da}}{U_o}$ is increases from -0.15 at $\frac{x}{D}=1.5$ to 0.6 at $\frac{x}{D}=3.2$ and the rate of increase slows down and the maximum $\frac{u_{da}}{U_o}=0.8$ occurs at $\frac{x}{D}=5.8$. $\frac{u_{da}}{U_o}$ remains constant until $\frac{x}{D}=7.2$ and thereafter it decreases as the flow approaches the downstream cylinder.

In the recirculating near wake zone, the recirculation near the water surface appears to be stronger than the near bed recirculation. In the far wake zone after the recirculating near wake zone, the velocity profiles can be categorized into two categories: jet type profiles and logarithmic type profile. The jet type profiles can be normalized with maximum velocity and z normalized by b , where b is the distance of u_{max} from bed. The normalized profiles are plotted in Figure 4.3. For the 3D spacing, only one profile at $\frac{x}{D}=2.2$ shows jet type shape. For the 6D and 9D spacings, profiles of $\frac{x}{D}=2.2$ to 4.5 have been plotted which shows that all the profiles are jet type but the profiles at $\frac{x}{D}=2.5$ to 4.5 for 6D and $\frac{x}{D}=2.5$ to 3.8 for 9D show self-similarity such that they will fall close to the same curve for respective case.

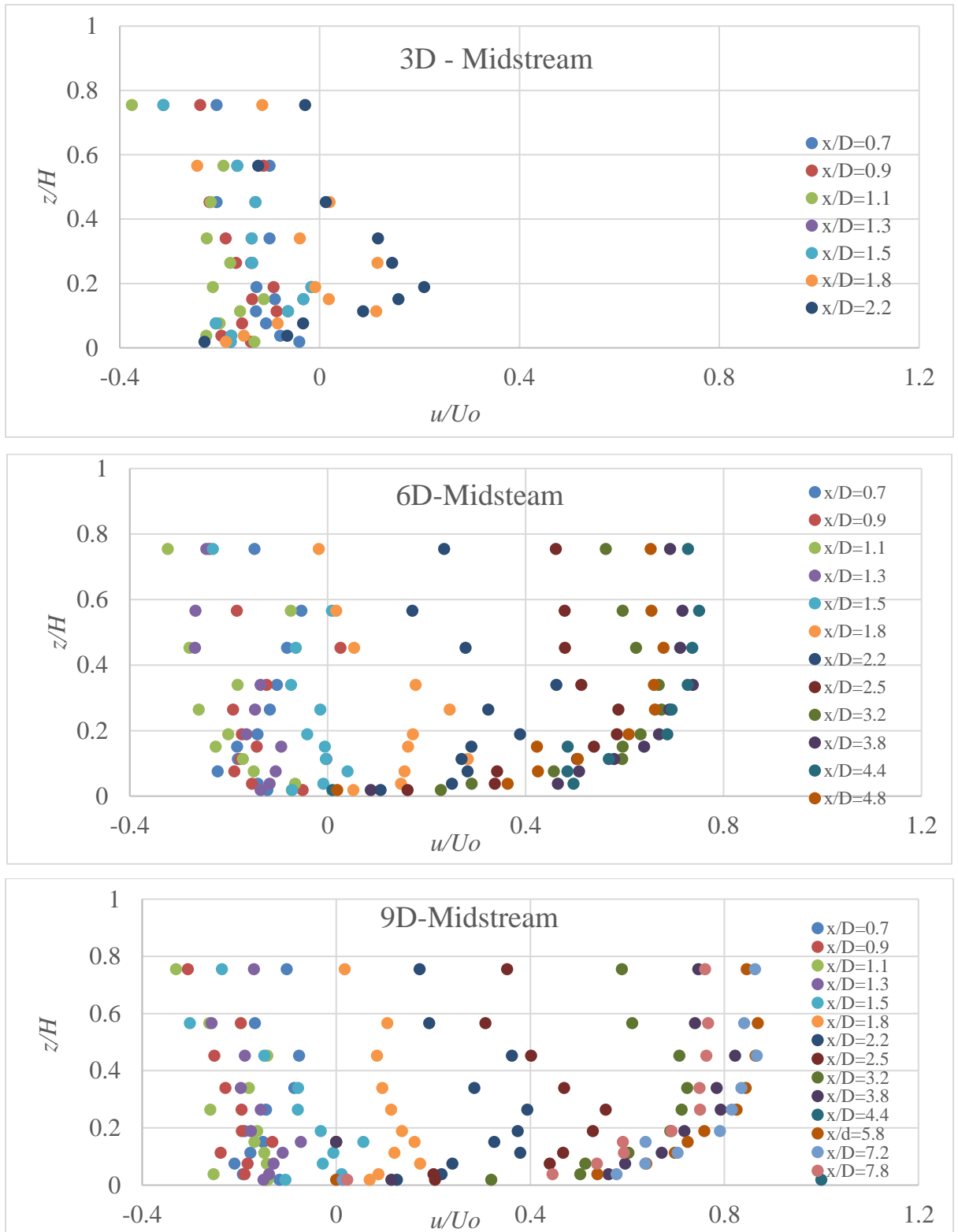


Figure 4.1: Normalized Longitudinal Velocity Profiles along plane of symmetry between two cylinders

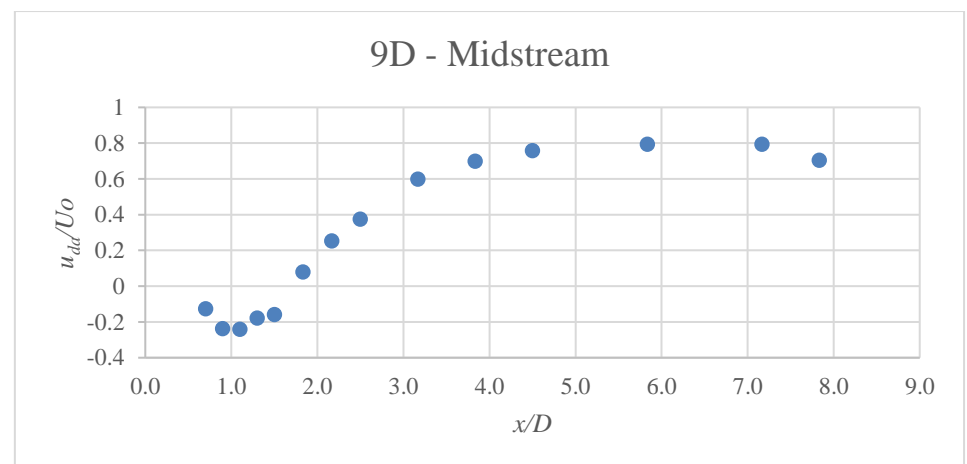
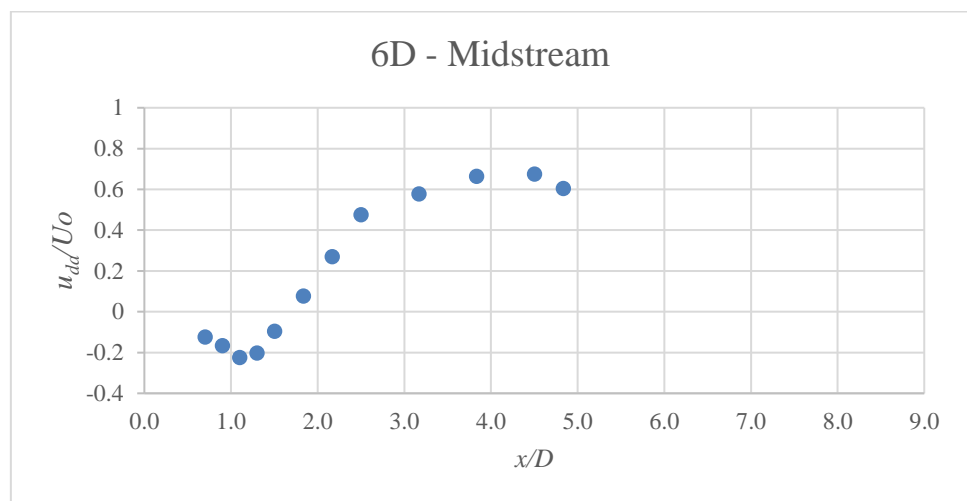
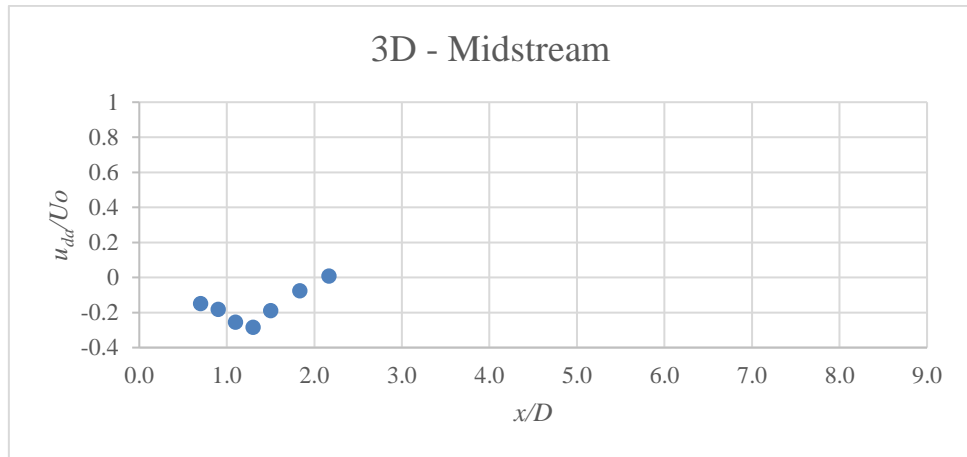


Figure 4.2: Normalized Longitudinal Depth-Averaged Velocity along a plane of symmetry between two cylinders

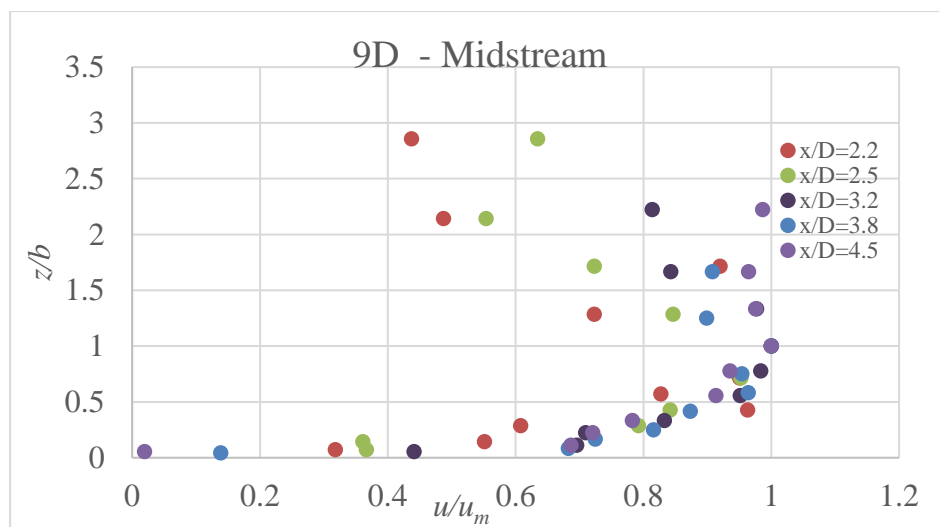
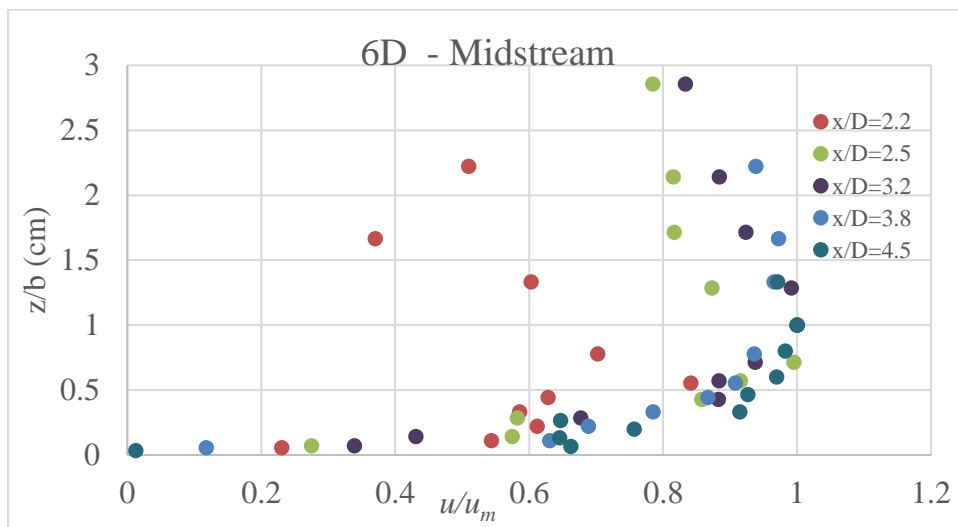
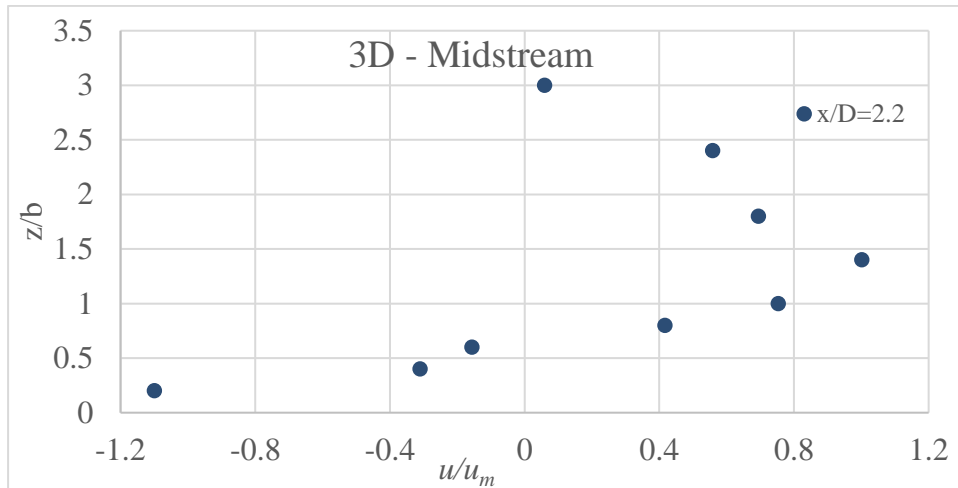
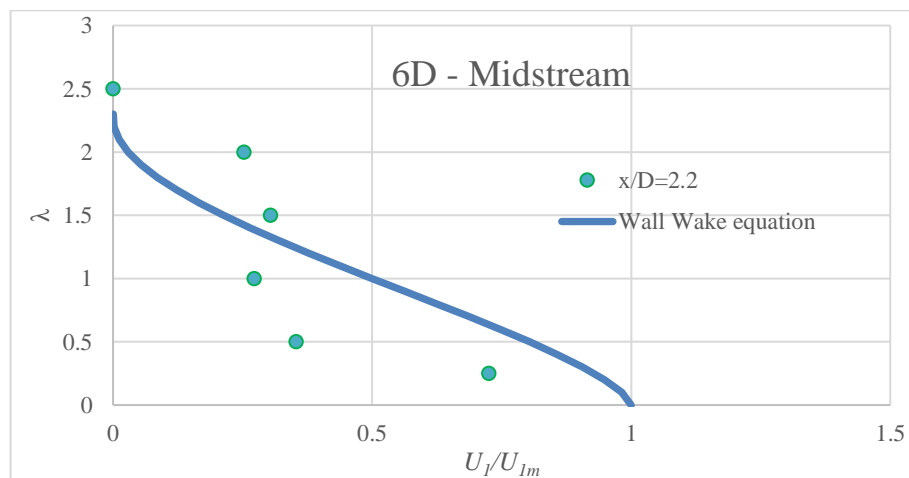


Figure 4.3: Jet-like longitudinal velocity profiles along with POS between two cylinders

4.3 Wall Wake Similarity Profile along the POS in Midstream

An ideal plane or wall wake has a free stream velocity equal to the maximum velocity and very low velocity behind an obstruction. However, for the experiments of this study, there is no possibility of obtaining an ideal wall wake just behind the cylinders along the plane of symmetry due to the absence of free stream velocity which cannot be obtained as the cylinders were not submerged. However, assuming that there is a free stream above the maximum velocity for each profile, wall wake similarity of the profiles below the maximum velocity can be obtained. Therefore, for the 3 cases, the longitudinal velocity profiles below their maximum velocity have been used to investigate their wall wake similarity of Schlichting as described in Chapter 2. The wall wake profile with λ vs $\frac{U_1}{U_{1m}}$ is plotted to investigate the wall wake similarity profiles for each selected stations along the centerline where velocity defect $U_1 = u_e - u$ with u_e = free stream velocity and is assumed to be equal to the maximum velocity for the respective profiles, U_{1m} is the maximum of U and $\lambda = \frac{z}{b_1}$, with b_1 equal to the distance from bed of the location where $U_1 = 0.5 U_{1m}$ following Rajaratnam, et al. [18]. For the experiments in this study, there is no profile that is similar to wall wake in the midstream for the 3D case as there is only near wake zone in this case. But for 6D and 9D spacing, as shown in Figure 4.4, profiles at $\frac{x}{D} = 2.2$ shows slight similarity with wall wake. This happens because the profiles after the near wake zone develops very rapidly within relatively short distance.



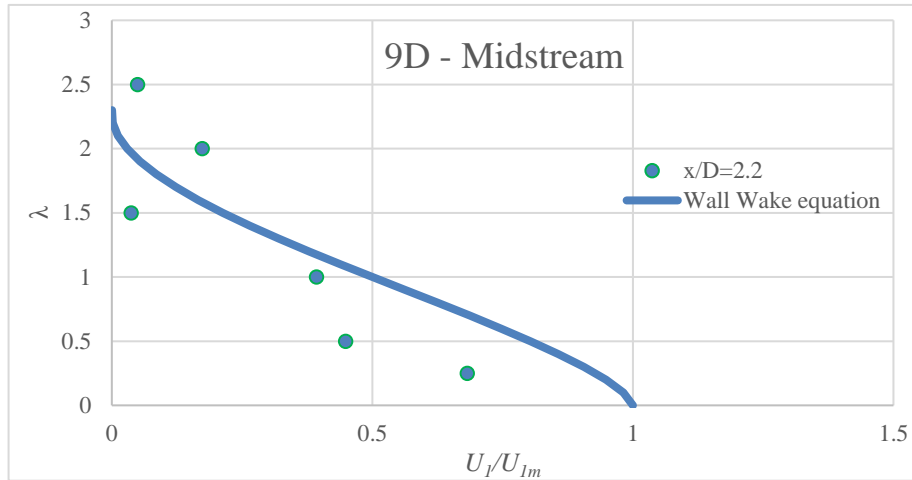


Figure 4.4: Wall wake similarity for longitudinal velocity profiles in midstream

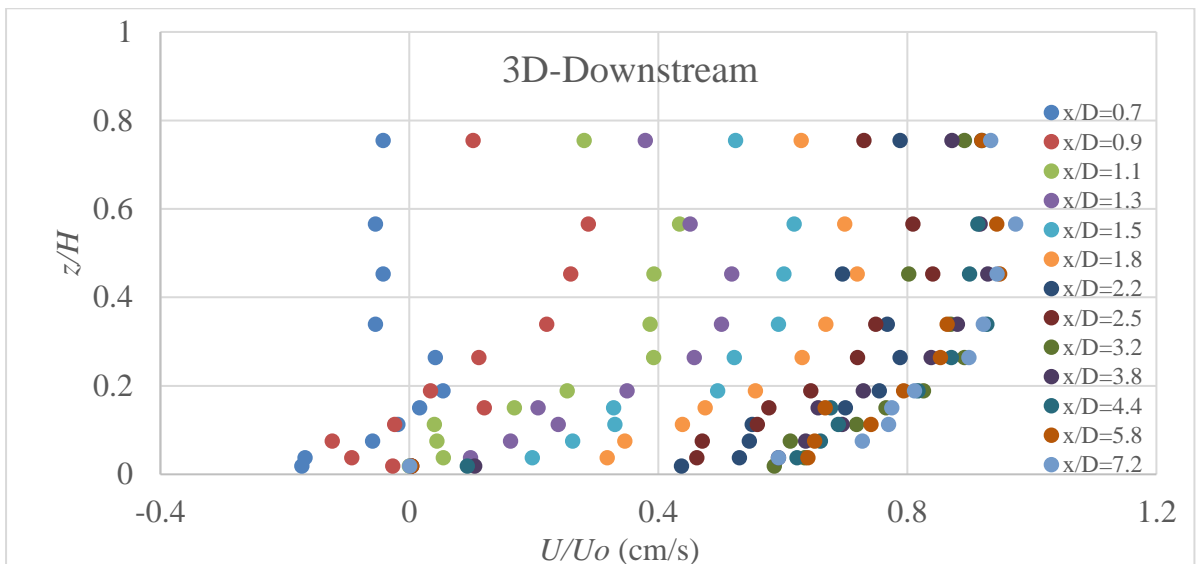
4.4 Normalized Longitudinal Velocity Variation along POS (Down-Stream Section)

To assess the longitudinal variation of mean turbulent flow characteristics at downstream section, point velocity was measured similarly by ADV at different depths of verticals for the selected points along the POS of the flume. The cylinders were placed at 3D, 6D and 9D c/c spacing for three different cases whereas the depth of water and discharge were kept unchanged as similar to the midstream section. Normalized profiles of $\frac{u}{U_0}$ vs $\frac{z}{H}$ at downstream are plotted in Figure 4.5 for 3D, 6D and 9D c/c spacings. The corresponding depth averaged velocity is plotted in Figure 4.6. For downstream analysis, x indicates the longitudinal distance from the center of the downstream pier along the POS. For the 3D c/c spacing, the velocity profiles show that near the bed and near the surface the velocities are negative from $\frac{x}{D}=0.7$ to 0.9. The corresponding depth averaged values of the profiles show that the recirculation zone occupies a small zone near the $\frac{x}{D}=0.7$ at the downstream for 3D c/c spacing.

For the 6D and 9D spacings, the velocity profiles are almost completely negative for $\frac{x}{D}=0.7$ and 0.9. Based on the depth averaged velocity, the recirculation zone is confined up to $\frac{x}{D}=0.9$ as obtained from interpolation. Thereafter, the profiles become positive and there is a rapid increase in velocity between $\frac{x}{D}=1.5$ to 2.5. This

can also be found in terms of depth averaged velocity as shown in Figure 4.6 where the $\frac{u_{da}}{U_o}$ increases from 0.25 at $\frac{x}{D}=1.5$ to 0.60 at $\frac{x}{D}=2.5$ for 6D case and then the rate of increase slows down and the maximum $\frac{u_{da}}{U_o}=0.83$ occurs at $\frac{x}{D}=7.2$. For 9D case, $\frac{u_{da}}{U_o}$ increases from 0.25 at $\frac{x}{D}=1.5$ to 0.55 at $\frac{x}{D}=2.5$ and the rate of increase slows down and reaches a value of $\frac{u_{da}}{U_o}=0.77$ at $\frac{x}{D}=7.2$.

As mentioned earlier, the recirculation near the water surface appears to be stronger than the near bed recirculation in the recirculating near wake zone for the midstream sections. In the near wake of downstream section, the reverse is true, where the recirculation zone near the bottom appears to be stronger. The jet type profiles can be normalized with maximum velocity and z normalized by b , where b is the distance of u_{max} from bed. The normalized profiles are plotted in Figure 4.7. For the 3D spacing, almost all profiles show jet type shape from $\frac{x}{D}=0.7$ to $\frac{x}{D}=3.8$. For the 6D and 9D spacings, profiles of $\frac{x}{D}=1.8$ to 3.8 have been plotted which shows that all the profiles are jet type. Additionally, all of these profiles for 6D and 9D spacings show self-similarity such that they will fall close to the same curve for respective case.



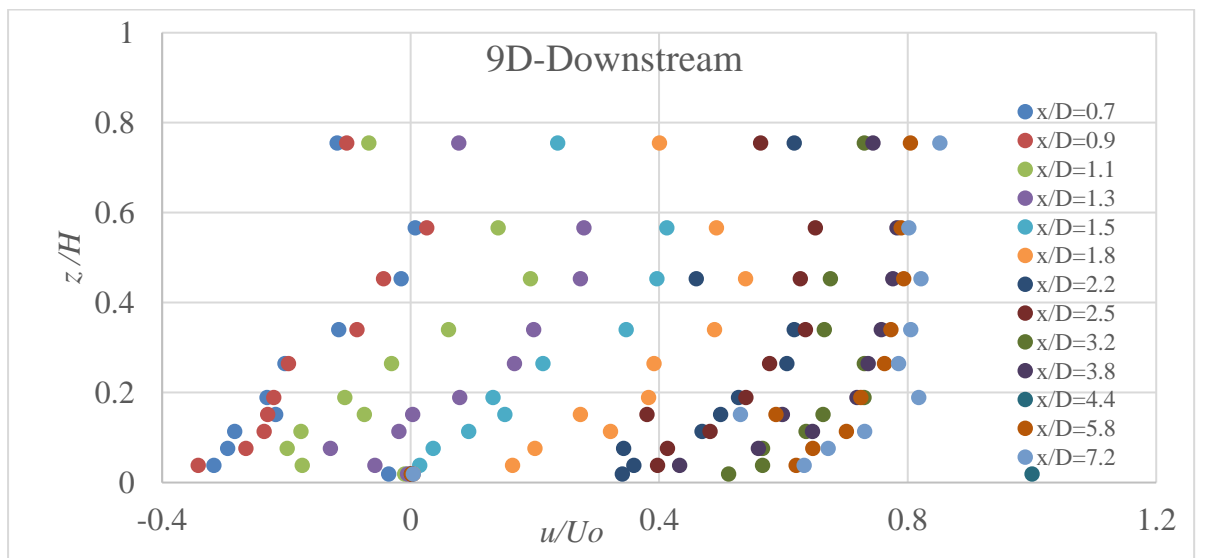
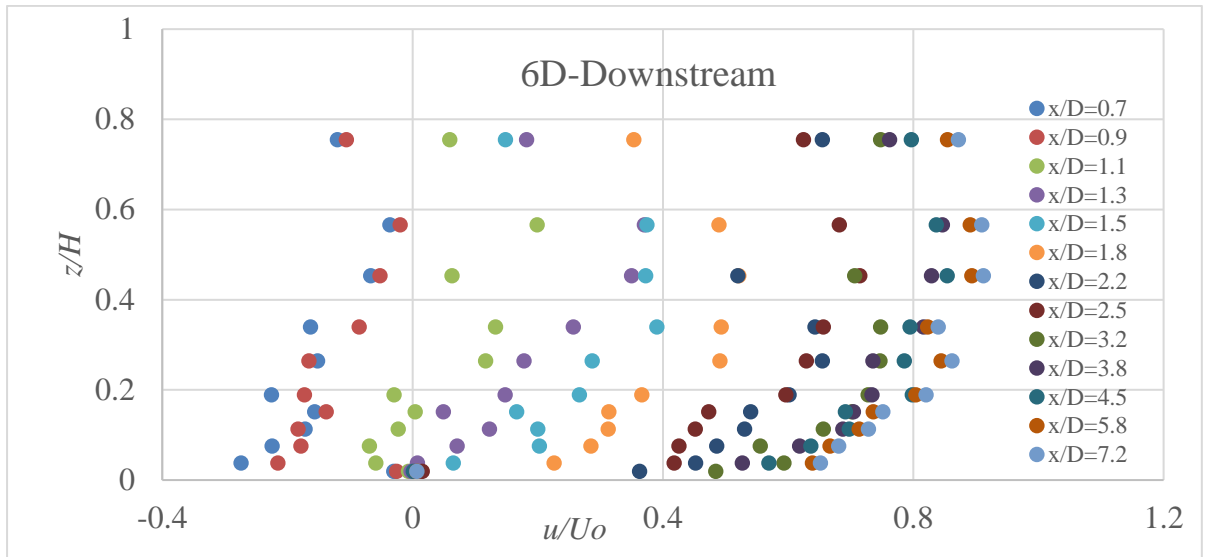


Figure 4.5: Normalized Longitudinal Velocity Profiles along plane of symmetry at downstream

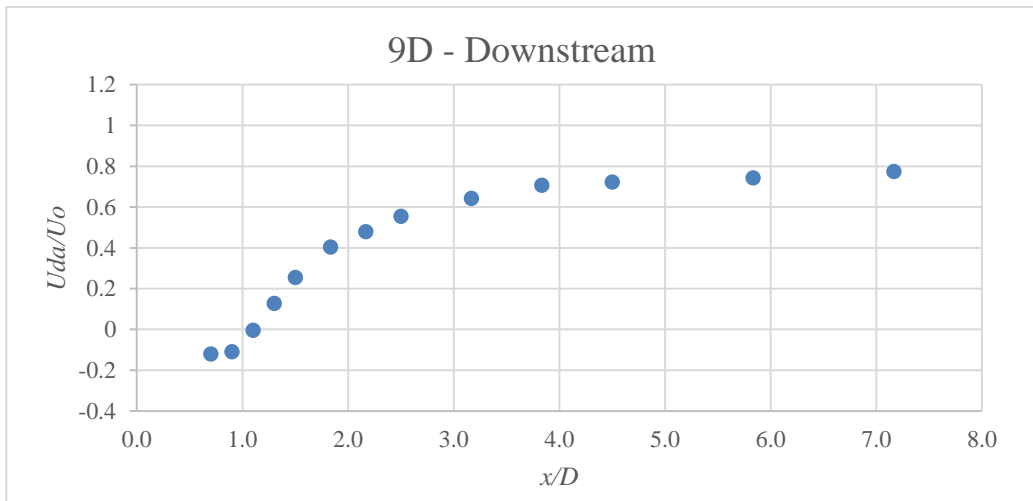
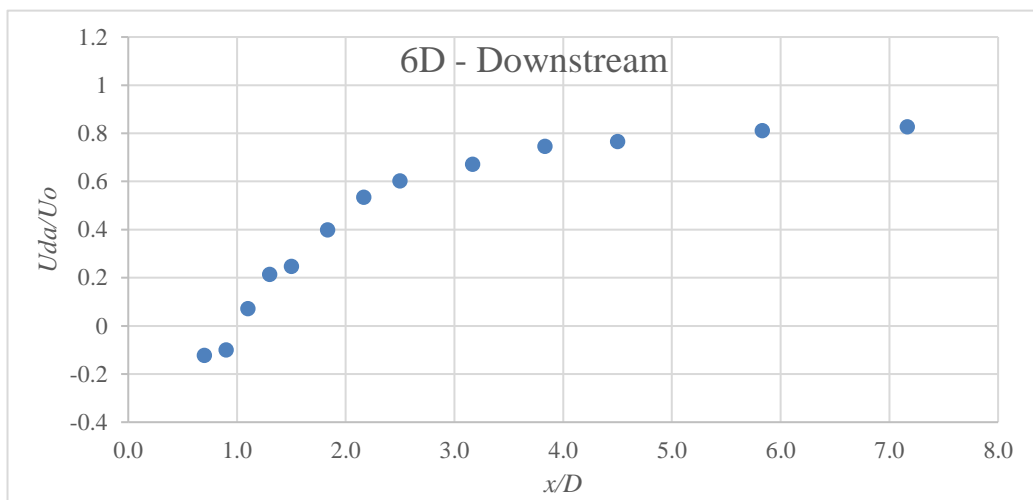
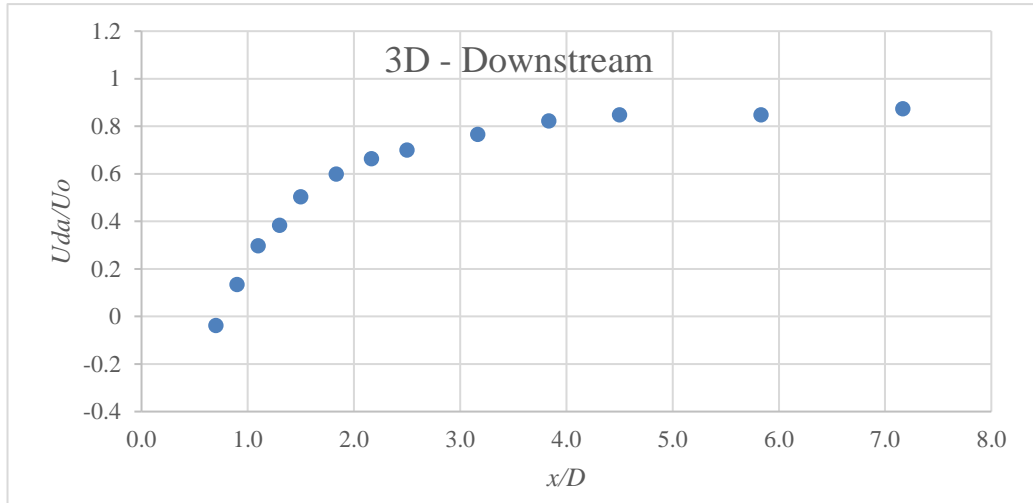


Figure 4.6: Normalized Longitudinal Depth-Averaged Velocity along a plane of symmetry at downstream

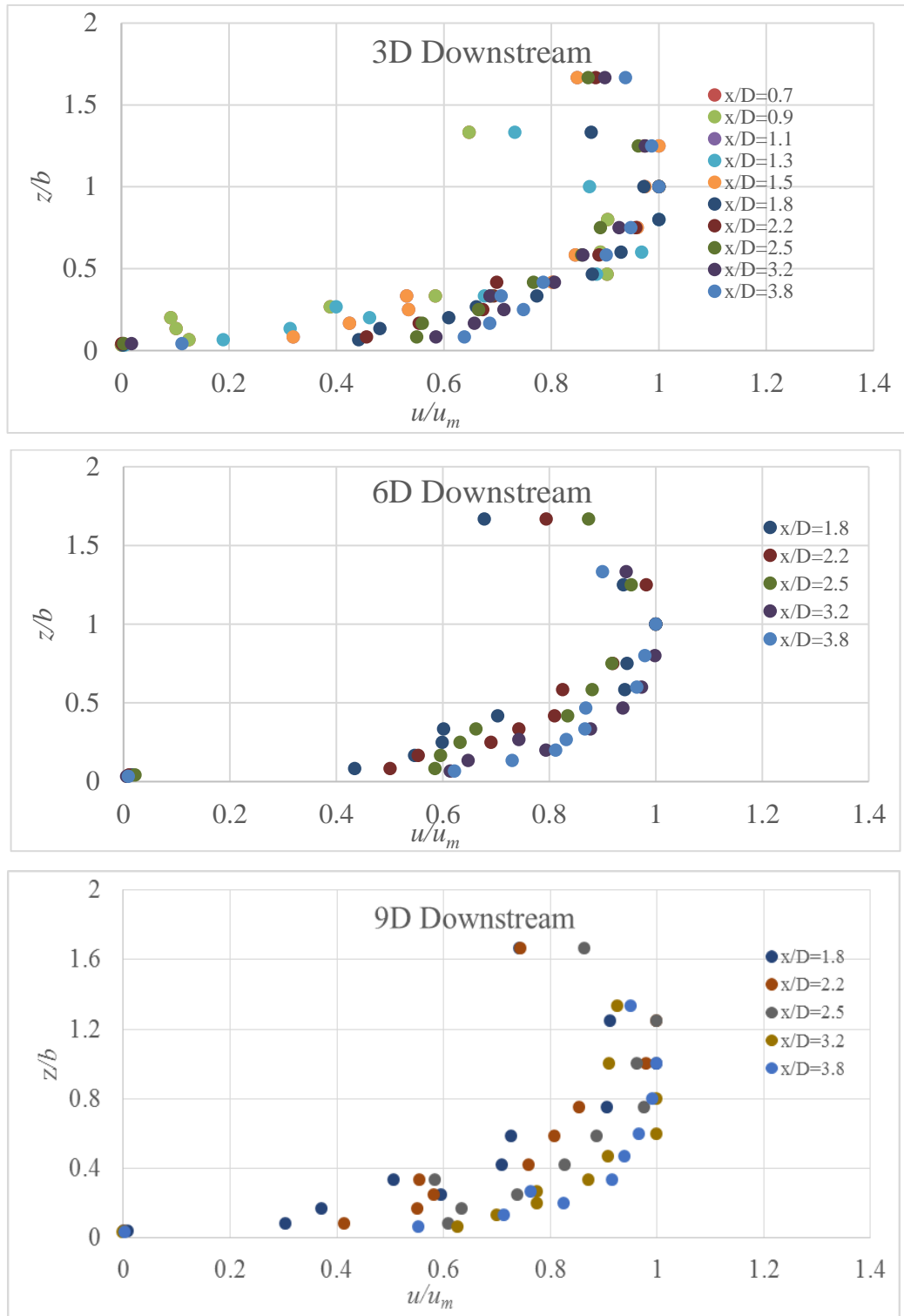
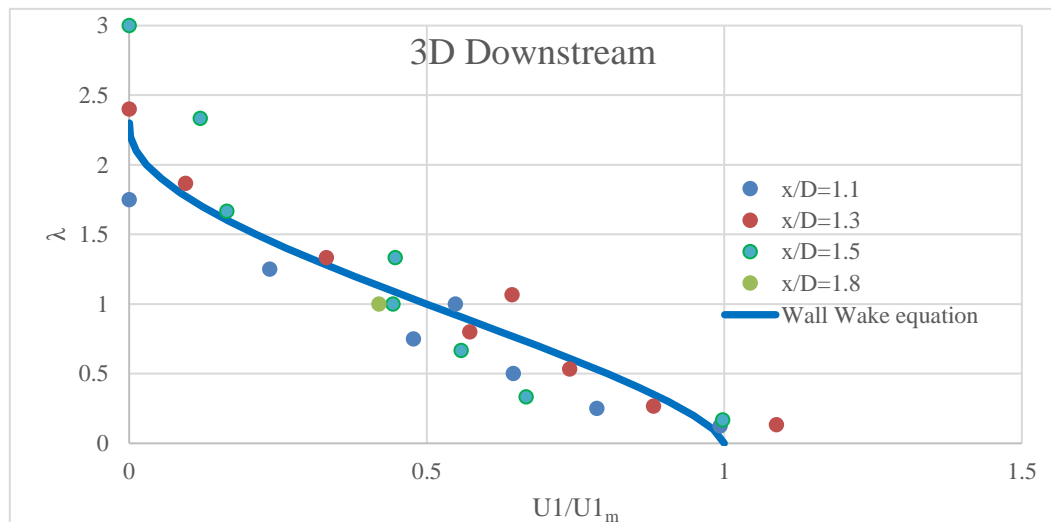


Figure 4.7: Jet-like longitudinal velocity profiles along with POS at downstream

4.5 Wall Wake Similarity Profile along the POS in Downstream

As stated earlier, for the sake of this experimental study, a free stream above the maximum velocity for each profile has been assumed so that wall wake similarity of the profiles below the maximum velocity can be obtained. Therefore, for the 3 cases, the longitudinal velocity profiles below their maximum velocity have been used to investigate their wall wake similarity of Schlichting as described in Chapter 2. The wall wake profile with λ vs $\frac{U_1}{U_{1m}}$ is plotted to investigate the wall wake similarity profiles for each selected stations along the centerline where velocity defect $U_1 = u_e - u$ with u_e = free stream velocity and is assumed to be equal to the maximum velocity for the respective profiles, U_{1m} is the maximum of U and $\lambda = \frac{z}{b_1}$, with b_1 equal to the distance from bed of the location where $U_1 = 0.5 U_{1m}$ following Rajaratnam, et al. [18]. For the experiments in this study, there are 4 profiles that are similar to wall wake in the downstream for the 3D case at $\frac{x}{D} = 1.1, 1.3, 1.5$ and 1.8 . However, for 6D spacing, velocity profile at $\frac{x}{D} = 1.3, 1.5$ and 1.8 show similarities with wall wake whereas, velocity profiles at $\frac{x}{D} = 1.3$ and 1.5 are closely congruent with wall wake profile and for 9D spacing similarities observed for $\frac{x}{D} = 1.5$ and 1.8 shown in Figure 4.8.



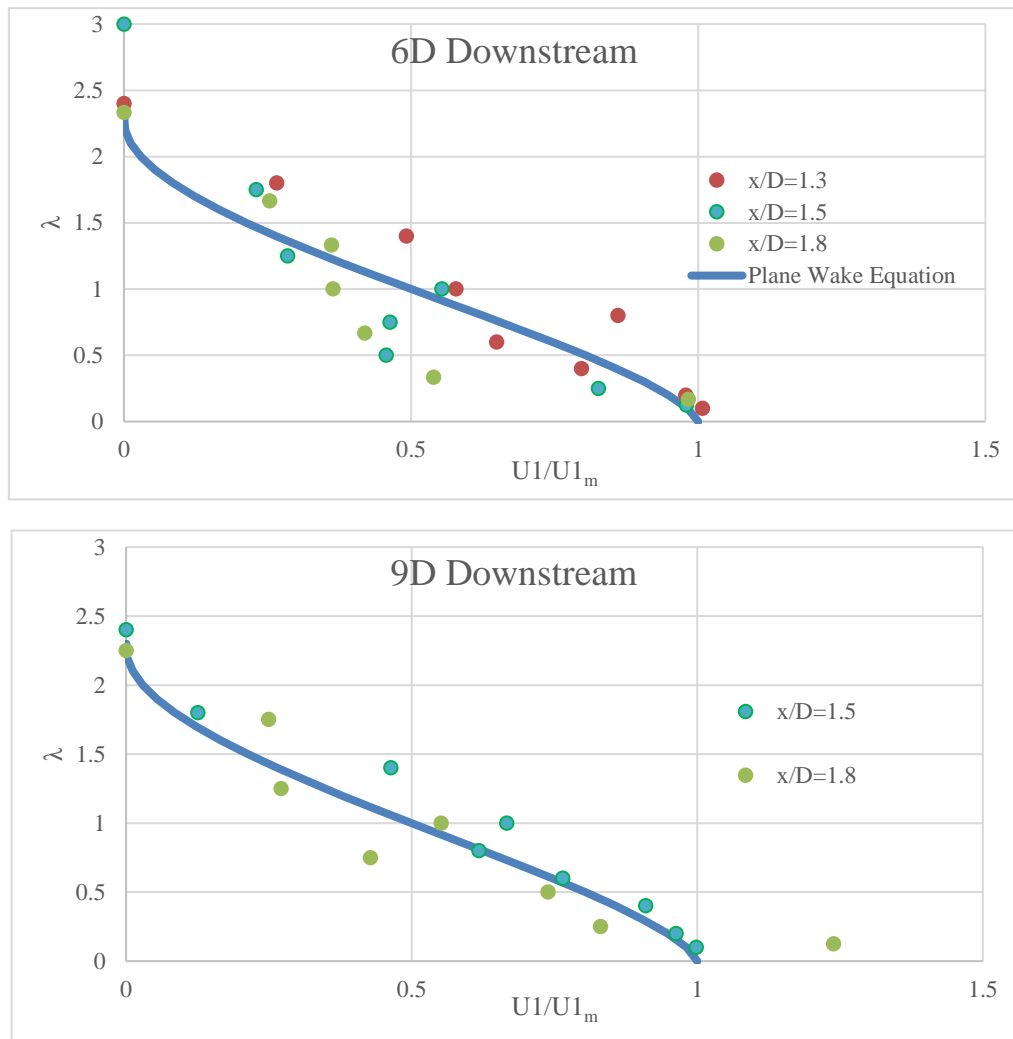


Figure 4.8: Wall wake similarity for longitudinal velocity profiles at downstream

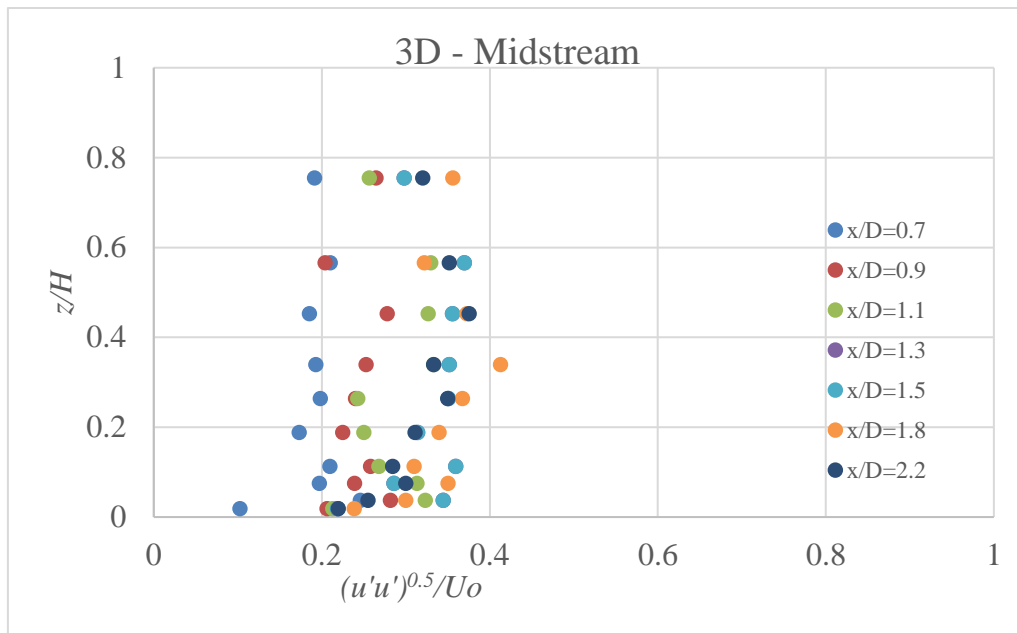
4.6 Turbulence Parameters at Mid-stream

Turbulent intensity in longitudinal, transverse and vertical direction is investigated for different spacing for mid-stream. Additionally, the variations of profile for specified sections are plotted to understand the behavior of turbulent flow around the cylinders.

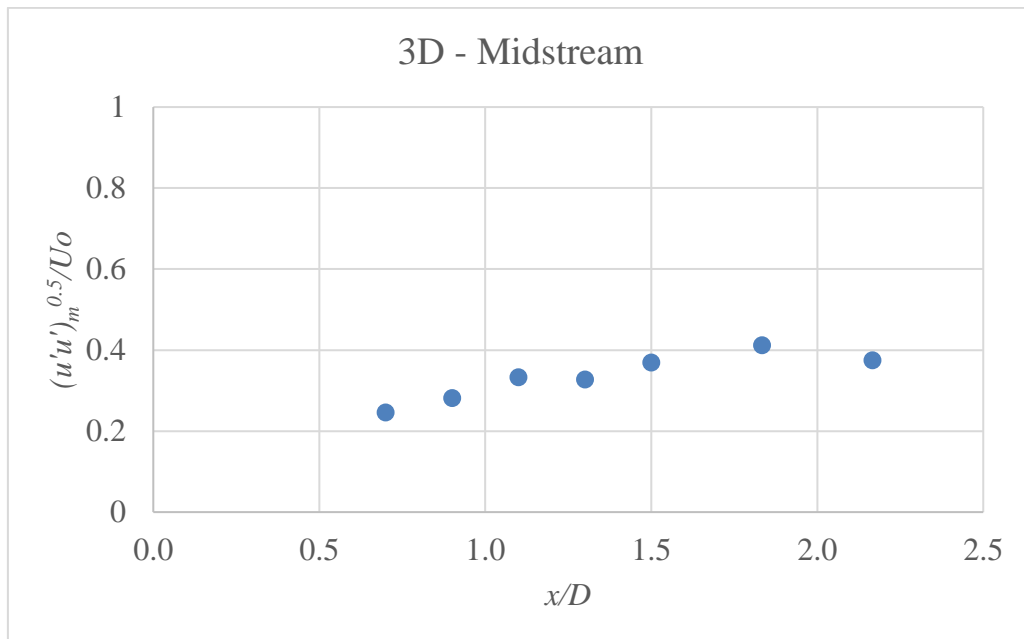
4.6.1 Turbulent intensity at mid-stream of 3D c/c spacing

Analysis shows in Figure 4.9(a) that the turbulent intensity increases as the flow progresses and maximum normalized intensity has been observed at $\frac{x}{D}=1.8$ for

$\frac{z}{H}=0.34$ which is equal to 0.41. The profiles are apparently logarithmic at maximum number of sections. Figure 4.9(b) shows a mapping for maximum values of normalized longitudinal turbulent intensities at different longitudinal distances. It shows a gradual increase of about 67% as the longitudinal distance is increased from $\frac{x}{D}=0.7$ to $\frac{x}{D}=1.8$. After that, the turbulent intensity decreases again due to the presence of recirculation before the second pier.



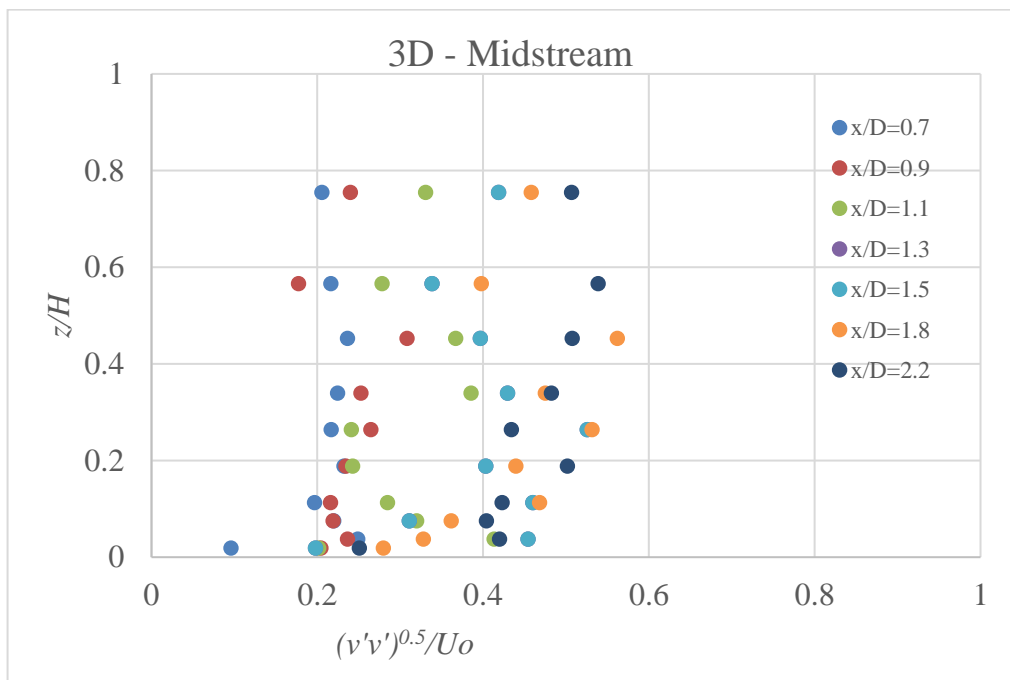
(a)



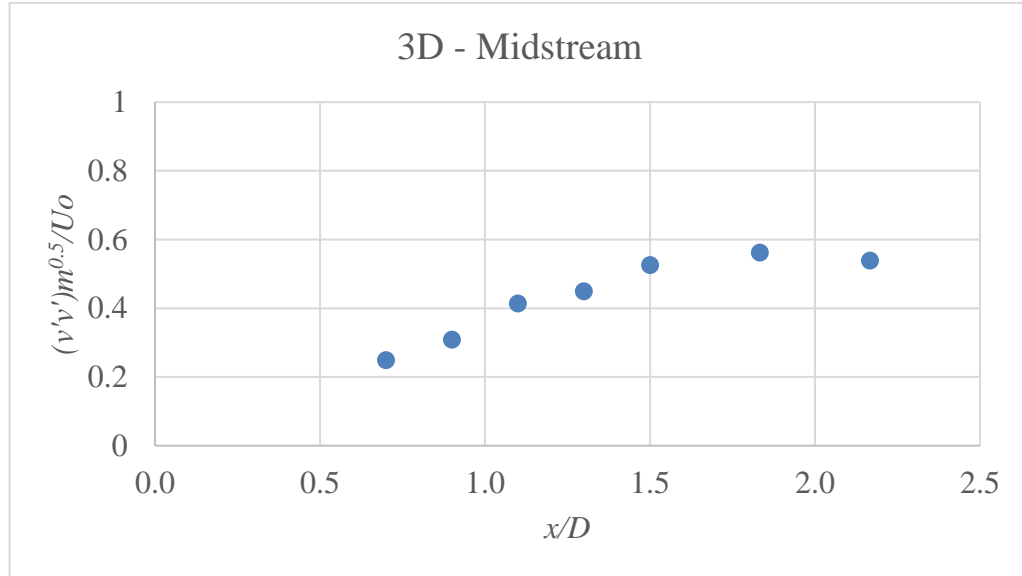
(b)

Figure 4.9: (a) Variation of Normalized Turbulent Intensity Profile (b) Variation of Maximum Turbulent Intensity in longitudinal direction along plane of symmetry between two cylinders (3D)

Figure 4.10(a) shows turbulent intensity profiles at transverse direction for 3D c/c spacing at between two cylinders. Analysis of this plot shows that the turbulent intensity increases as the flow progresses and maximum normalized intensity has been observed at $\frac{x}{D}=1.8$ which is equal to 0.56. So, it has been observed the turbulent intensity is higher at transverse direction compared to longitudinal direction. Figure 4.10(b) shows a mapping for maximum values of normalized longitudinal turbulent intensities at different longitudinal distances. It shows a gradual increase of about 116% as the longitudinal distance is increased from $\frac{x}{D}=0.7$ to $\frac{x}{D}=1.8$. After that, the turbulent intensity decreases again due to the presence of recirculation before the second pier as shown in the study of turbulent intensity at longitudinal direction.



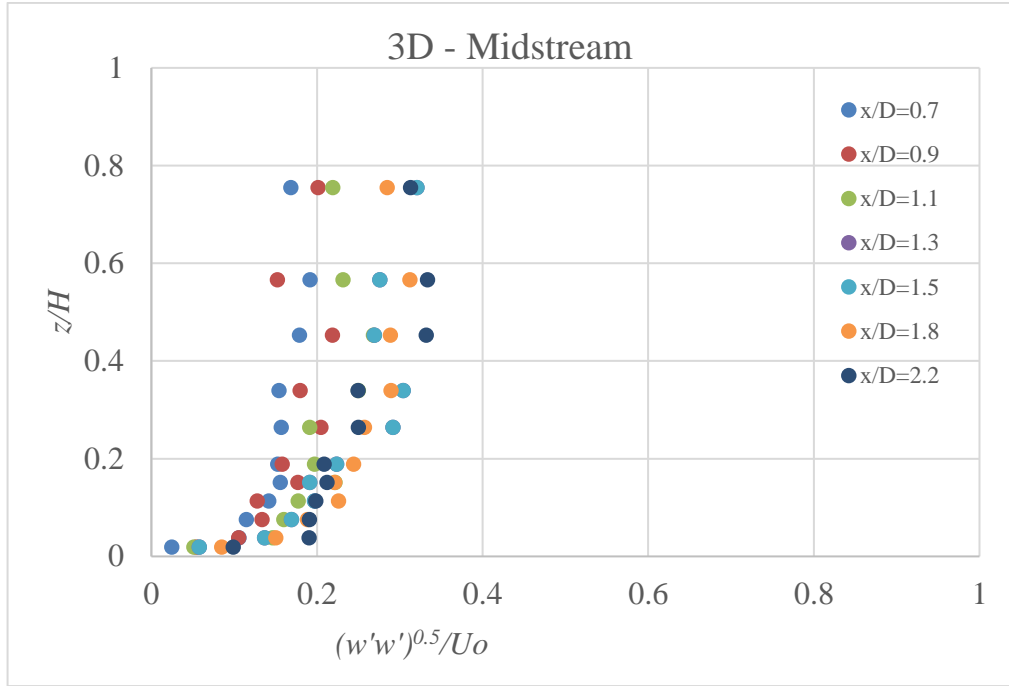
(a)



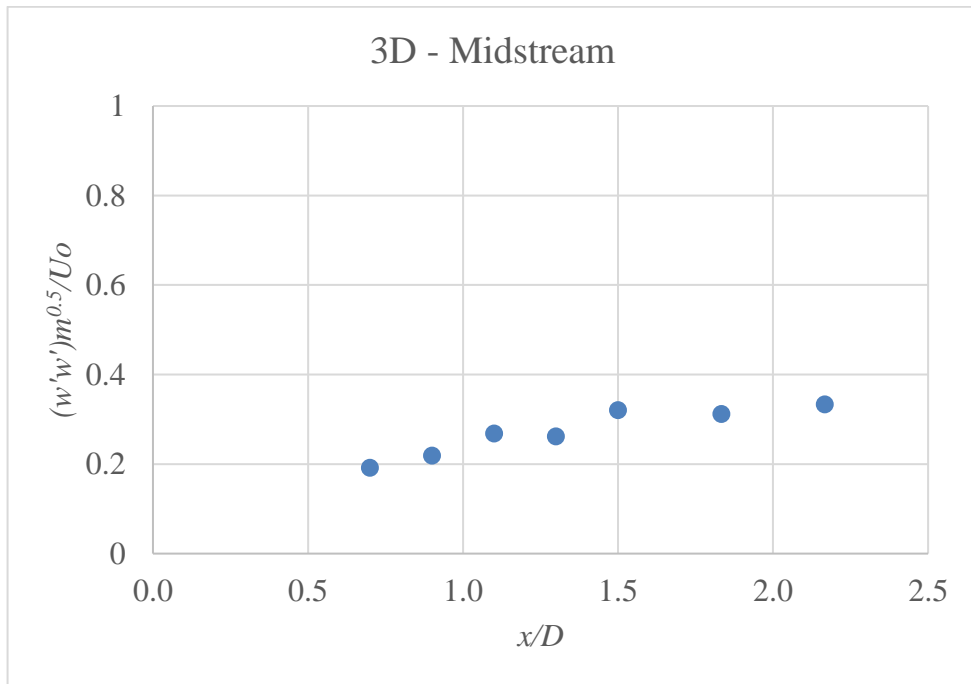
(b)

Figure 4.10: (a) Variation of Normalized Turbulent Intensity Profile (b) Variation of Maximum Turbulent Intensity in transverse direction along plane of symmetry between two cylinders (3D)

Figure 4.11(a) shows turbulent intensity profiles at vertical direction for 3D c/c spacing. Analysis of this plot shows that the turbulent intensity increases as the flow progresses and maximum normalized intensity has been observed at $\frac{x}{D}=2.2$ for $\frac{z}{H}=0.45$ which is equal to 0.33. So, it has been observed that the turbulent intensity is the smallest at the vertical direction. However, Logarithmic profiles are visible at the higher longitudinal distances. Figure 4.11(b) shows a mapping for maximum values of normalized longitudinal turbulent intensities at different longitudinal distances. It shows a gradual increase of about 74% as the longitudinal distance is increased from $\frac{x}{D}=0.7$ to $\frac{x}{D}=2.2$. Turbulent intensity at vertical direction has been observed to increase with a slight fall at $\frac{x}{D}=1.8$. However, the maximum turbulent intensity kept an apparent constant value from $\frac{x}{D}=1.5$ to $\frac{x}{D}=2.2$.



(a)

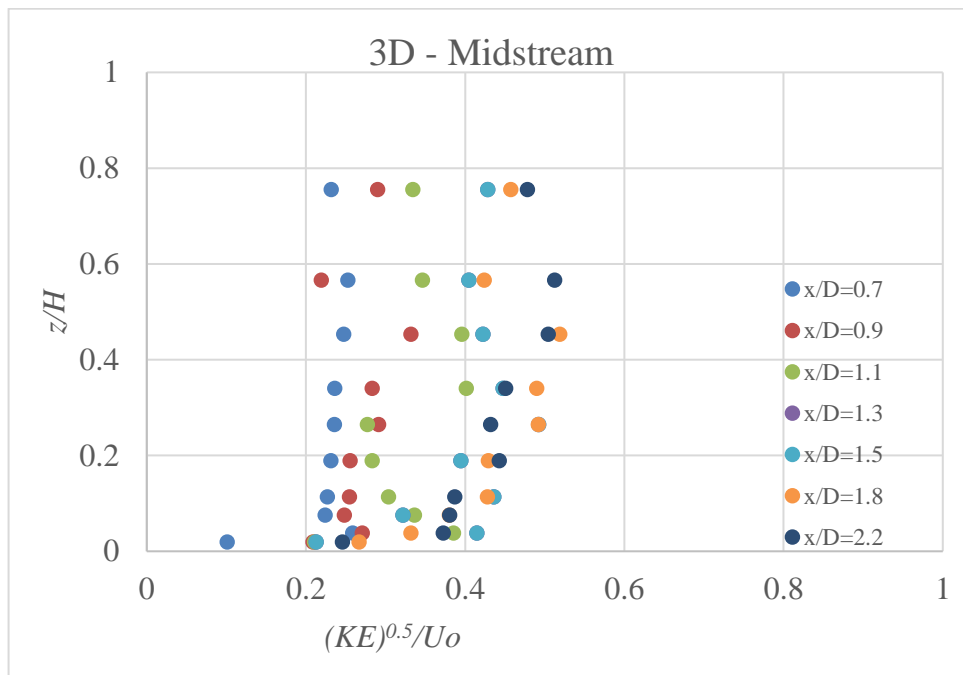


(b)

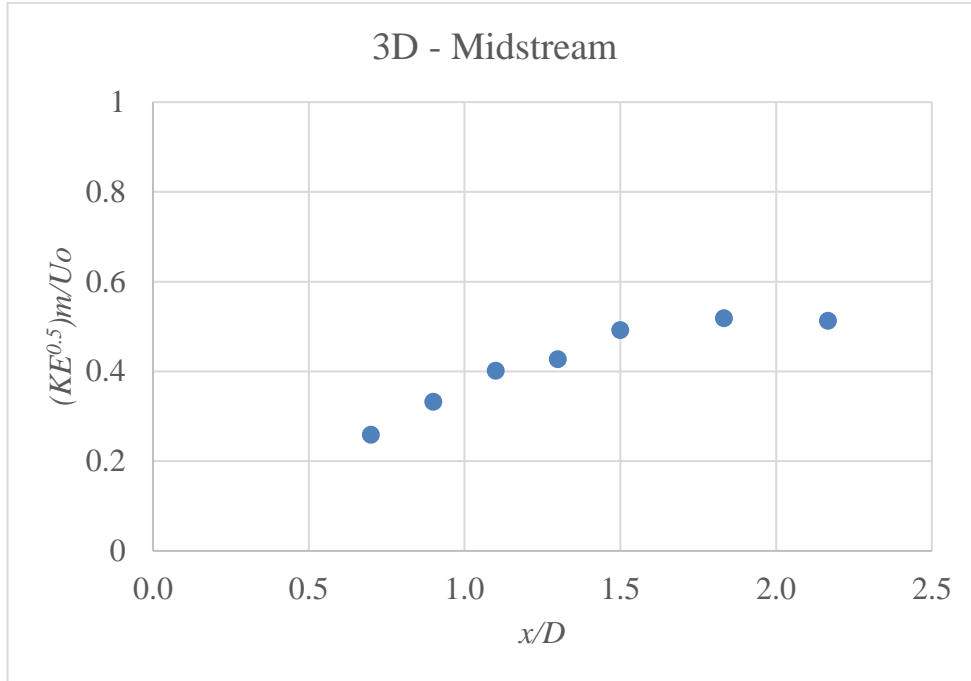
Figure 4.11: (a) Variation of Normalized Turbulent Intensity Profile (b) Variation of Maximum Turbulent Intensity in vertical direction along plane of symmetry between two cylinders (3D)

4.6.2 Kinetic Energy at mid-stream of 3D c/c spacing

Figure 4.12(a) shows kinetic energy profiles at different vertical depths for 3D c/c spacing. Analysis reveals that the kinetic energy also keeps on increasing as the flow progresses as similar to the turbulent intensities. Additionally, maximum normalized kinetic energy has been observed at $\frac{x}{D}=1.8$ for $\frac{z}{H}=0.45$ which is equal to 0.50. Figure 4.12(b) shows a mapping for maximum values of normalized kinetic energy at different longitudinal distances. It shows a gradual increase of about 96% as the longitudinal distance is increased from $\frac{x}{D}=0.7$ to $\frac{x}{D}=1.8$. After that, the kinetic energy decreases only about 0.8% as the flow progresses from $\frac{x}{D}=1.8$ to $\frac{x}{D}=2.2$. Cause of the reduction can be predicted as the presence of recirculation zone before the second pier.



(a)

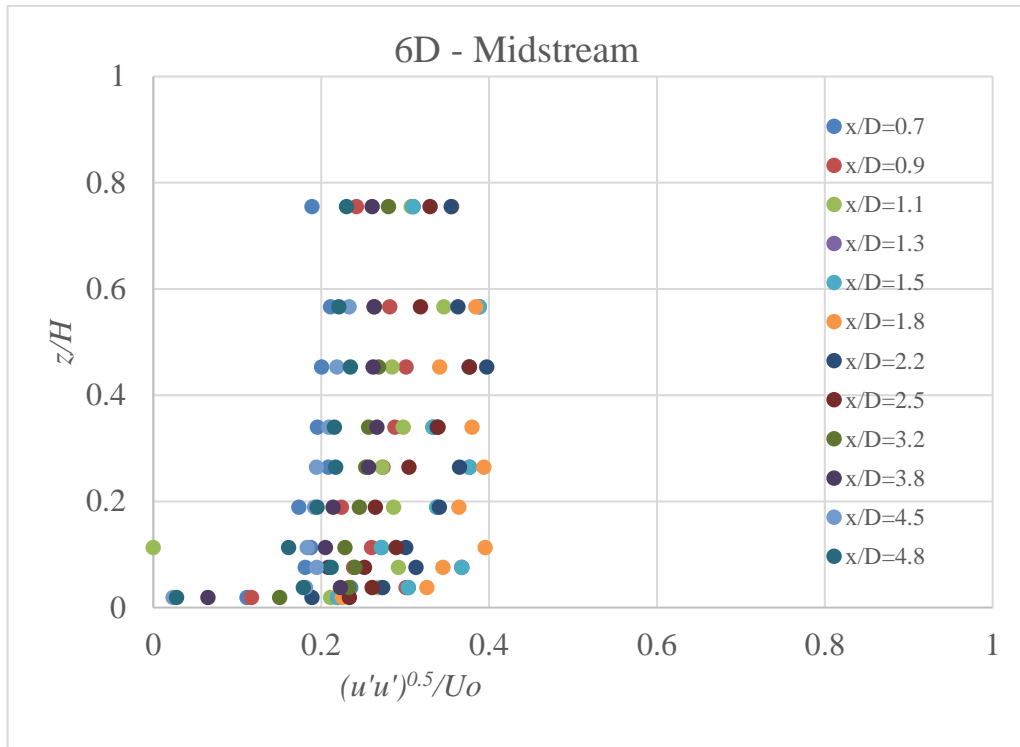


(b)

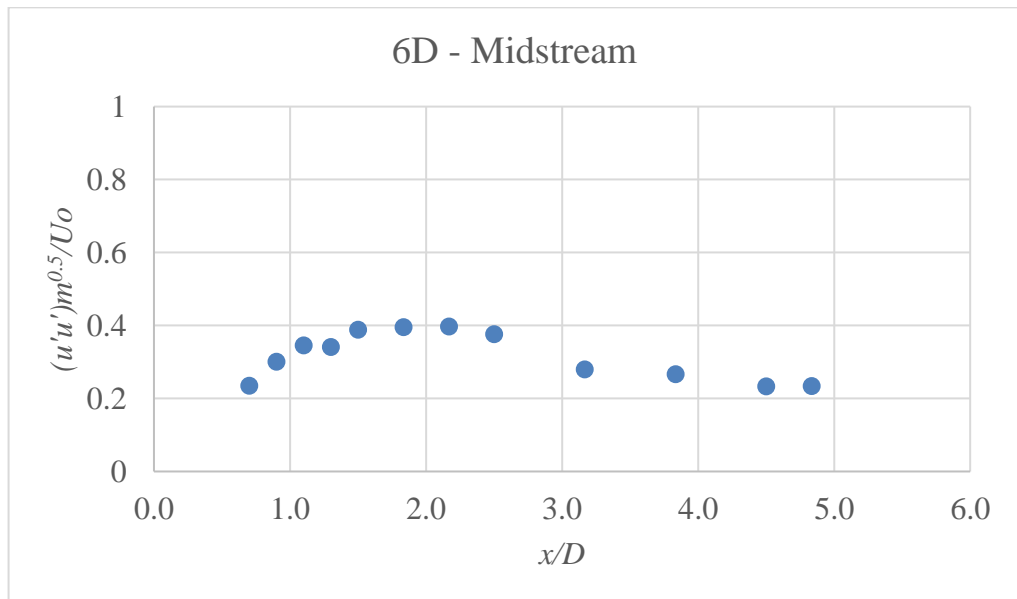
Figure 4.12: (a) Variation of Normalized Kinetic Energy Profile (b) Variation of Maximum Kinetic Energy in vertical direction along plane of symmetry between two cylinders (3D)

4.6.3 Turbulent intensity at mid-stream of 6D c/c spacing

Figure 4.13(a) shows turbulent intensity profiles at longitudinal direction for 6D c/c spacing. From the analysis it is observed that turbulent intensity increases initially as the flow progresses and maximum normalized intensity has been observed at $\frac{x}{D} = 2.2$ for $\frac{z}{H} = 0.45$ which is equal to 0.40. Almost each profile is logarithmic compared to the 3D c/c spacing case study where some of the sections have not showed logarithmic profiles. So, it can be said that flow gets more space to form fully logarithmic profiles. Figure 4.13(b) shows a mapping for maximum values of normalized longitudinal turbulent intensities at different longitudinal distances. It shows a gradual increase of about 67% as the longitudinal distance is increased from $\frac{x}{D} = 0.7$ to $\frac{x}{D} = 2.2$. After that, the turbulent intensity decreases about 43% from $\frac{x}{D} = 2.2$ to $\frac{x}{D} = 4.8$.



(a)

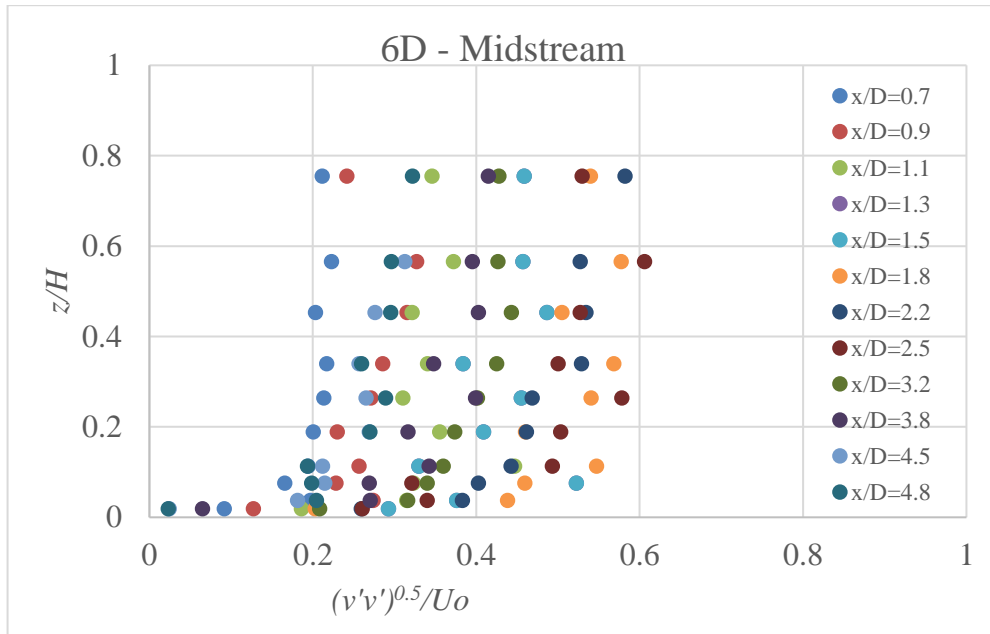


(b)

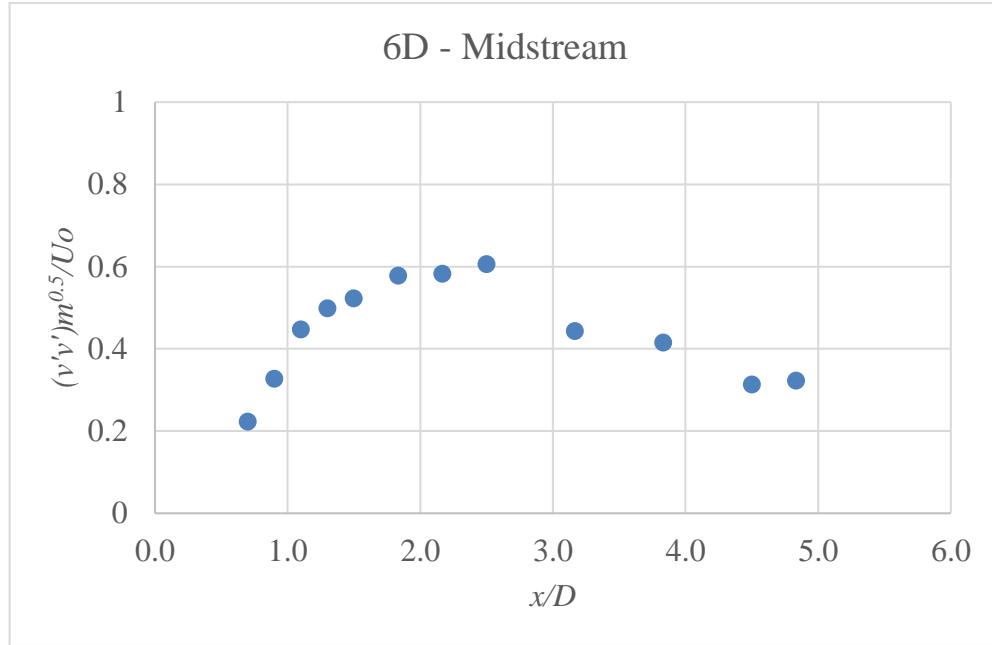
Figure 4.13: (a) Variation of Normalized Turbulent Intensity Profile (b) Variation of Maximum Turbulent Intensity in longitudinal direction along plane of symmetry between two cylinders (6D)

Figure 4.14(a) compares between turbulent intensity profiles at transverse direction for 6D c/c spacing. It is observed that at $\frac{x}{D}=2.5$ for $\frac{z}{H}=0.57$ which is equal to

0.61. So, it has been observed that the turbulent intensity is higher at transverse direction compared to longitudinal direction similar to 3D case study. Profiles are found logarithmic similar to the longitudinal direction at 6D c/c spacing. From Figure 4.14(b) it is observed that a gradual increase of about 177% as the longitudinal distance is increased from $\frac{x}{D}=0.7$ to $\frac{x}{D}=2.5$. After that, the turbulent intensity decreases about 47% from $\frac{x}{D}=2.5$ to $\frac{x}{D}=4.8$.



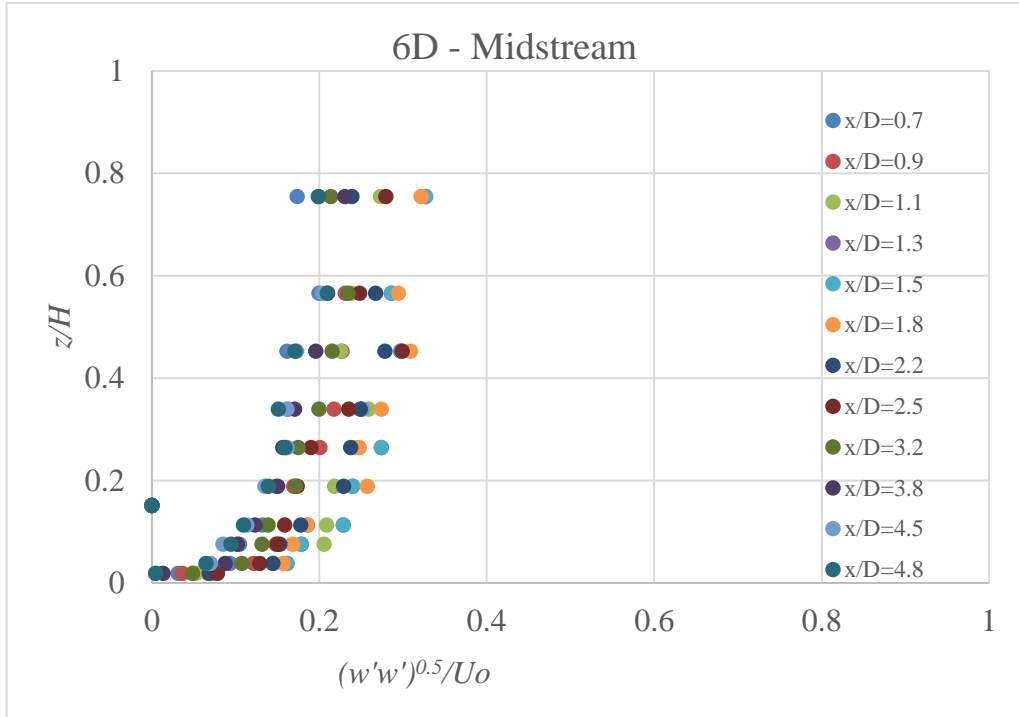
(a)



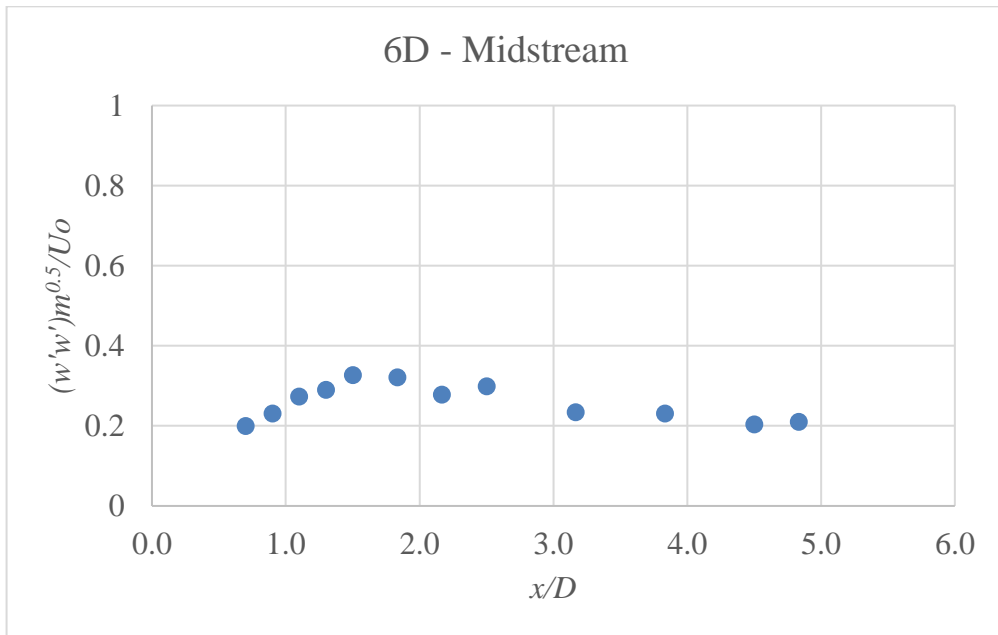
(b)

Figure 4.14: (a) Variation of Normalized Turbulent Intensity Profile (b) Variation of Maximum Turbulent Intensity in transverse direction along plane of symmetry between two cylinders (6D)

Figure 4.15(a) shows turbulent intensity profiles at vertical direction for 6D c/c spacing. Results reveal that the turbulent intensity increases initially as the flow progresses similar as found along both longitudinal and vertical directions and maximum normalized intensity has been observed at $\frac{x}{D}=1.5$ for $\frac{z}{H}=0.75$ which is equal to 0.33. So, it has been observed the turbulent intensity is the smallest at the vertical direction as found earlier in 3D case study and similarly profiles are logarithmic in this case. Figure 4.15(b) shows that an increment of about 65% as the longitudinal distance is increased from $\frac{x}{D}=0.7$ to $\frac{x}{D}=1.5$. After that, the turbulent intensity decreases about 34% from $\frac{x}{D}=1.5$ to $\frac{x}{D}=4.8$.



(a)

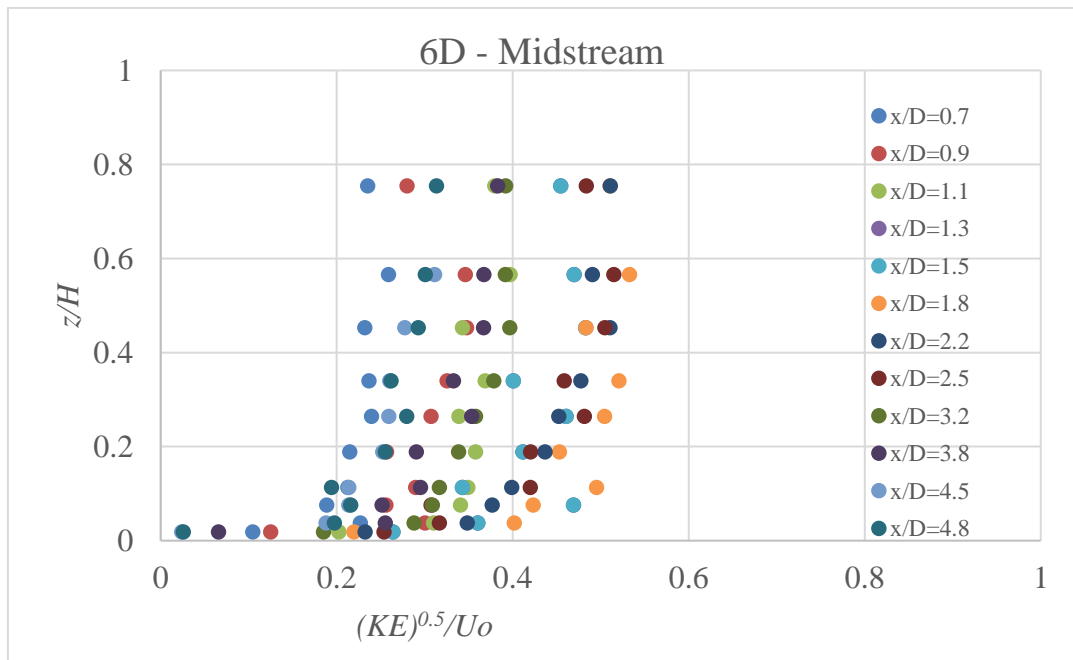


(b)

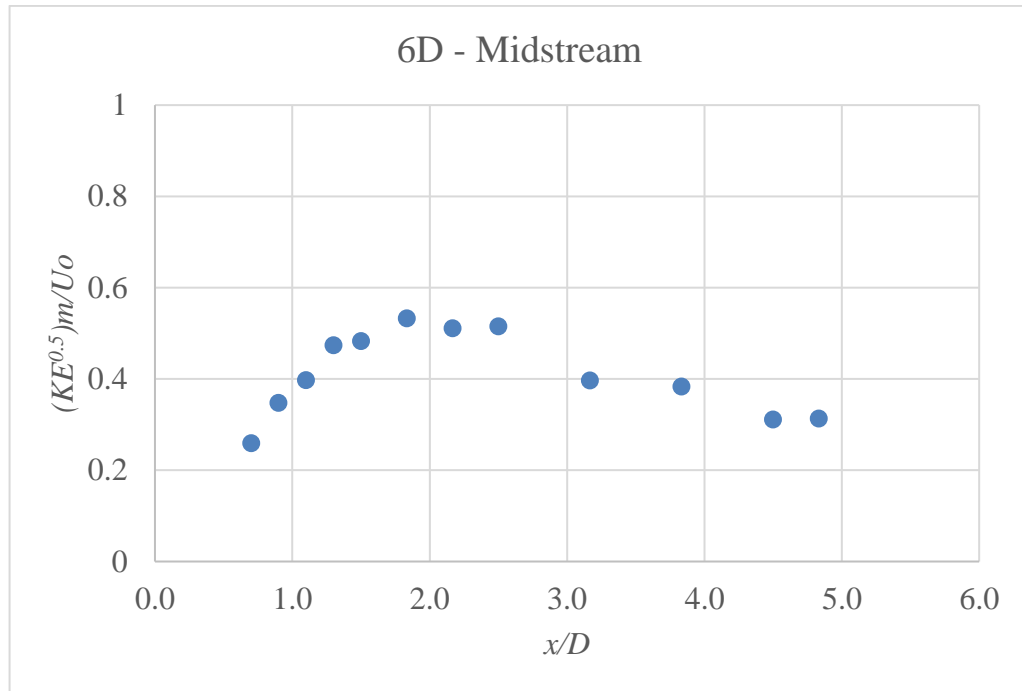
Figure 4.15: (a) Variation of Normalized Turbulent Intensity Profile (b) Variation of Maximum Turbulent Intensity in vertical direction along plane of symmetry between two cylinders (6D)

4.6.4 Kinetic Energy at mid-stream of 6D c/c spacing

Figure 4.16(a) compares between kinetic energy profiles at different vertical depths for 6D c/c spacing. Analysis shows that the kinetic energy also keeps on increasing initially as the flow progresses as similar to the turbulent intensities. Additionally, maximum normalized kinetic energy has been observed at $\frac{x}{D}=1.8$ for $\frac{z}{H}=0.57$ which is equal to 0.53. Similar to turbulent intensity profiles, kinetic energy profiles show logarithmic profile too at each longitudinal distance. Figure 4.16(b) shows a mapping for maximum values of normalized kinetic energy at different longitudinal distances. Similarly, like other cases it shows a gradual increase of 104% as the longitudinal distance is increased from $\frac{x}{D}=0.7$ to $\frac{x}{D}=1.8$. After that, the turbulent intensity decreases about 43% as the flow progresses from $\frac{x}{D}=1.8$ to $\frac{x}{D}=4.8$. However, the reduction is significantly higher compared to 3D case.



(a)

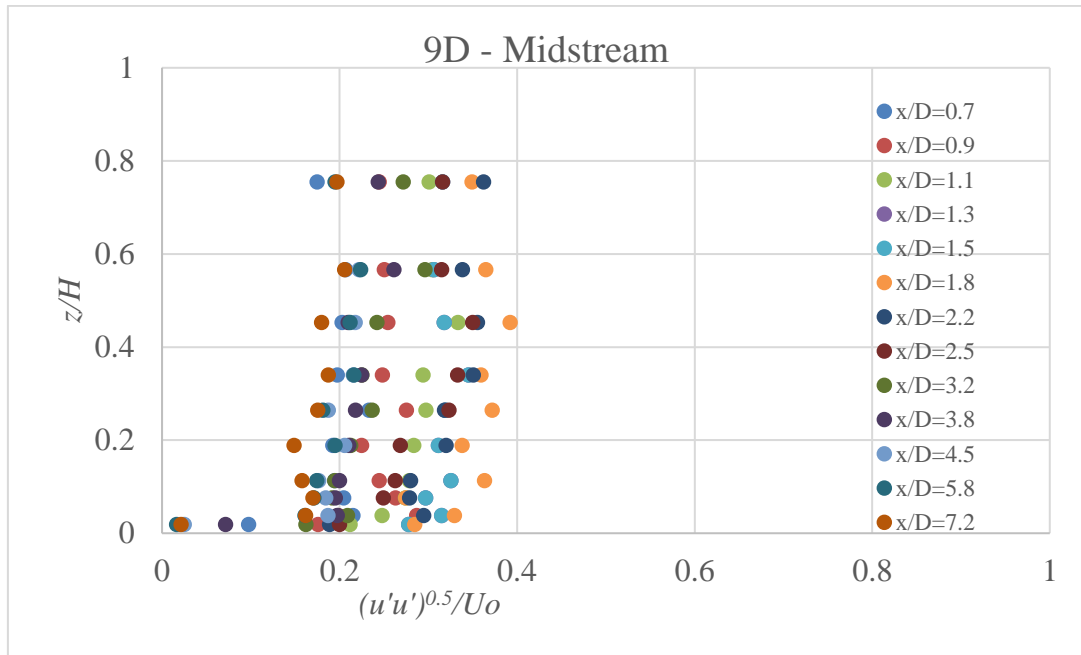


(b)

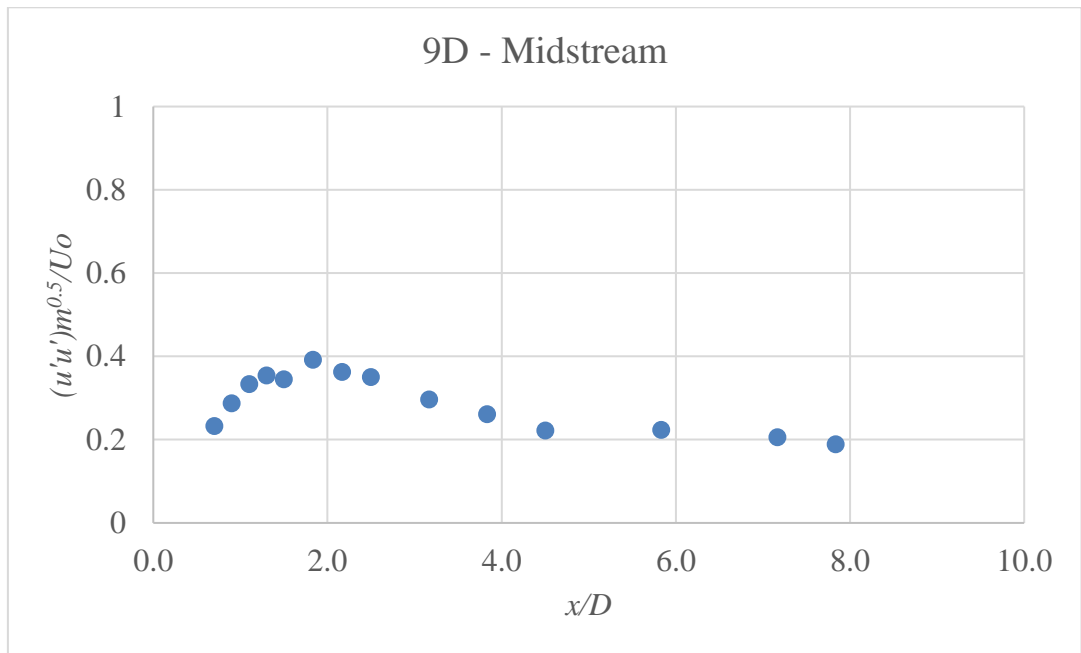
Figure 4.16: (a) Variation of Normalized Kinetic Energy Profile (b) Variation of Maximum Kinetic Energy in vertical direction along plane of symmetry between two cylinders (6D)

4.6.5 Turbulent intensity at mid-stream of 9D c/c spacing

Figure 4.17(a) shows turbulent intensity profiles at longitudinal direction for 9D c/c spacing. Analysis of this plot shows that the turbulent intensity increases initially as the flow progresses as similar to 6D c/c spacing and maximum normalized intensity has been observed at $\frac{x}{D}=1.8$ for $\frac{z}{H}=0.46$ which is equal to 0.40. Profiles at all of the longitudinal distances are logarithmic as similar to 6D c/c spacing. Figure 4.17(b) shows a mapping for maximum values of normalized longitudinal turbulent intensities at different longitudinal distances. It shows a gradual increase of about 74% as the longitudinal distance is increased from $\frac{x}{D}=0.7$ to $\frac{x}{D}=1.8$. After that, the turbulent intensity decreases about 53% from $\frac{x}{D}=1.8$ to $\frac{x}{D}=7.8$.



(a)

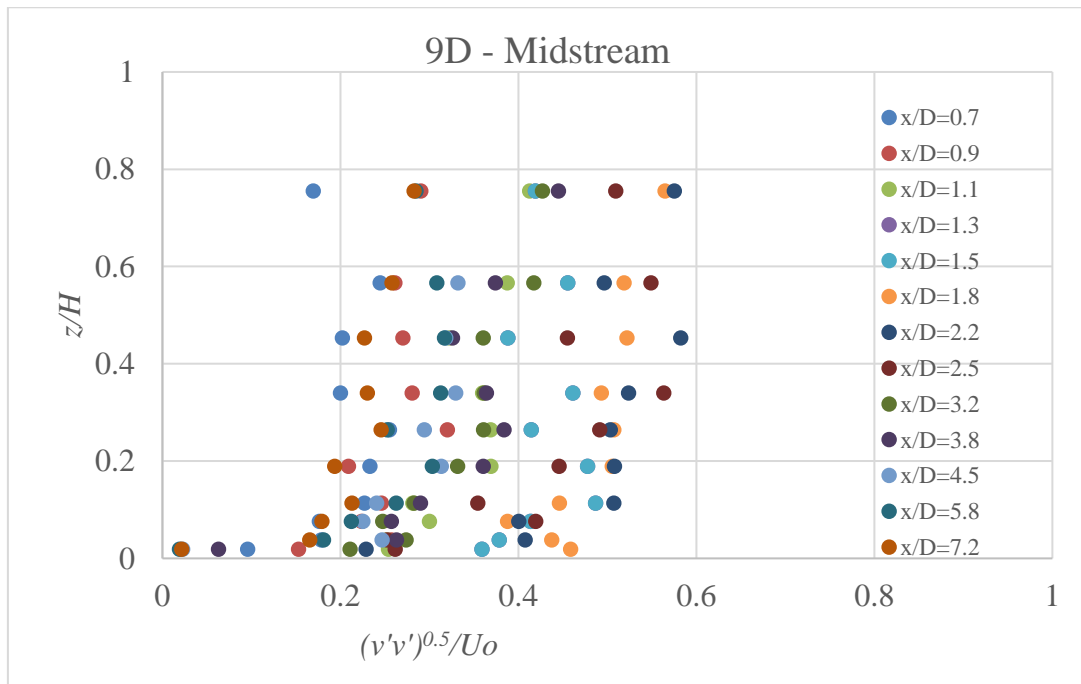


(b)

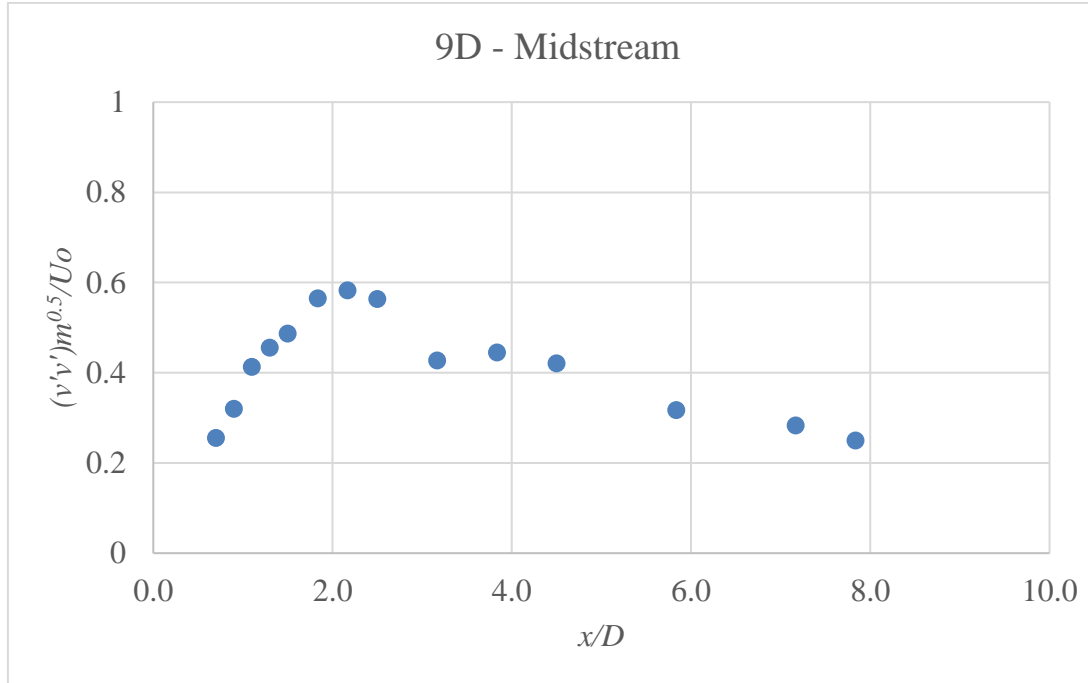
Figure 4.17: (a) Variation of Normalized Turbulent Intensity Profile (b) Variation of Maximum Turbulent Intensity in longitudinal direction along plane of symmetry between two cylinders (9D)

Turbulent intensity profiles at transverse direction for 9D c/c spacing is investigated shown in Figure 4.18(a). Analysis of this plot shows that the turbulent

intensity increases initially as the flow progresses similar along longitudinal direction as similar to 6D c/c spacing and maximum normalized intensity has been observed at $\frac{x}{D}=2.2$ for $\frac{z}{H}=0.45$ which equals to 0.58. So, it has been observed that the turbulent intensity is higher at transverse direction compared to longitudinal direction similar to 3D and 6D case studies. Figure 4.14(b) shows a mapping for maximum values of normalized longitudinal turbulent intensities at different longitudinal distances. It shows a gradual increase of about 123% as the longitudinal distance is increased from $\frac{x}{D}=0.7$ to $\frac{x}{D}=2.2$. After that, the turbulent intensity decreases about 57% from $\frac{x}{D}=2.2$ to $\frac{x}{D}=7.8$.



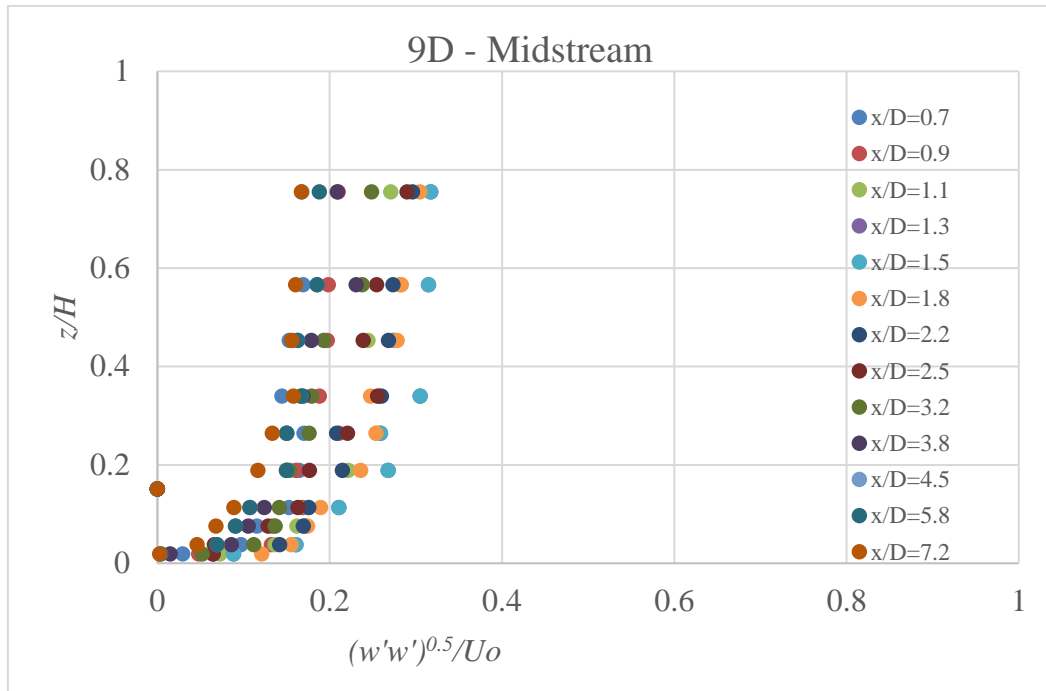
(a)



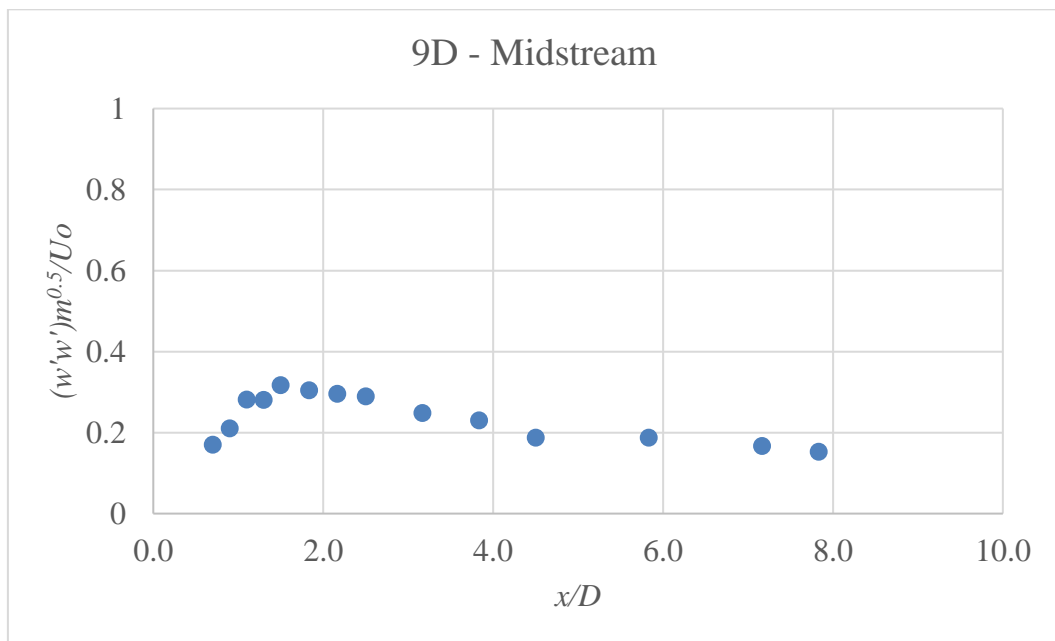
(b)

Figure 4.18: (a) Variation of Normalized Turbulent Intensity Profile (b) Variation of Maximum Turbulent Intensity in transverse direction along plane of symmetry between two cylinders (9D)

Figure 4.19(a) compares the turbulent intensity profiles at vertical direction for 9D c/c spacing. Results shows that the turbulent intensity increases initially as the flow progresses similar as found in both longitudinal and vertical directions and maximum normalized intensity has been observed at $\frac{x}{D}=1.5$ for $\frac{z}{H}=0.75$ which is equal to 0.32. So, it has been observed that the turbulent intensity is the smallest at the vertical direction as found earlier in 3D and 6D c/c spacing. Profiles at all of the longitudinal distances are logarithmic similar to the longitudinal direction intensity profiles at 9D c/c spacing. Figure 4.19(b) shows a gradual increase of about 88% as the longitudinal distance is increased from $\frac{x}{D}=0.7$ to $\frac{x}{D}=1.5$. After that, the turbulent intensity decreases about 53% from $\frac{x}{D}=1.5$ to $\frac{x}{D}=4.8$.



(a)

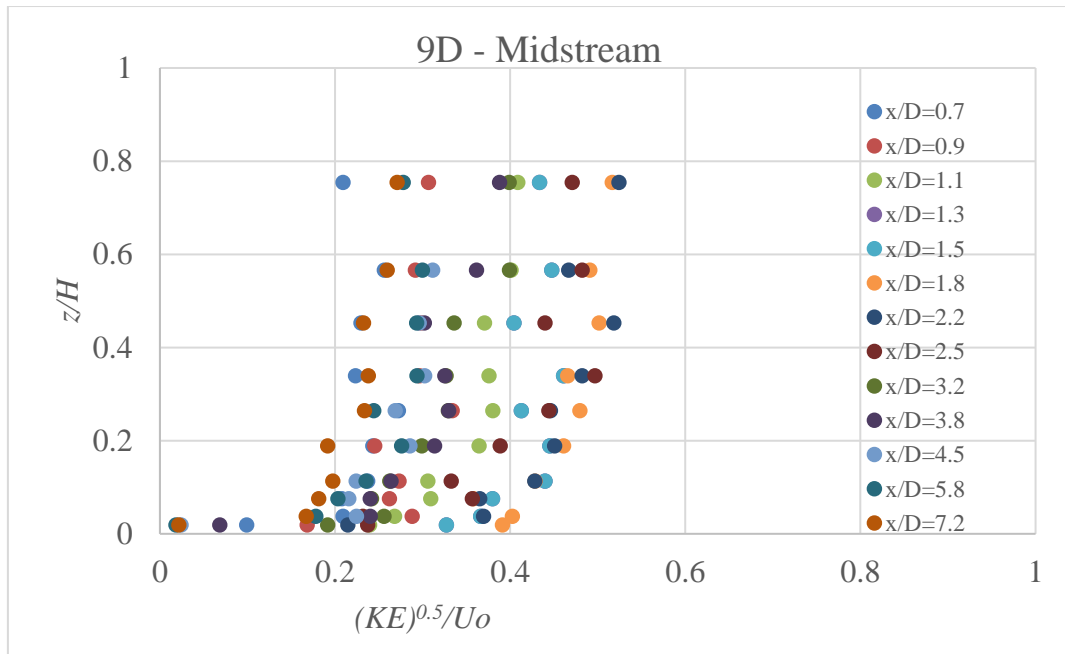


(b)

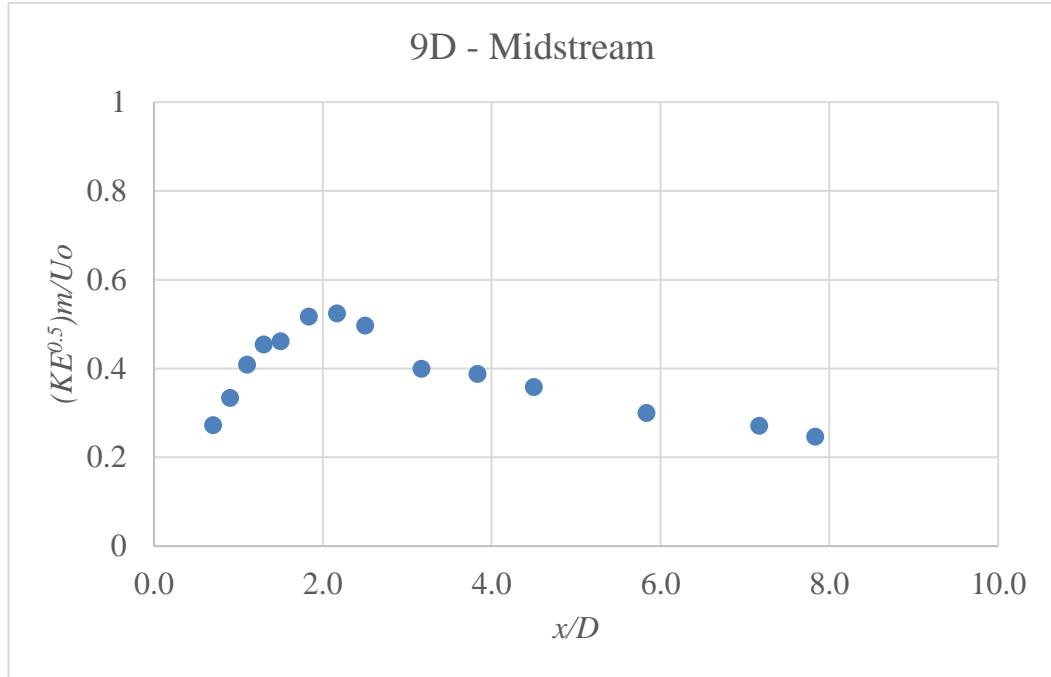
Figure 4.19: (a) Variation of Normalized Turbulent Intensity Profile (b) Variation of Maximum Turbulent Intensity in vertical direction along plane of symmetry between two cylinders (9D)

4.6.6 Kinetic Energy at mid-stream of 9D c/c spacing

Figure 4.20(a) shows that kinetic energy profiles at different vertical depths for 9D c/c spacing. Analysis of this plot shows that the kinetic energy also continues on increasing initially as the flow progresses as similar to the turbulent intensities. Additionally, maximum normalized kinetic energy has been observed at $\frac{x}{D}=2.2$ for $\frac{z}{H}=0.75$ which is equal to 0.52. Figure 4.20(b) shows a gradual increase of about 93% as the longitudinal distance is increased from $\frac{x}{D}=0.7$ to $\frac{x}{D}=2.2$. After that, the turbulent intensity decreases about 52% as the flow progresses from $\frac{x}{D}=1.8$ to $\frac{x}{D}=7.8$.



(a)



(b)

Figure 4.20: (a) Variation of Normalized Kinetic Energy Profile (b) Variation of Maximum Kinetic Energy in vertical direction along plane of symmetry between two cylinders (9D)

4.6.7 Turbulent shear stress at midstream

Variation of normalized maximum turbulent shear stress per unit mass in the x direction on the xy plane ($\frac{\sqrt{u'w'}}{U_0}$) at different verticals along the POS in the midstream of 3D, 6D and 9D are plotted in Figure 4.20. Similar to kinetic energy, the maximum of ($\frac{\sqrt{u'w'}}{U_0}$) increases to a peak, and then reduces gradually to a lower value, however the variation is relatively chaotic compared to turbulent intensities and kinetic energy. For 3D, the maximum value of around 0.6 occurs at $\frac{x}{D}=1.3$ and 1.8 and for 6D the maximum occurs at $\frac{x}{D}=1.3$ with a value of 0.46. For 9D, the maximum occurs at $\frac{x}{D}=1.5$ with a value of 0.54. It appears that the maximum of ($\frac{\sqrt{u'w'}}{U_0}$) tend to occur before the end of the recirculation zone in the midstream for all cases.

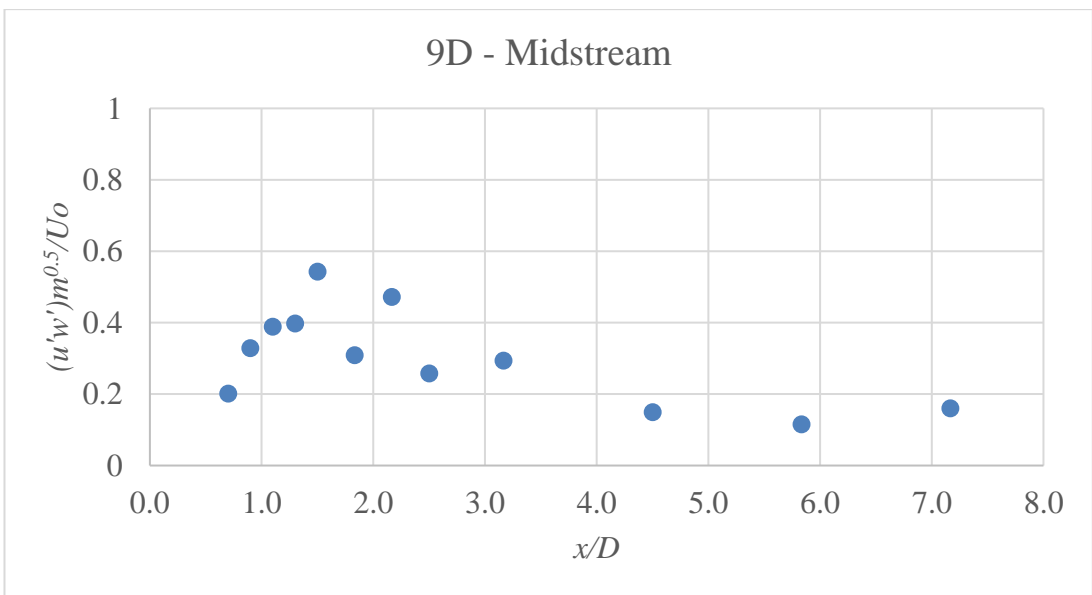
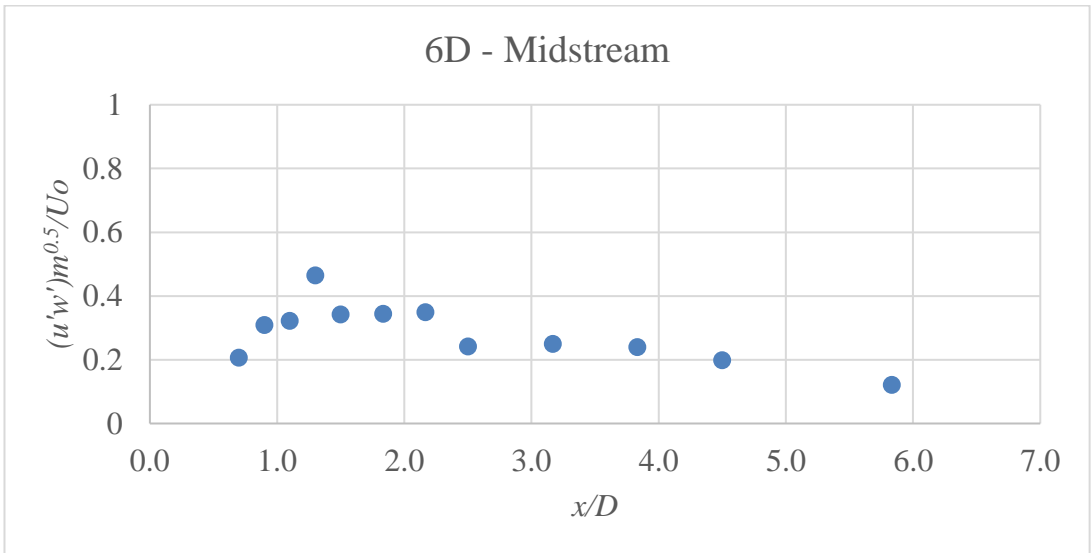
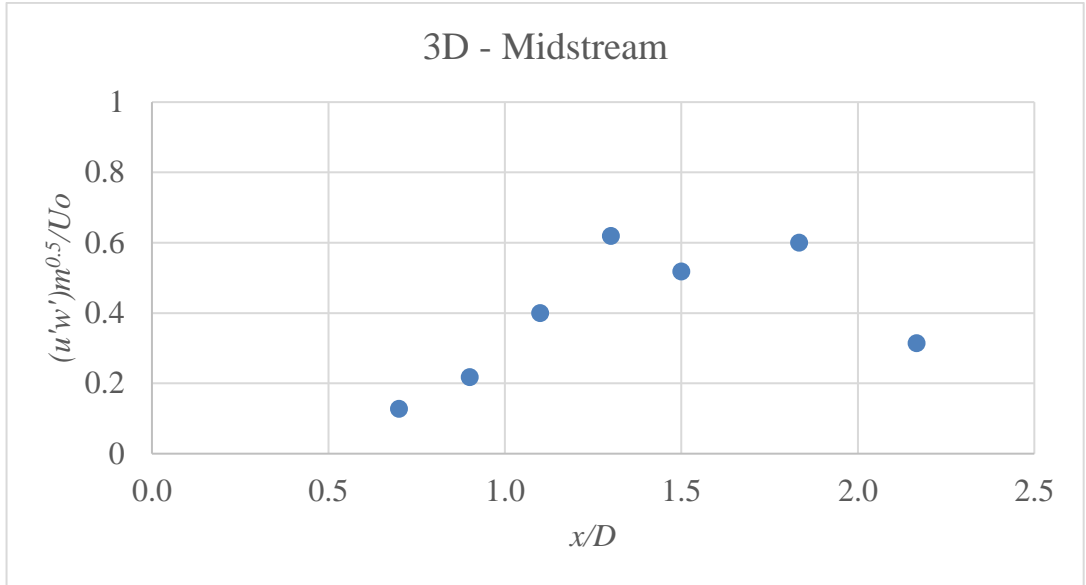


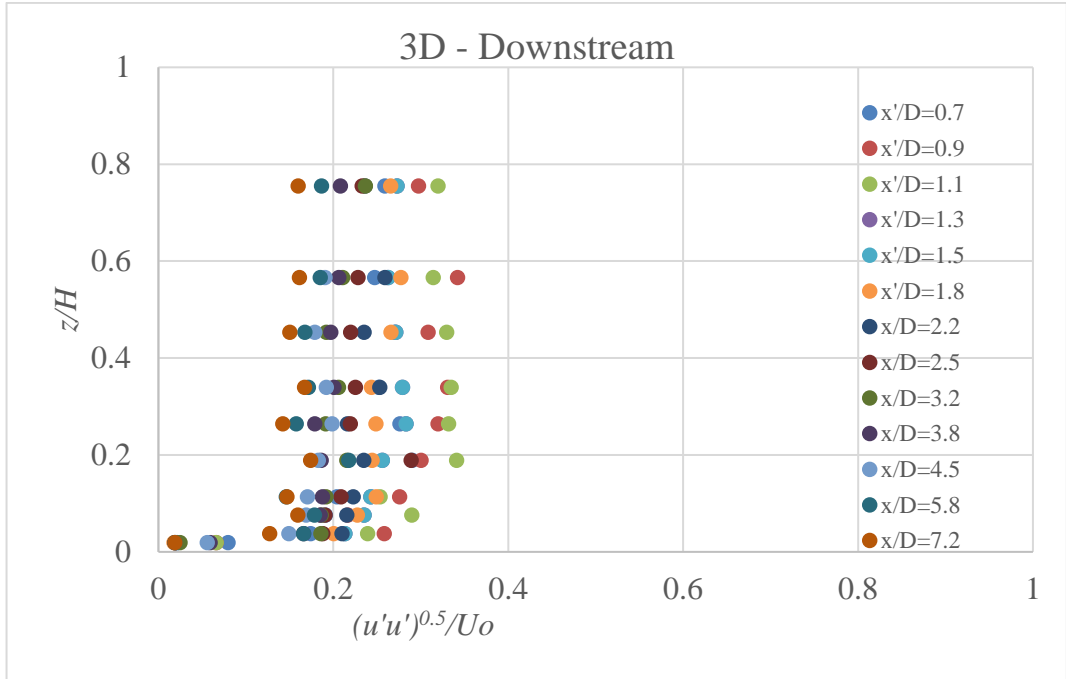
Figure 4. 21: Variation of normalized maximum turbulent shear stress for three cases at midstream section

4.7 Turbulence Parameters at Downstream

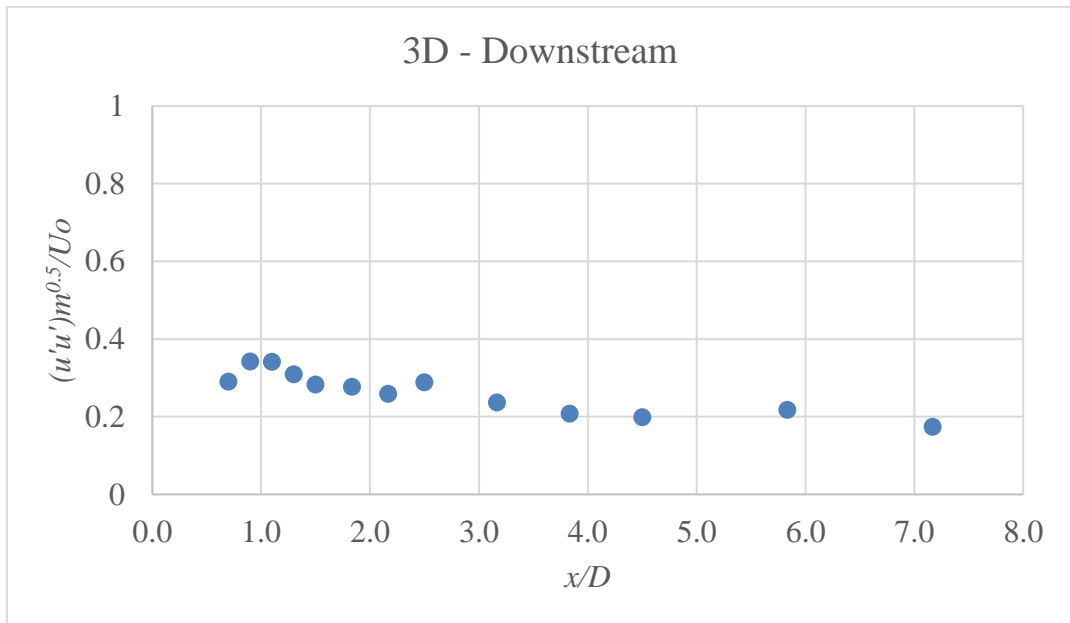
Turbulent intensity in longitudinal, transverse and vertical direction is investigated for three case studies at downstream. Additionally, the variation of profiles for specified sections are plotted to understand the behavior of turbulent flow around the cylinders.

4.7.1 Turbulent intensity at downstream of 3D c/c spacing

Figure 4.22(a) shows the turbulent intensity profiles at longitudinal direction for 3D c/c spacing at downstream. Analysis of this plot shows that the turbulent intensity increases initially at a relatively shorter longitudinal distance ($\frac{x}{D} < 1.1$) as the flow progresses and maximum normalized intensity has been observed at $\frac{x}{D} = 1.1$ for $\frac{z}{H} = 0.18$ which is equal to 0.34. Logarithmic profiles are visible at all longitudinal distances. The maximum value of normalized intensity is smaller compared to the normalized intensity observed at mid-stream. Figure 4.22(b) shows a mapping for maximum values of normalized longitudinal turbulent intensities at different longitudinal distances. It shows a gradual increase of about 17% as the longitudinal distance is increased from $\frac{x}{D} = 0.7$ to $\frac{x}{D} = 0.9$. After that, the turbulent intensity starts to decrease again.



(a)

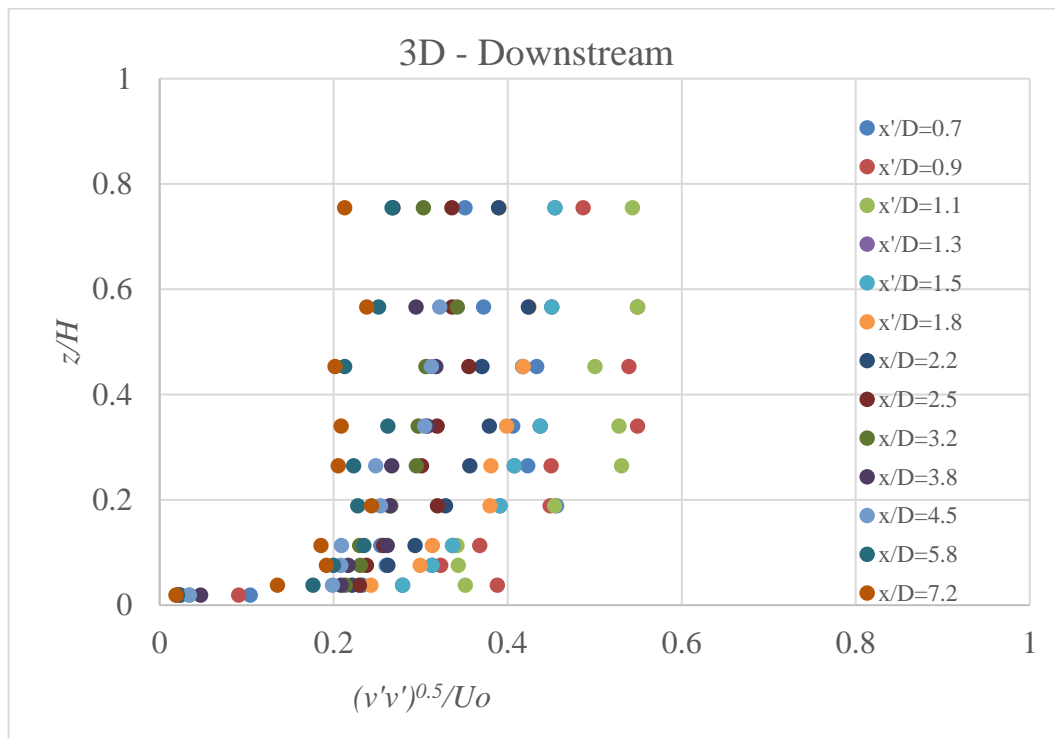


(b)

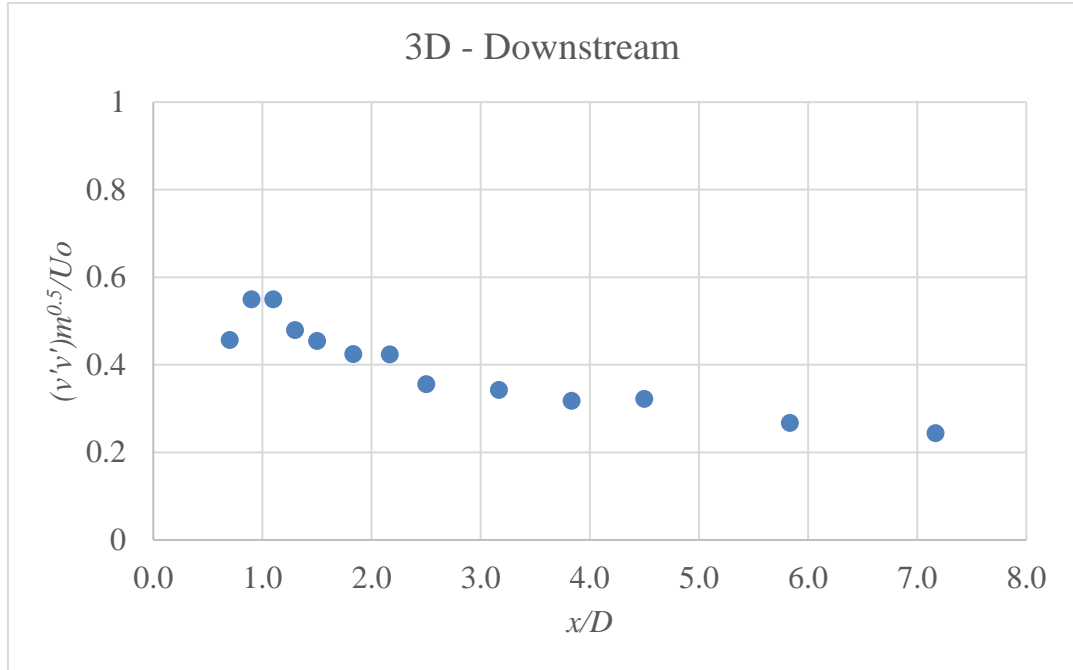
Figure 4.22: (a) Variation of Normalized Turbulent Intensity Profile (b) Variation of Maximum Turbulent Intensity in longitudinal direction along plane of symmetry downstream of second cylinder(3D)

Figure 4.23(a) shows turbulent intensity profiles at transverse direction for 3D c/c spacing at downstream of second cylinder. Analysis of this plot shows that the turbulent intensity increases initially as the flow progresses and maximum normalized

intensity has been observed at $\frac{x}{D}=1.1$ for $\frac{z}{H}=0.57$ which is equal to 0.55. So, it has been observed the turbulent intensity is higher at transverse direction compared to longitudinal direction which is compatible with the findings measured at between two cylinders. Logarithmic profiles are visible at all of the longitudinal distances as found for earlier sections. Figure 4.23(b) shows a mapping for maximum values of normalized longitudinal turbulent intensities at different longitudinal distances. It shows an increase of about 20% as the longitudinal distance is increased from $\frac{x}{D}=0.7$ to $\frac{x}{D}=1.1$. After that, the turbulent intensity decreases by 56% when the flow progresses from $\frac{x}{D}=1.1$ to $\frac{x}{D}=7.2$.



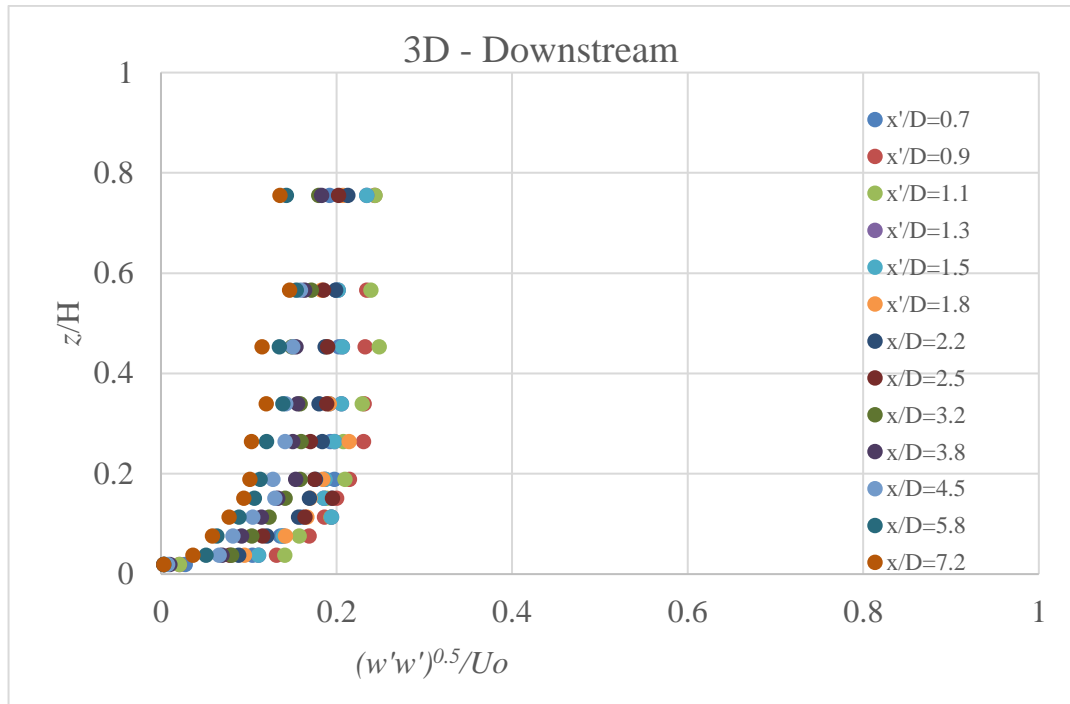
(a)



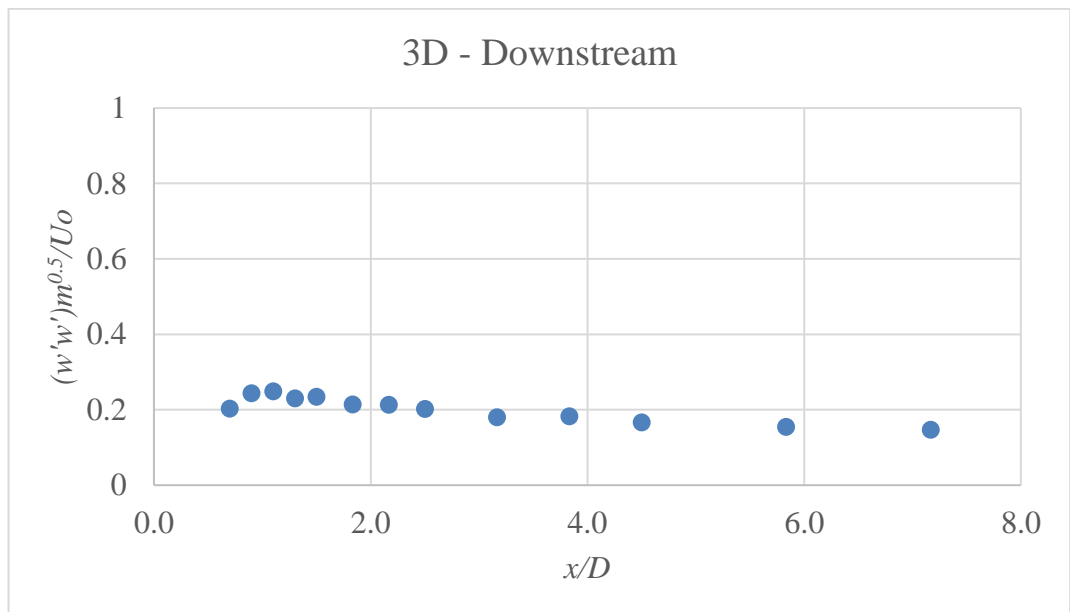
(b)

Figure 4.23: (a) Variation of Normalized Turbulent Intensity Profile (b) Variation of Maximum Turbulent Intensity in transverse direction along plane of symmetry downstream of second cylinders (3D)

Figure 4.24(a) shows the turbulent intensity profiles at vertical direction for 3D c/c spacing at downstream section. Analysis of this plot shows that the turbulent intensity increases initially as the flow progresses and maximum normalized intensity has been observed at $\frac{x}{D}=1.1$ for $\frac{z}{H}=0.45$ which is equal to 0.25. So, it has been observed that the values are of small scale in turbulent intensity at vertical direction. Logarithmic profiles are visible each distance as found earlier along longitudinal sections. Figure 4.24(b) shows an increase of about 20% as the longitudinal distance is increased from $\frac{x}{D}=0.7$ to $\frac{x}{D}=1.1$. After that, the turbulent intensity decreases by 40% when the flow progresses from $\frac{x}{D}=1.1$ to $\frac{x}{D}=7.2$.



(a)

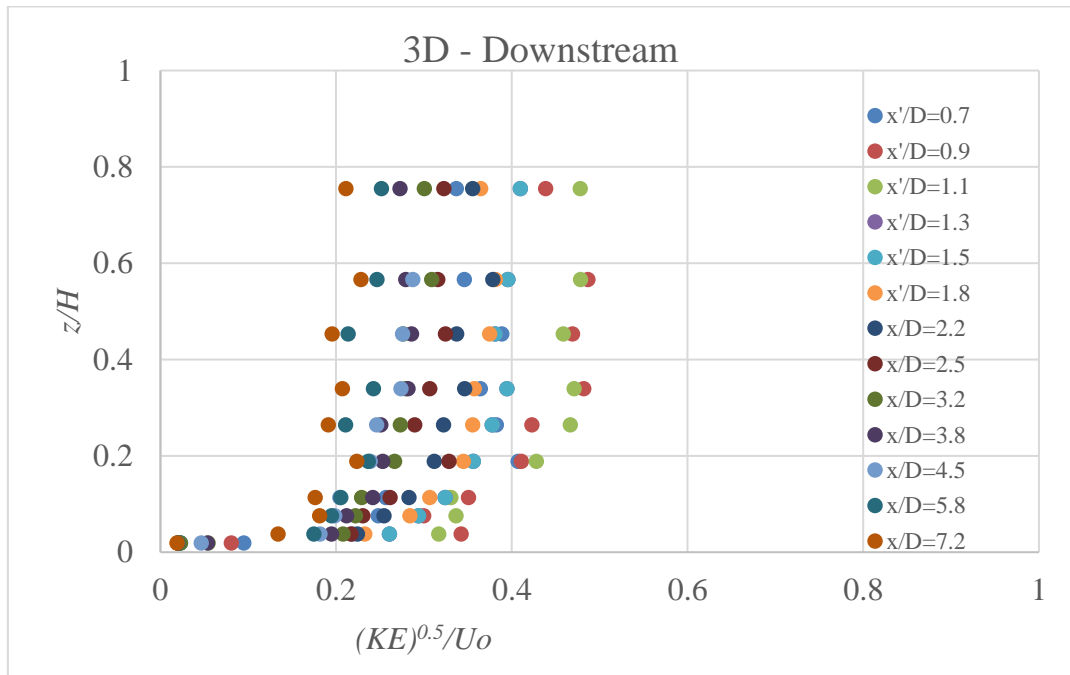


(b)

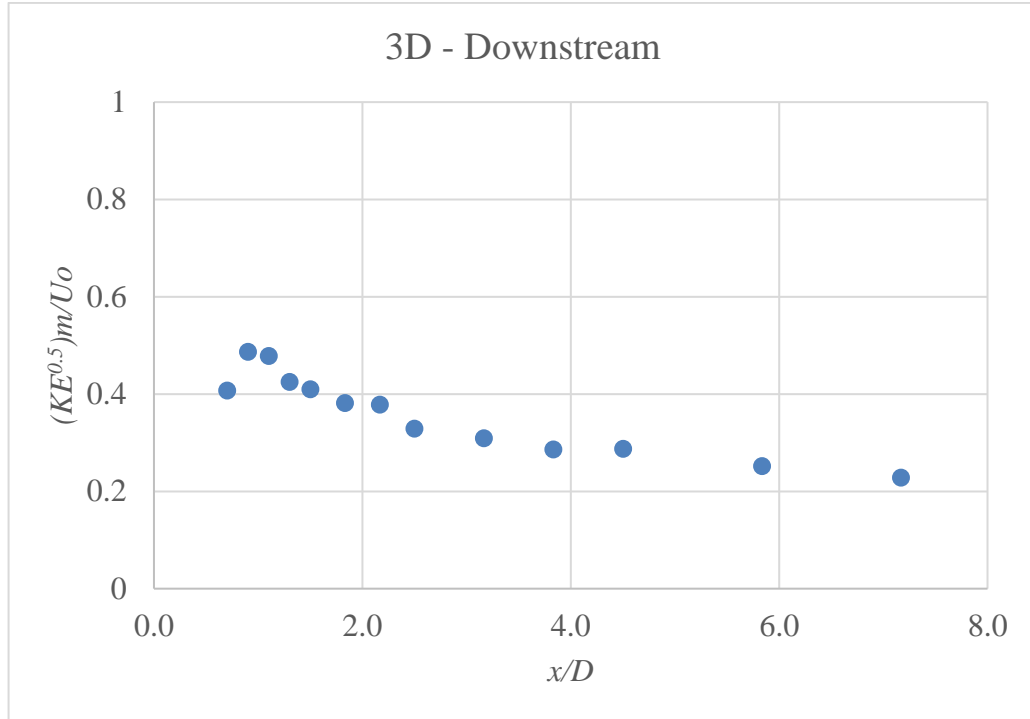
Figure 4.24: (a) Variation of Normalized Turbulent Intensity Profile (b) Variation of Maximum Turbulent Intensity in vertical direction along plane of symmetry downstream of second cylinders(3D)

4.7.2 Kinetic Energy at downstream of 3D c/c spacing

Figure 4.25(a) shows the plot of kinetic energy profiles at different vertical depths for 3D c/c spacing at downstream section. Analysis of this plot shows that the kinetic energy follows the same pattern of decrement after reaching a peak at relatively shorter longitudinal distance as the turbulent intensities. Moreover, maximum normalized kinetic energy has been observed at $\frac{x}{D}=0.9$ for $\frac{z}{H}=0.57$ which is equal to 0.49. Logarithmic profiles are visible at all of the longitudinal distances as found earlier in case of turbulent intensities. Figure 4.25(b) shows an increase of about 23% as the longitudinal distance is increased from $\frac{x}{D}=0.7$ to $\frac{x}{D}=0.9$. After that, the kinetic energy decreases by 53% when the flow progresses from $\frac{x}{D}=0.7$ to $\frac{x}{D}=7.2$.



(a)

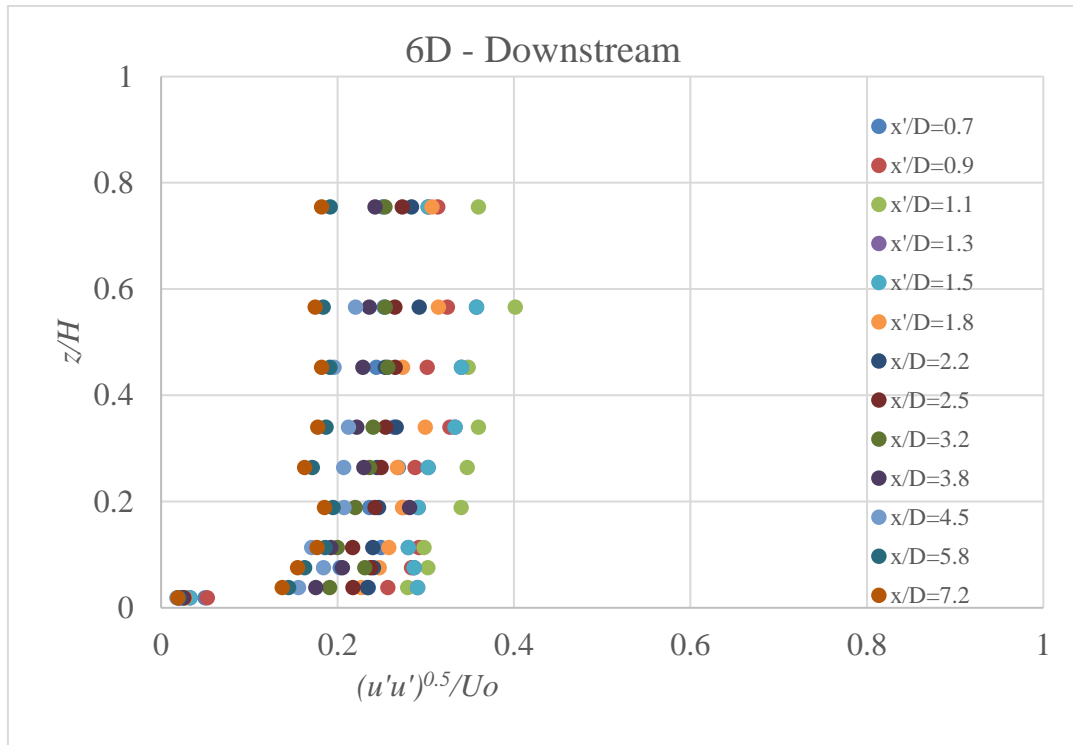


(b)

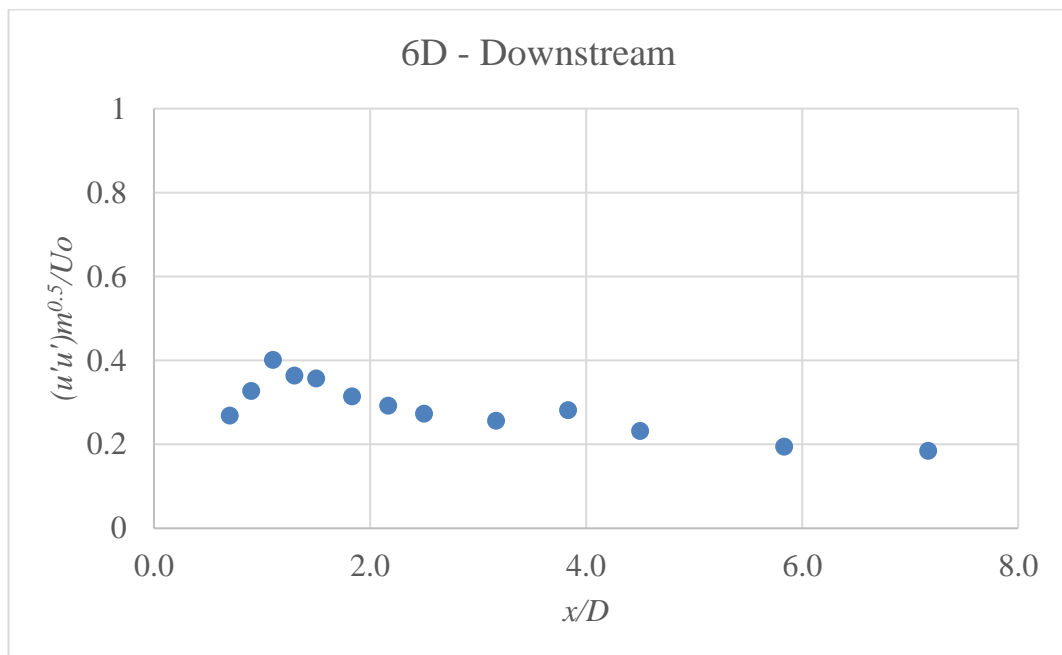
Figure 4.25: (a) Variation of Normalized Kinetic Energy Profile (b) Variation of Maximum Kinetic Energy in vertical direction along plane of symmetry downstream of second cylinders(3D)

4.7.3 Turbulent intensity at downstream of 6D c/c spacing

Figure 4.26(a) reveals turbulent intensity profiles at longitudinal direction for 6D c/c spacing at downstream section. Analysis of this plot shows that the turbulent intensity increases initially as the flow progresses and maximum normalized intensity has been observed at $\frac{x}{D}=1.1$ for $\frac{z}{H}=0.57$ which is equal to 0.40. The maximum turbulent intensity found at 3D case study at downstream section is approximately 18% lower than the value found in this study. Figure 4.26(b) shows an increase of about 48% as the longitudinal distance is increased from $\frac{x}{D}=0.7$ to $\frac{x}{D}=1.1$. After that, the turbulent intensity decreases about 55% from $\frac{x}{D}=1.1$ to $\frac{x}{D}=7.2$.



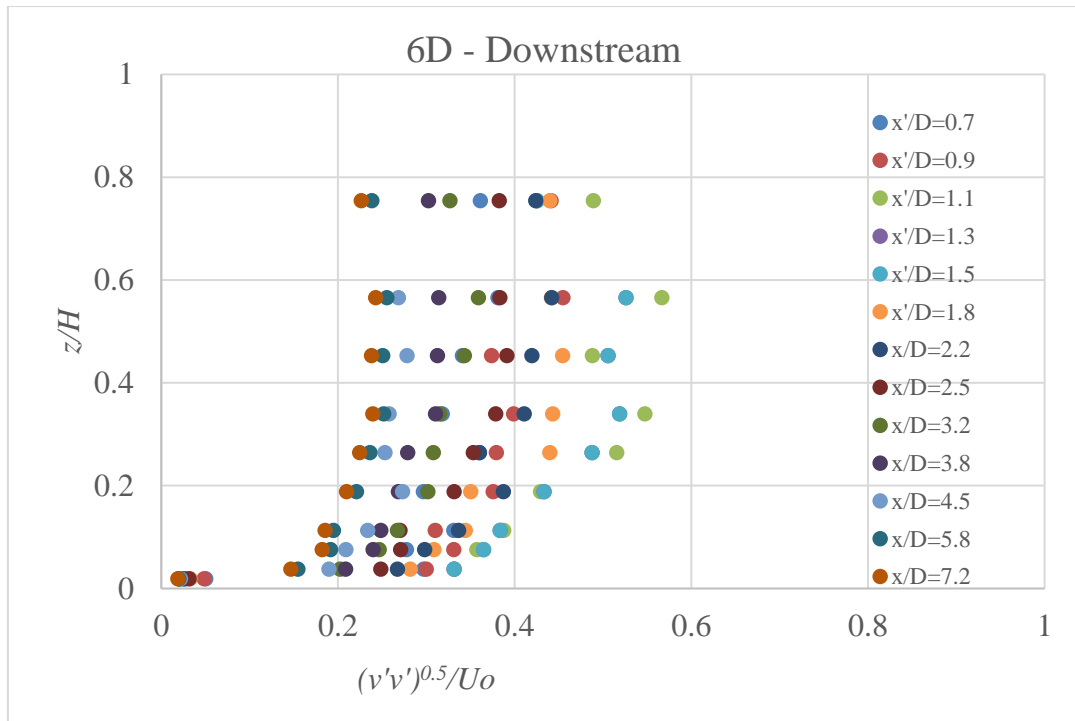
(a)



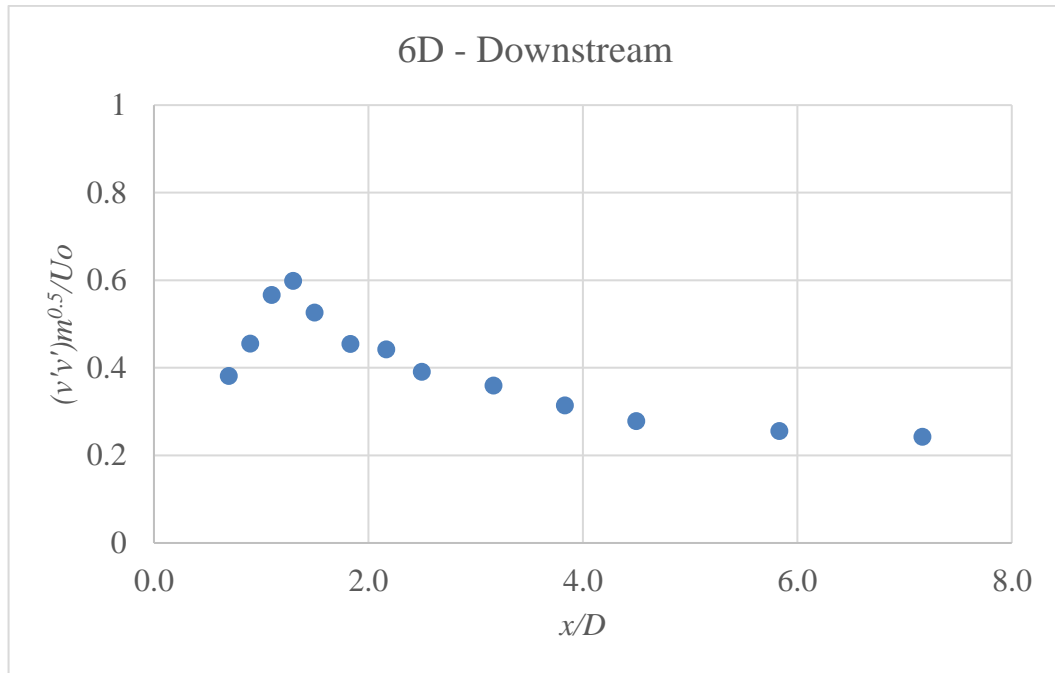
(b)

Figure 4.26: (a) Variation of Normalized Turbulent Intensity Profile (b) Variation of Maximum Turbulent Intensity in longitudinal direction along plane of symmetry downstream of second cylinders (6D)

Figure 4.27(a) shows turbulent intensity profiles at transverse direction for 6D c/c spacing at downstream section. Similarly, maximum normalized intensity has been observed at $\frac{x}{D}=1.3$ for $\frac{z}{H}=0.57$ which is equal to 0.60. So, it has been observed that the turbulent intensity is higher at transverse direction in this case study also. Figure 4.27(b) shows a mapping for maximum values of normalized traverse turbulent intensities at different longitudinal distances. It shows an increase of about 54% as the longitudinal distance is increased from $\frac{x}{D}=0.7$ to $\frac{x}{D}=1.3$. After that, the turbulent intensity decreases about 60% from $\frac{x}{D}=1.3$ to $\frac{x}{D}=7.2$.



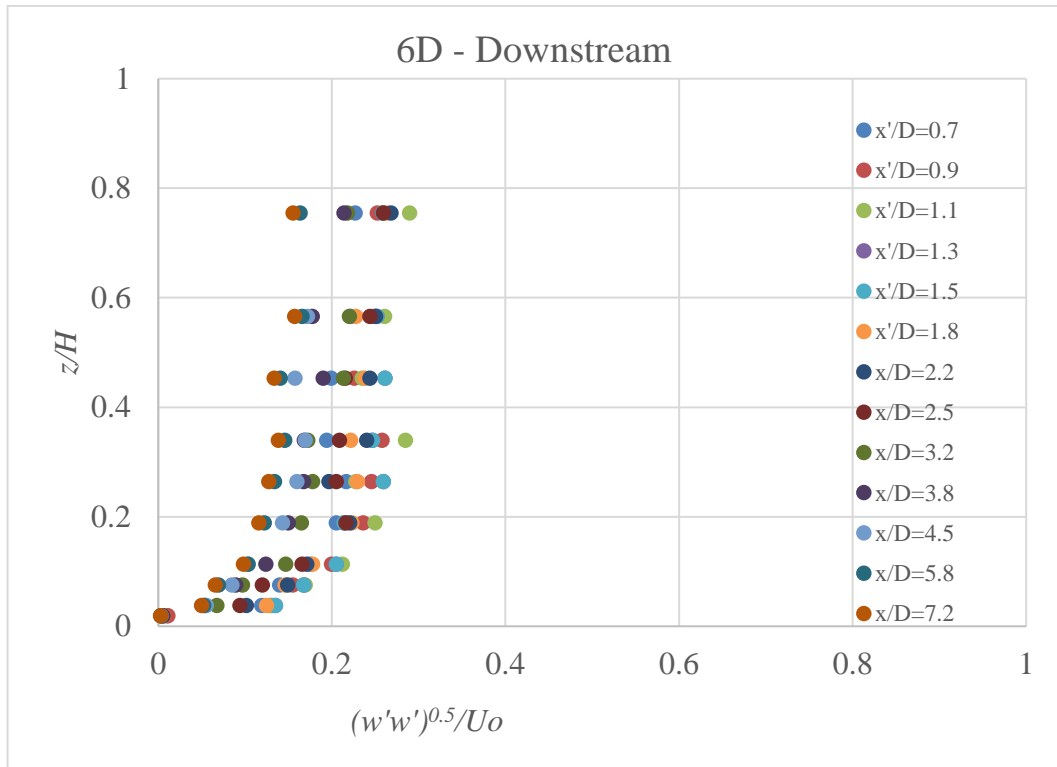
(a)



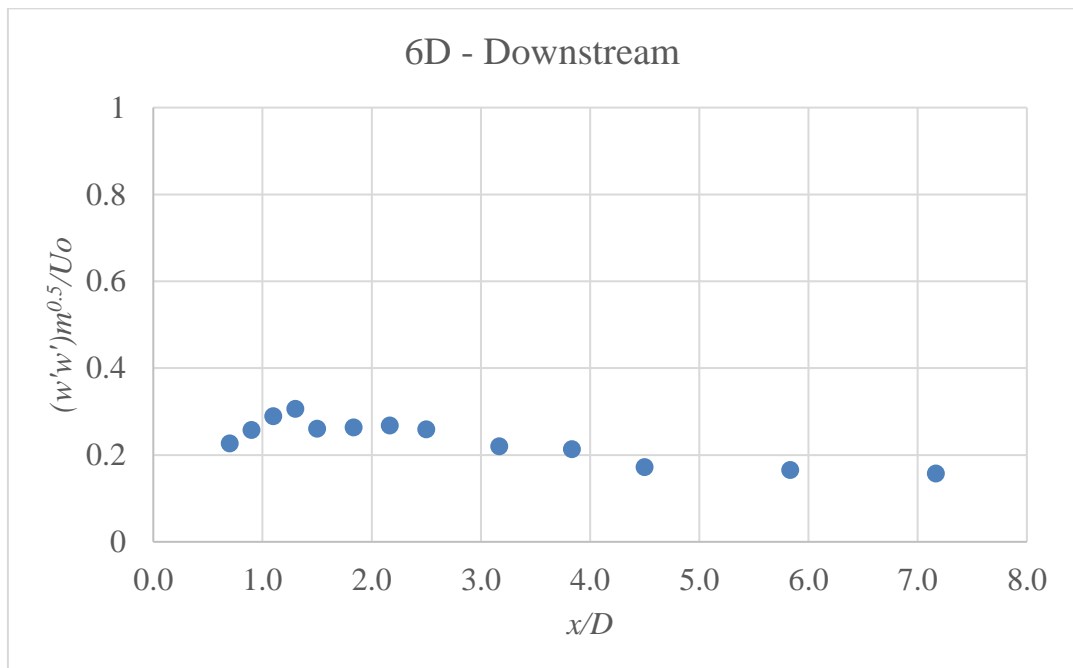
(b)

Figure 4.27: (a) Variation of Normalized Turbulent Intensity Profile (b) Variation of Maximum Turbulent Intensity in transverse direction along plane of symmetry downstream of second cylinders (6D)

From Figure 4.28(a), turbulent intensity profiles at vertical direction for 6D c/c spacing at downstream section can be observed. Analysis shows that the turbulent intensity increases initially as the flow progresses and maximum normalized intensity has been observed at $\frac{x}{D}=1.3$ for $\frac{z}{H}=0.76$ which is equal to 0.31. Profiles at all of the longitudinal distances are logarithmic as found in the earlier case studies of downstream section. Figure 4.28(b) shows a mapping for maximum values of normalized vertical turbulent intensities at different longitudinal distances. It shows an increase of about 35% as the longitudinal distance is increased from $\frac{x}{D}=0.7$ to $\frac{x}{D}=1.3$. After that, the turbulent intensity decreases about 48% from $\frac{x}{D}=1.3$ to $\frac{x}{D}=7.2$.



(a)

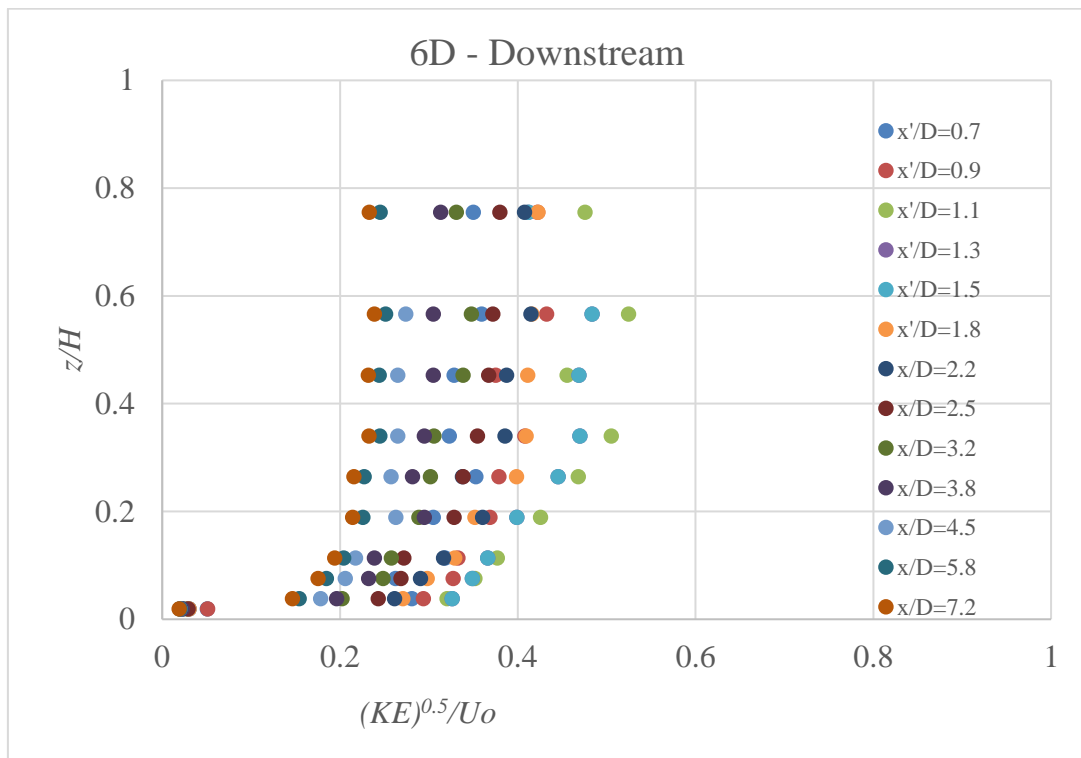


(b)

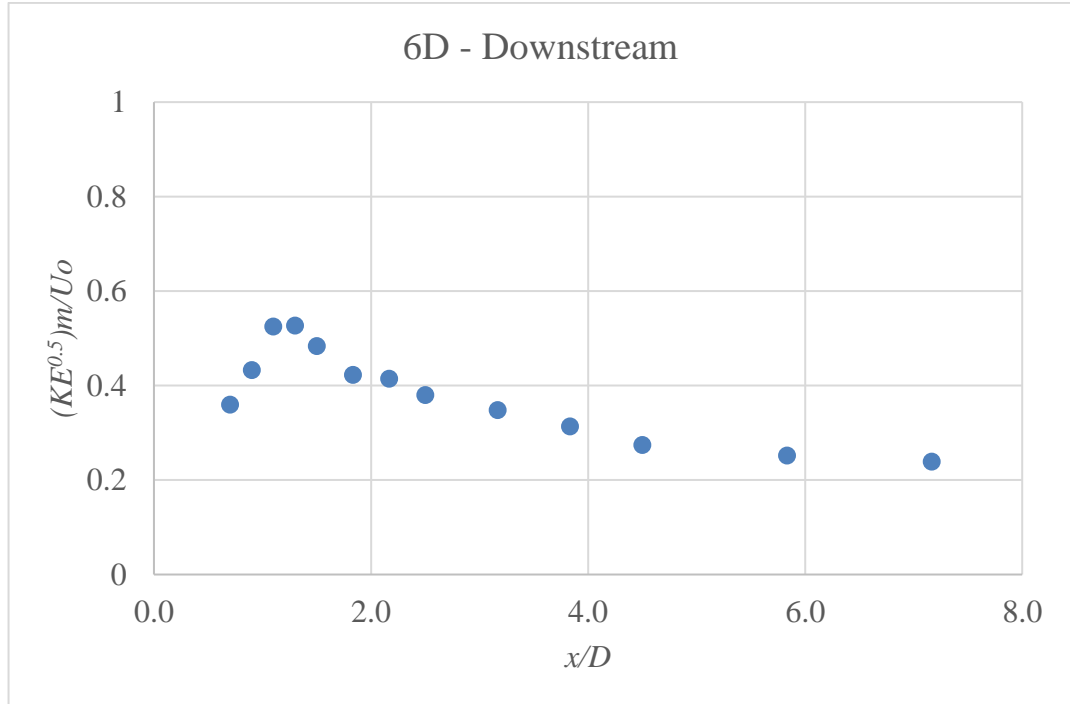
Figure 4.28: (a) Variation of Normalized Turbulent Intensity Profile (b) Variation of Maximum Turbulent Intensity in vertical direction along plane of symmetry downstream of second cylinders (6D)

4.7.4 Kinetic Energy at downstream of 6D c/c spacing

kinetic energy profiles at different vertical depths for 6D c/c spacing at downstream section shown in Figure 4.29(a) and from the plot it shows that the kinetic energy follows the same pattern of decrement after reaching a peak at relatively shorter longitudinal distance as the turbulent intensities. Moreover, maximum normalized kinetic energy has been observed at $\frac{x}{D}=1.3$ for $\frac{z}{H}=0.57$ which is equal to 0.53. Logarithmic profiles are visible at all of the longitudinal distances as found earlier in case of turbulent intensities. Figure 4.29(b) shows a mapping for maximum values of normalized kinetic energy at different longitudinal distances. It shows an increase of about 47% as the longitudinal distance is increased from $\frac{x}{D}=0.7$ to $\frac{x}{D}=1.3$. After that, the kinetic energy decreases by 55% when the flow progresses from $\frac{x}{D}=1.3$ to $\frac{x}{D}=7.2$.



(a)

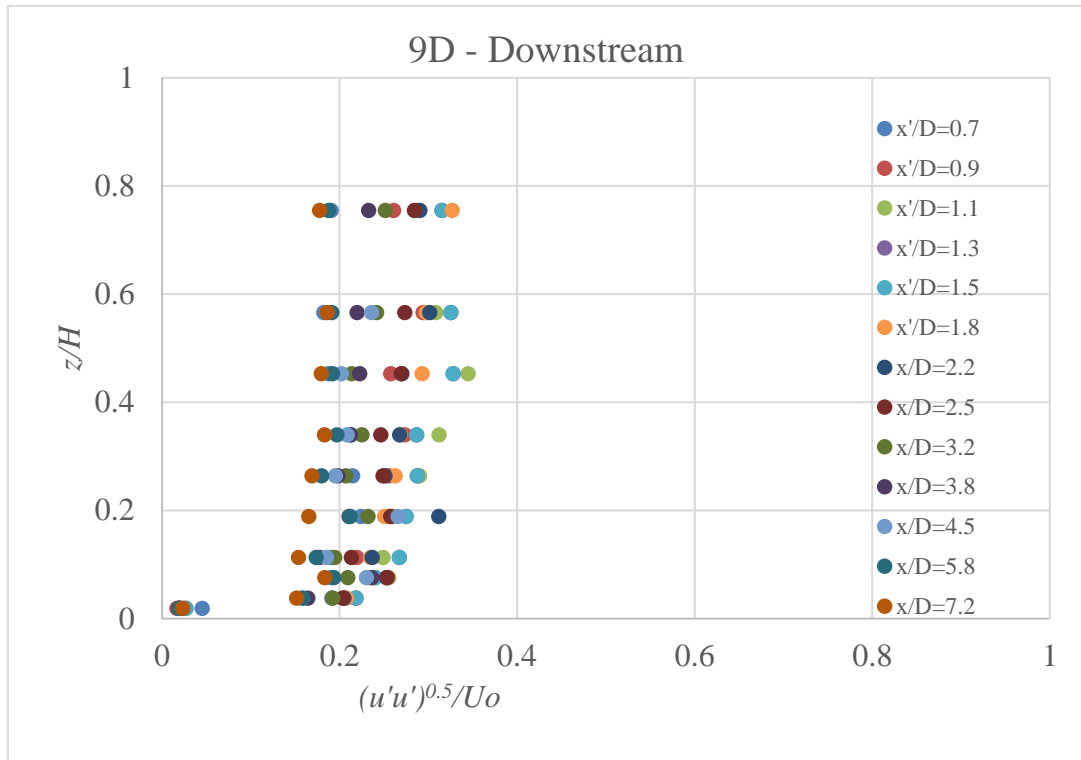


(b)

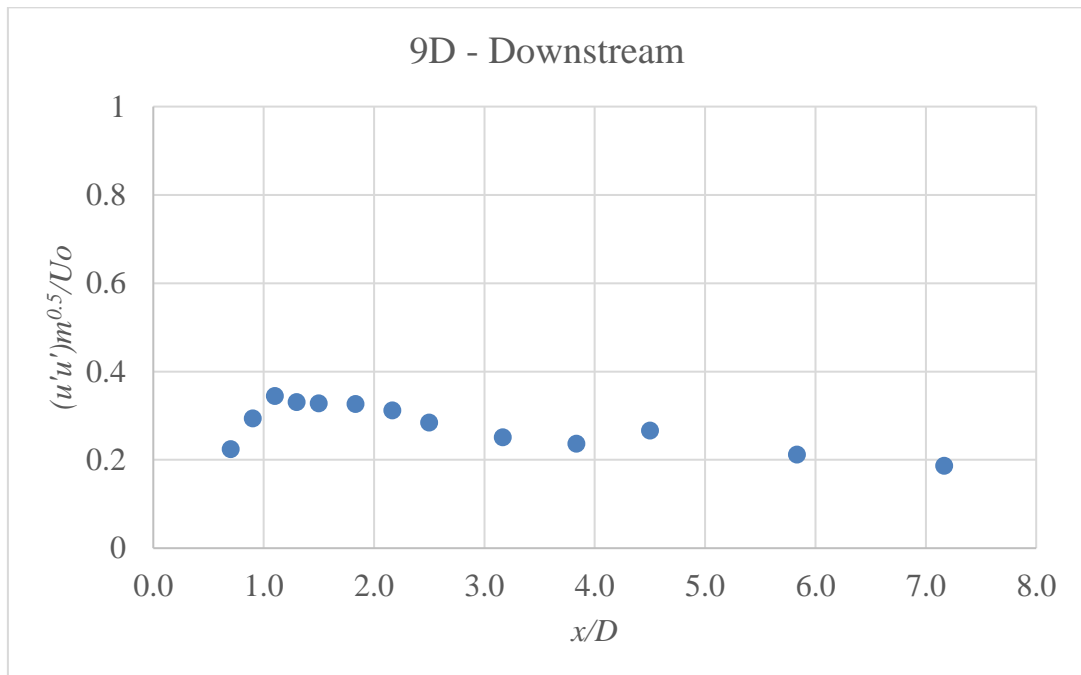
Figure 4.29: (a) Variation of Normalized Kinetic Energy Profile (b) Variation of Maximum Kinetic Energy in vertical direction along plane of symmetry downstream of second cylinders(6D)

4.7.1 Turbulent intensity at downstream of 9D c/c spacing

Comparison of turbulent intensity profiles at longitudinal direction for 9D c/c spacing at downstream is plotted in figure 4.30(a). Analysis of this plot shows that the turbulent intensity increases initially as the flow progresses as similar to 6D c/c spacing and maximum normalized intensity has been observed at $\frac{x}{D}=1.1$ for $\frac{z}{H}=0.45$ which is equal to 0.34. The maximum turbulent intensity found at 3D case study at downstream section is actually same as the value found in this study. Profiles at all of the longitudinal distances are logarithmic as similar to 6D c/c spacing. Figure 4.30(b) shows a mapping for maximum values of normalized longitudinal turbulent intensities at different longitudinal distances which shows an increase of about 54% as the longitudinal distance is increased from $\frac{x}{D}=0.7$ to $\frac{x}{D}=1.1$. After that, the turbulent intensity decreases about 44% from $\frac{x}{D}=1.1$ to $\frac{x}{D}=7.2$.



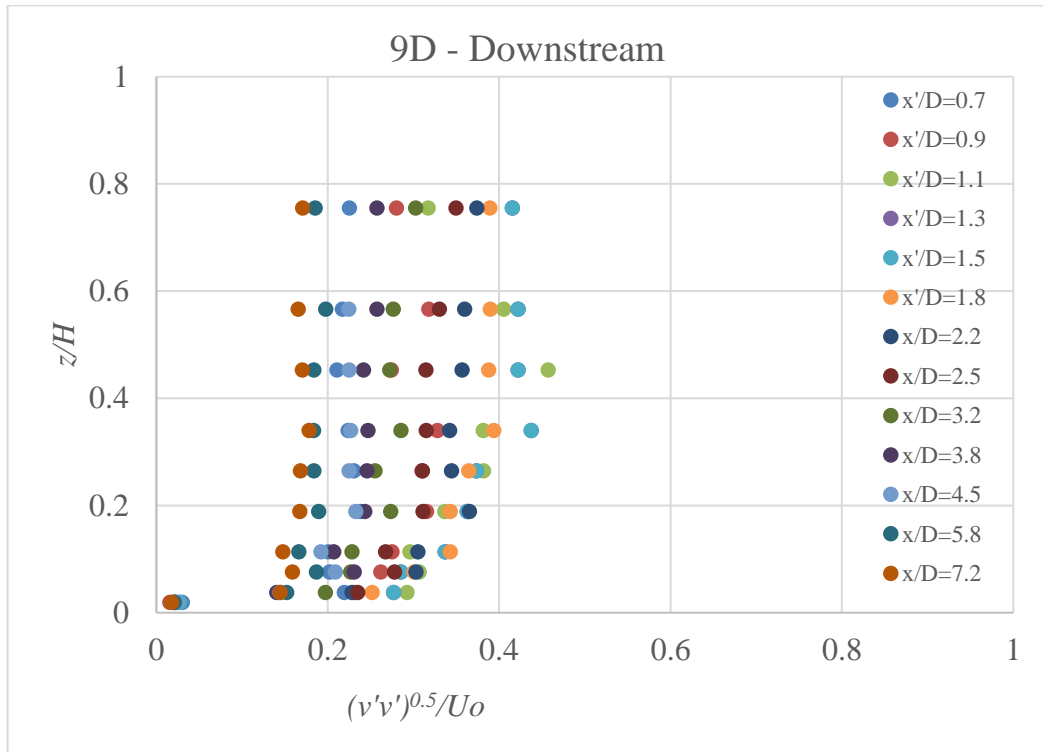
(a)

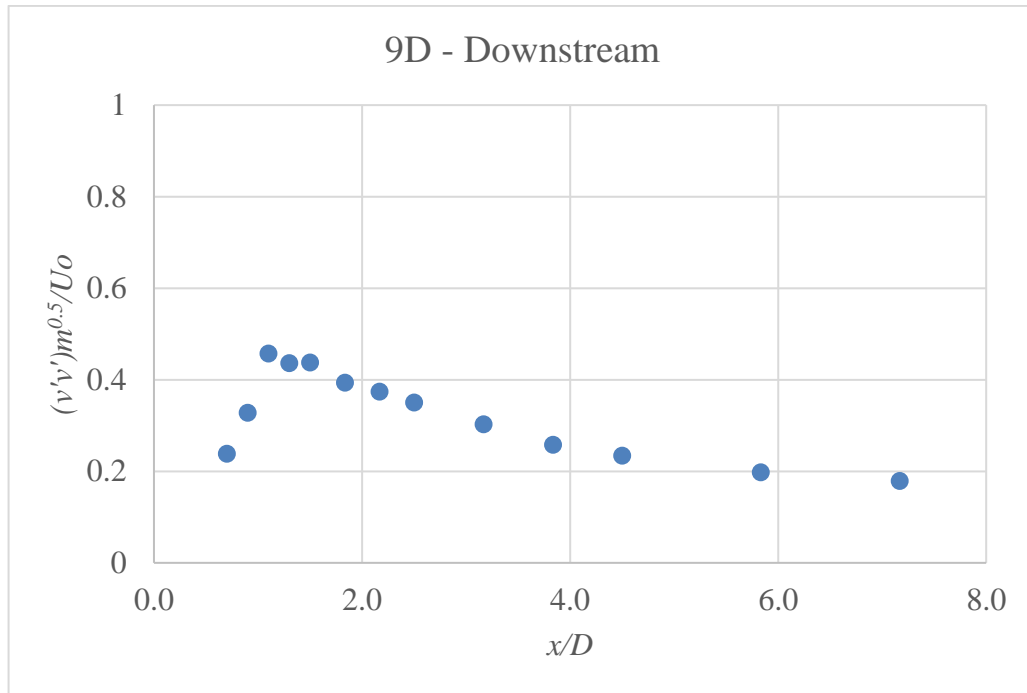


(b)

Figure 4.30: (a) Variation of Normalized Turbulent Intensity Profile (b) Variation of Maximum Turbulent Intensity in longitudinal direction along plane of symmetry downstream of second cylinder (9D)

Figure 4.31(a) shows that the turbulent intensity increases initially as flow progresses similar to 6D c/c spacing and maximum normalized intensity has been observed at $\frac{x}{D}=1.1$ for $\frac{z}{H}=0.45$ which is equal to 0.46. Figure 4.31(b) shows an increase of about 100% as the longitudinal distance is increased from $\frac{x}{D}=0.7$ to $\frac{x}{D}=1.1$. After that, the turbulent intensity decreases about 61% from $\frac{x}{D}=1.1$ to $\frac{x}{D}=7.2$.

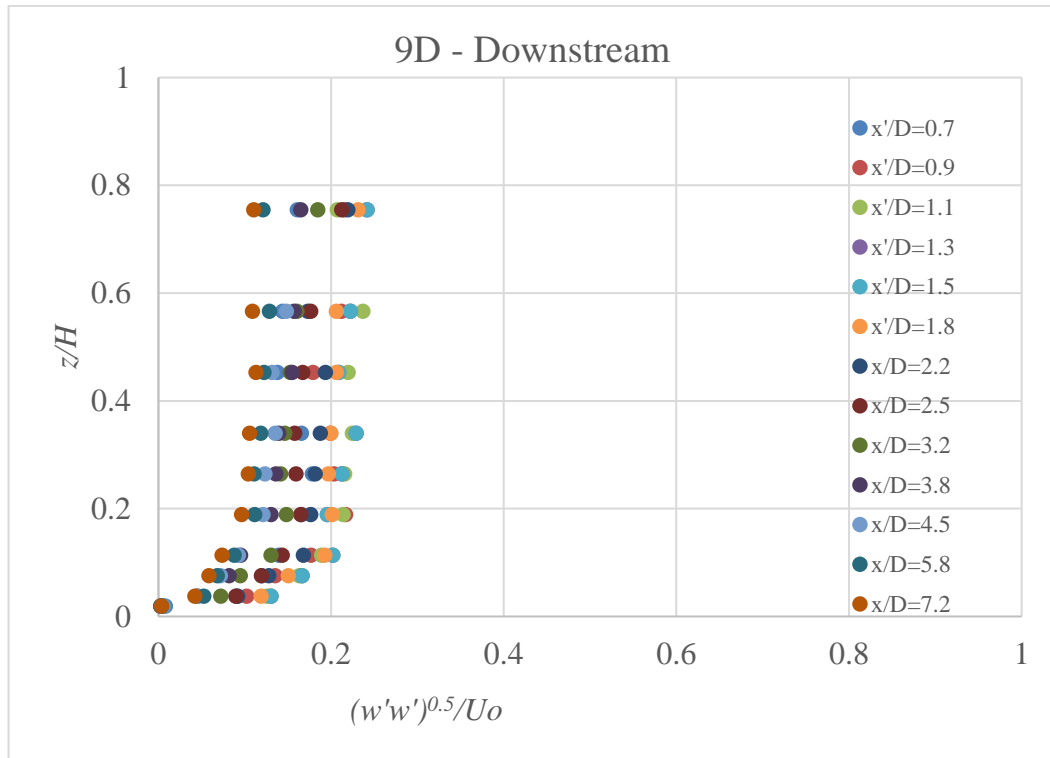




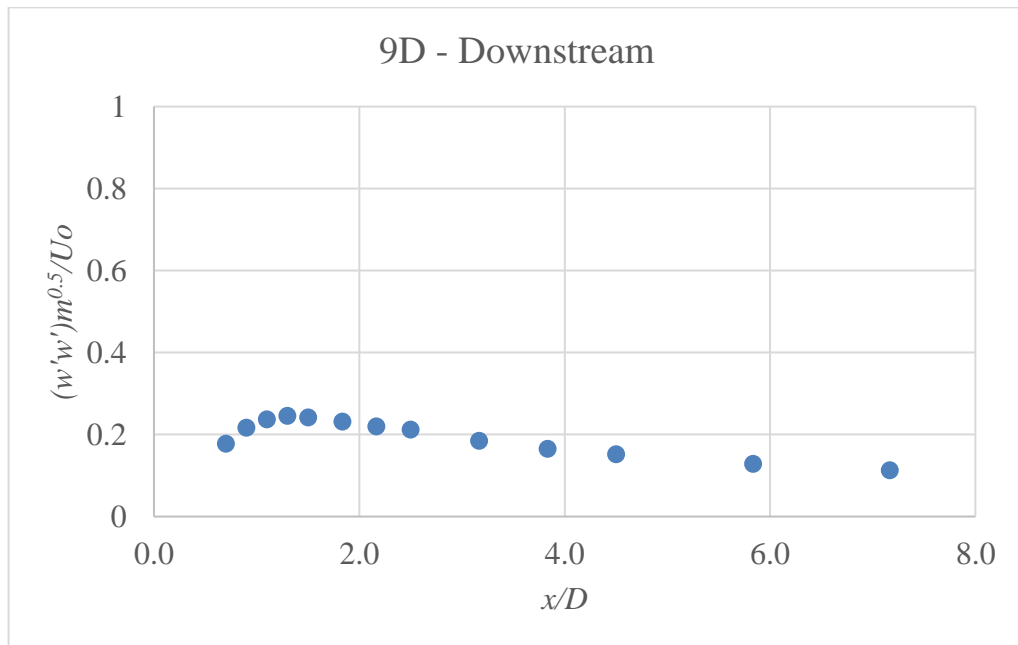
(b)

Figure 4.31: (a) Variation of Normalized Turbulent Intensity Profile (b) Variation of Maximum Turbulent Intensity in transverse direction along plane of symmetry downstream of second cylinder (9D)

Figure 4.32(a) shows that the turbulent intensity increases at vertical direction initially as the flow progresses as similar to 6D c/c spacing and maximum normalized intensity has been observed at $\frac{x}{D}=1.3$ for $\frac{z}{H}=0.75$ which is equal to 0.25. Figure 4.32(b) shows an increase of about 39% as the longitudinal distance is increased from $\frac{x}{D}=0.7$ to $\frac{x}{D}=1.3$. After that, the turbulent intensity decreases about 56% from $\frac{x}{D}=1.3$ to $\frac{x}{D}=7.2$.



(a)

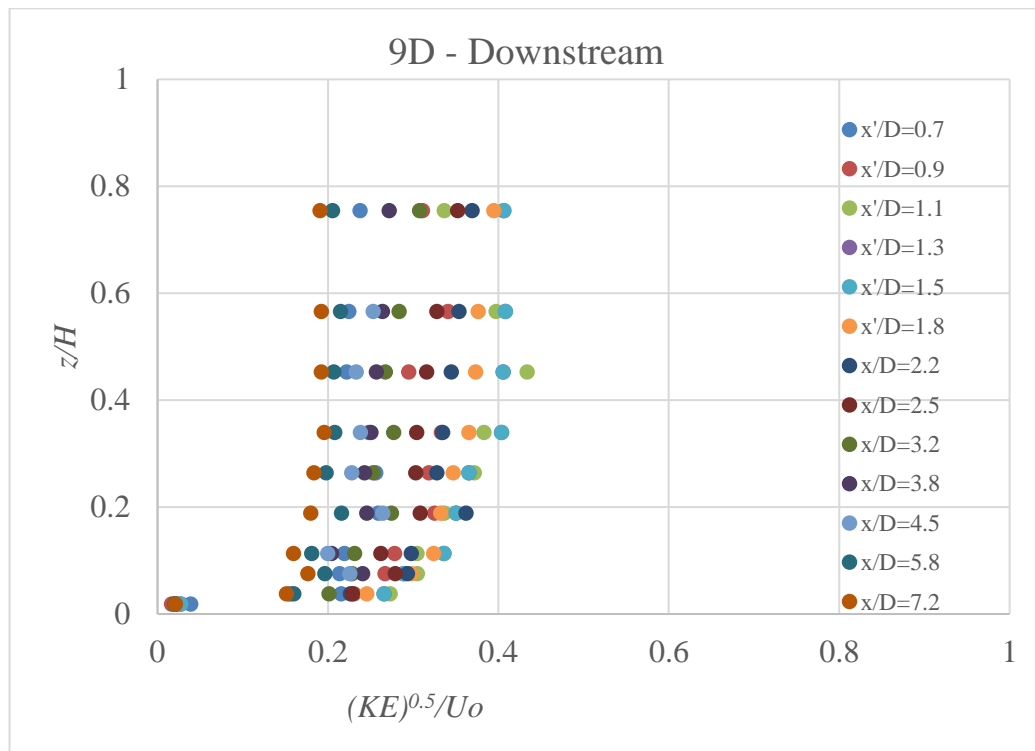


(b)

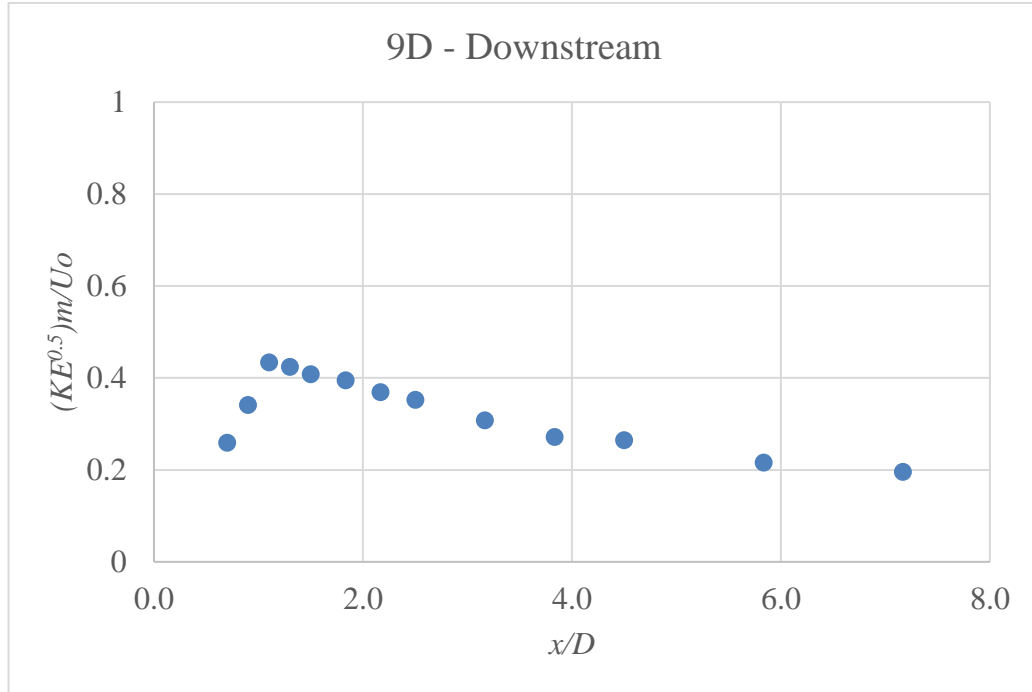
Figure 4.32: (a) Variation of Normalized Turbulent Intensity Profile (b) Variation of Maximum Turbulent Intensity in vertical direction along plane of symmetry downstream of second cylinders (9D)

4.7.2 Kinetic Energy at downstream of 9D c/c spacing

Figure 4.33(a) shows kinetic energy profiles at different vertical depths for 9D c/c spacing at downstream section. Analysis of this plot shows that the kinetic energy follows the same pattern of decrement after reaching a peak at relatively shorter longitudinal distance as the turbulent intensities. Moreover, maximum normalized kinetic energy has been observed at $\frac{x}{D}=1.1$ for $\frac{z}{H}=0.45$ which is equal to 0.43. Logarithmic profiles are visible at all of the longitudinal distances as found earlier in case of turbulent intensities. Similar to turbulent intensity profiles, kinetic energy profiles show logarithmic profile in this study also. Figure 4.33(b) shows an increase of about 74% as the longitudinal distance is increased from $\frac{x}{D}=0.7$ to $\frac{x}{D}=1.1$. After that, the kinetic energy decreases by 54% when the flow progresses from $\frac{x}{D}=1.1$ to $\frac{x}{D}=7.2$.



(a)



(b)

Figure 4.33: (a) Variation of Normalized Kinetic Energy Profile (b) Variation of Maximum Kinetic Energy in vertical direction along plane of symmetry downstream of second cylinders(9D)

4.7.3 Turbulent shear stress at downstream

Variation of normalized maximum turbulent shear stress per unit mass in the x direction on the xy plane ($\frac{\sqrt{u'w'}}{U_0}$) at different verticals along the POS in the downstream of 3D, 6D and 9D are plotted in Figure 4.34. Similar to the shear stress at midstream, the maximum of ($\frac{\sqrt{u'w'}}{U_0}$) increases to a peak, and then reduces gradually to a lower value, in a relatively chaotic way. For 3D, the maximum value of around 0.54 occurs at $\frac{x}{D}=1.3$ and for 6D the maximum occurs at $\frac{x}{D}=1.3$ with a value of 0.54. For 9D, the maximum occurs at $\frac{x}{D}= 1.1$ with a value of 0.55. In downstream the maximum values for all three cases are almost the same.

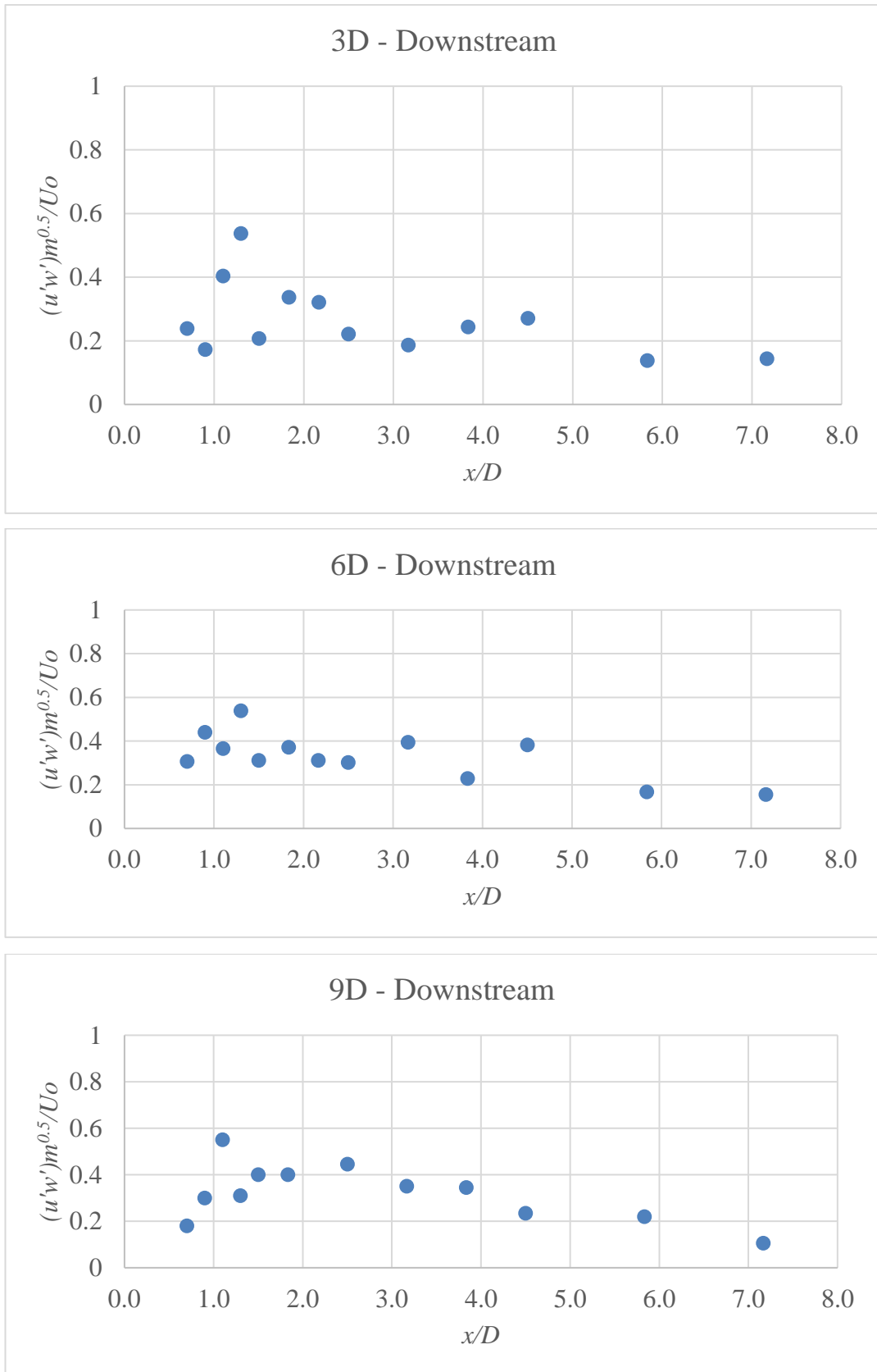


Figure 4. 34 Variation of normalized maximum turbulent shear stress for three cases at downstream section

4.8 Wake Similarity Profile in Term of Near Wake on Horizontal Plane at Mid-Depth

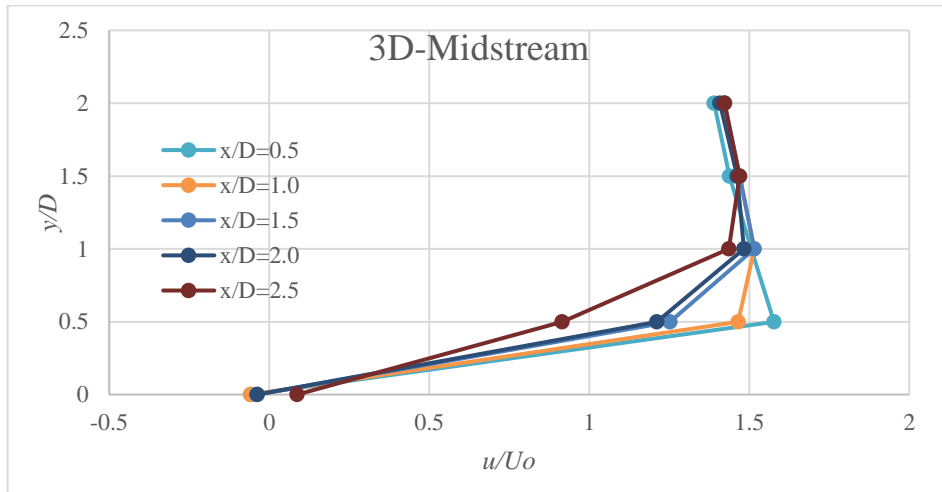
The wake profiles from these experimental data are compared with the Balachandar's equation for near wake region. Figure 4.35 shows the variation of normalized longitudinal velocity at mid depth in transverse direction between two cylinders for different c/c spacing. These figures show that decrement takes place in the value of longitudinal velocity as the c/c spacing is increased. While comparing the 3D and 6D data, it has been observed that about 19% decrement in normalized velocity occurs when c/c spacing is increased from 3D to 6D for $\frac{x}{D}=0.5$ at $\frac{y}{D}=0.5$. For 3D c/c spacing, the normalized velocity decreases 42% when the longitudinal distance is increased from $\frac{x}{D}=0.5$ to $\frac{x}{D}=2.5$. However, in case of 6D c/c spacing, the decrement is at most about 17% whereas the decrement is about 13% from 6D to 9D spacing.

Figure 4.36 shows the plane wake similarity of longitudinal velocity at mid-depth in the transverse direction between two cylinders at the mid-stream section. All of the plots show that at $\frac{y}{b_2}=0, \frac{U-U_{\min}}{U_2}=0$. In case of higher longitudinal distances, the experimental data more rigorously approaches towards the plane wake graph. The maximum value of $\frac{y}{b_2}$ in which the experimental results are closer to plane wake graph decreases significantly with the c/c spacing. For 3D c/c spacing, the $\frac{y}{b_2}$ is 5.625, for 6D c/c spacing, the corresponding $\frac{y}{b_2}$ is 5.0 and, for 9D c/c spacing, the corresponding $\frac{y}{b_2}$ is 4.748.

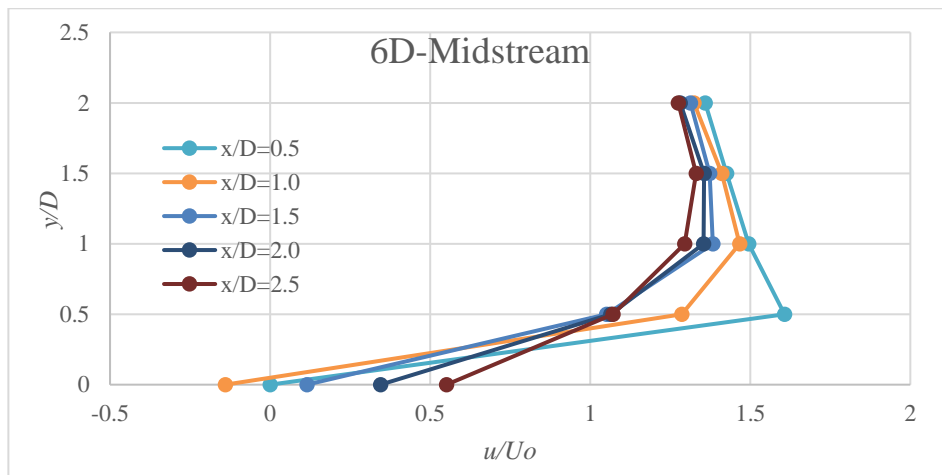
Figure 4.37 shows the variation of normalized longitudinal velocity at mid depth in transverse direction at downstream for different c/c spacing. These figures show that decrement takes place in the value of longitudinal velocity as the c/c spacing is increased similar to mid-stream findings. While comparing the 3D and 6D data, it has been observed that about 10% decrement in normalized velocity occurs when c/c spacing is increased from 3D to 6D for $\frac{x}{D}=0.5$ at $\frac{y}{D}=1.0$. For 3D c/c spacing, the normalized velocity decreases 11% when the longitudinal distance is increased from

$\frac{x}{D}=0.5$ to $\frac{x}{D}=2.5$. However, in case of 6D c/c spacing, the decrement is at most about 18% whereas the decrement is about 8% from 6D to 9D spacing.

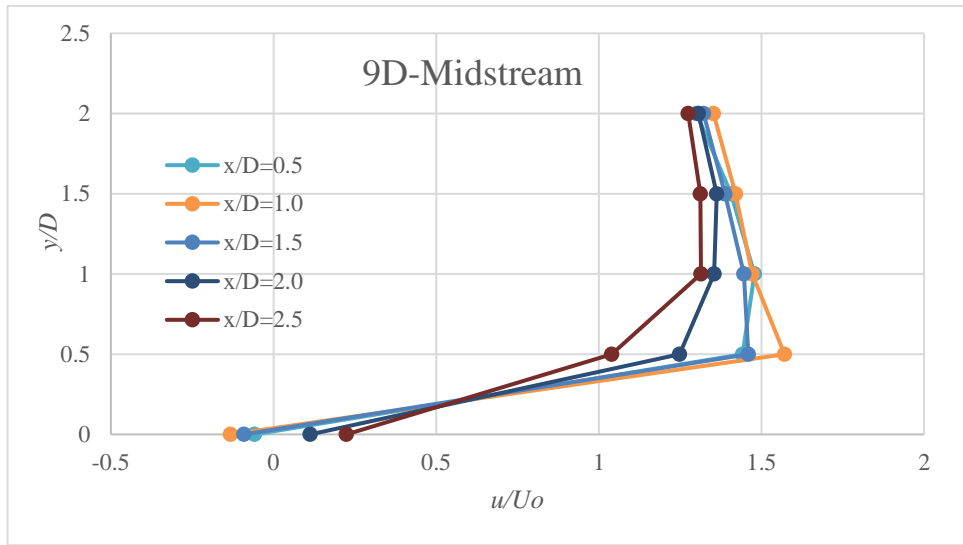
Figure 4.38 shows plane wake similarity of longitudinal velocity at mid-depth in the transverse direction at the downstream. By observing the plots, it can be explained that experimental results achieved at the downstream almost passes through the plane wake graph. For such reason, it could be concluded that after passing both the cylinders, as the characteristics of wake at this zone is well-defined and follow plane wake graph at a relatively shorter longitudinal distance.



(a)

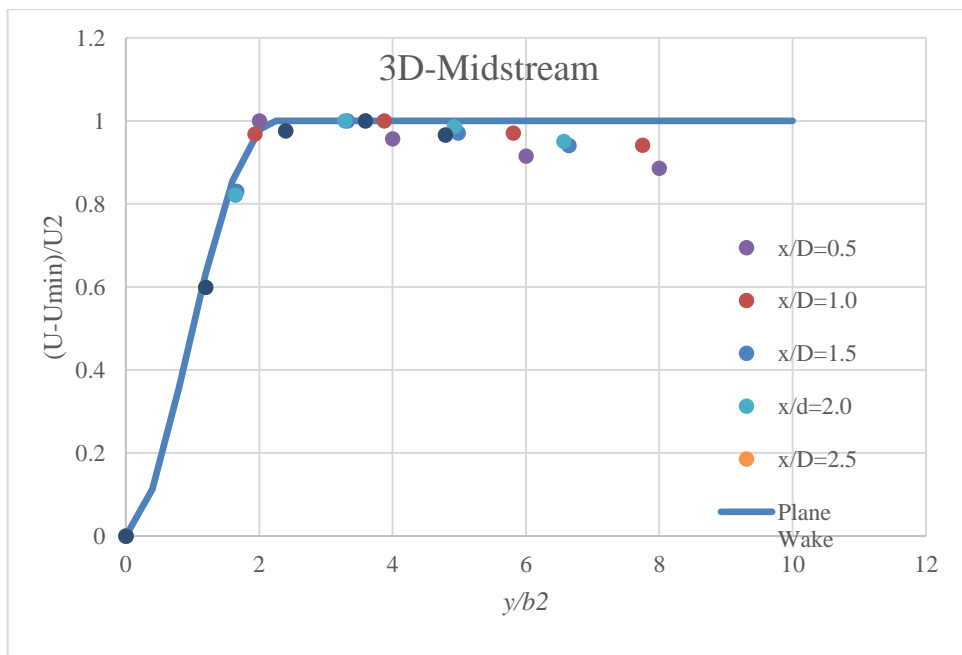


(b)

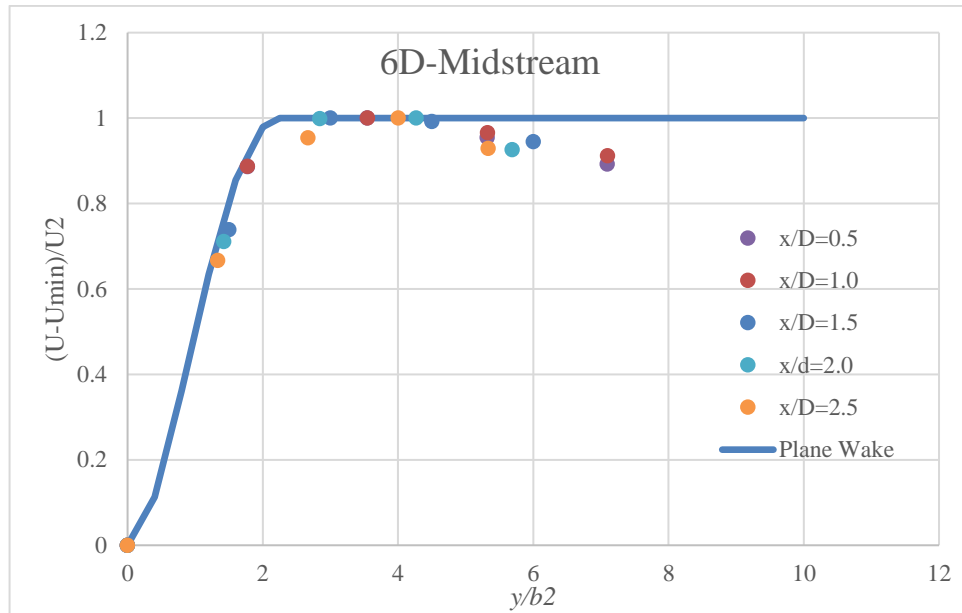


(c)

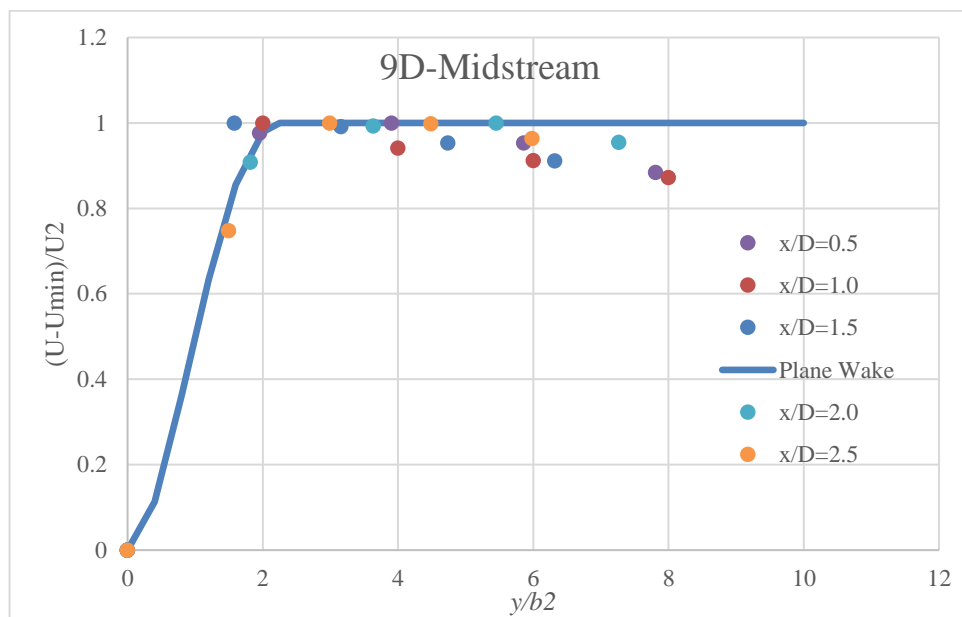
Figure 4.35: Normalized Longitudinal Velocity Variation at Mid Depth in Transverse Direction between Two Cylinders



(a)

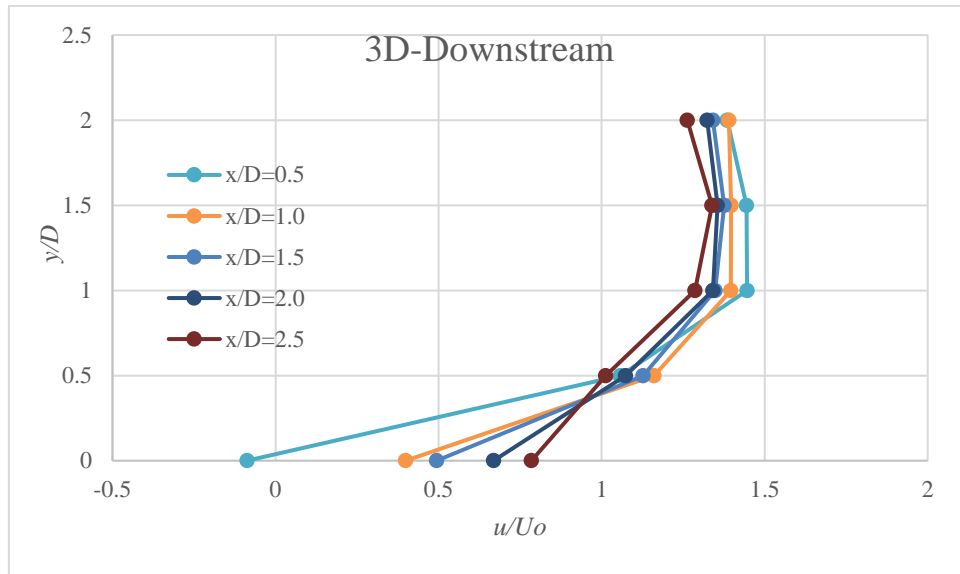


(b)

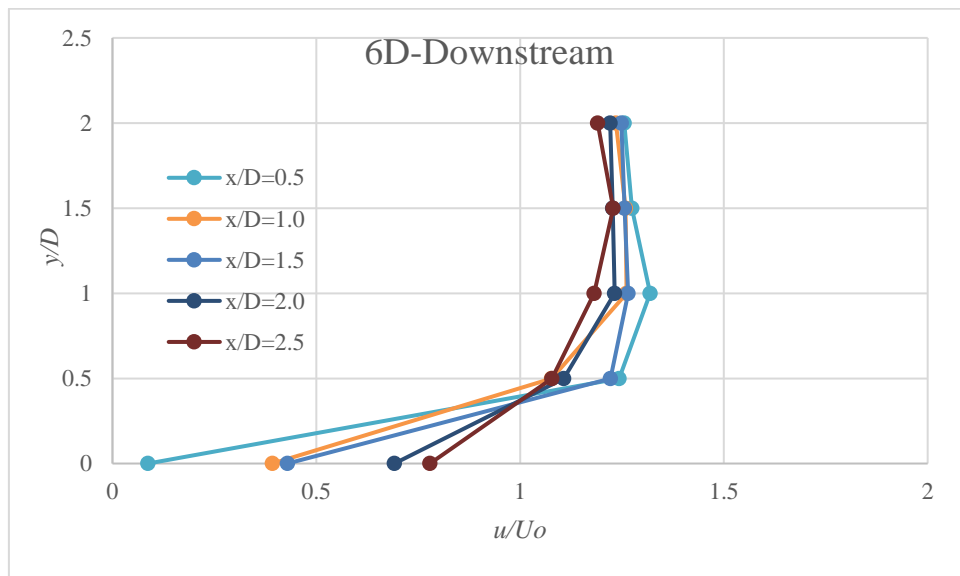


(c)

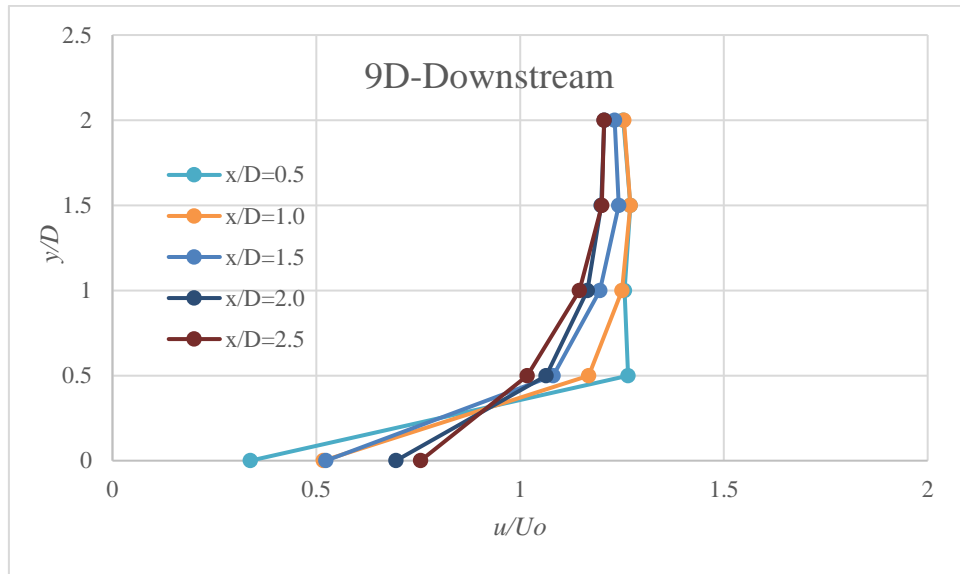
Figure 4.36: Plane Wake Similarity of longitudinal velocity at Mid-depth in the transverse direction between two cylinders



(a)

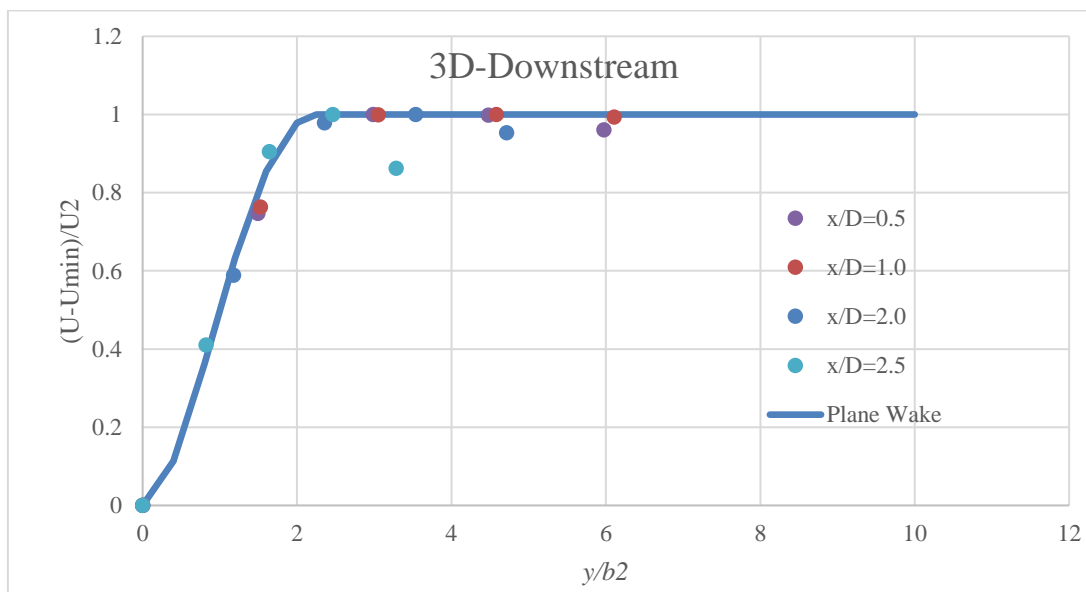


(b)

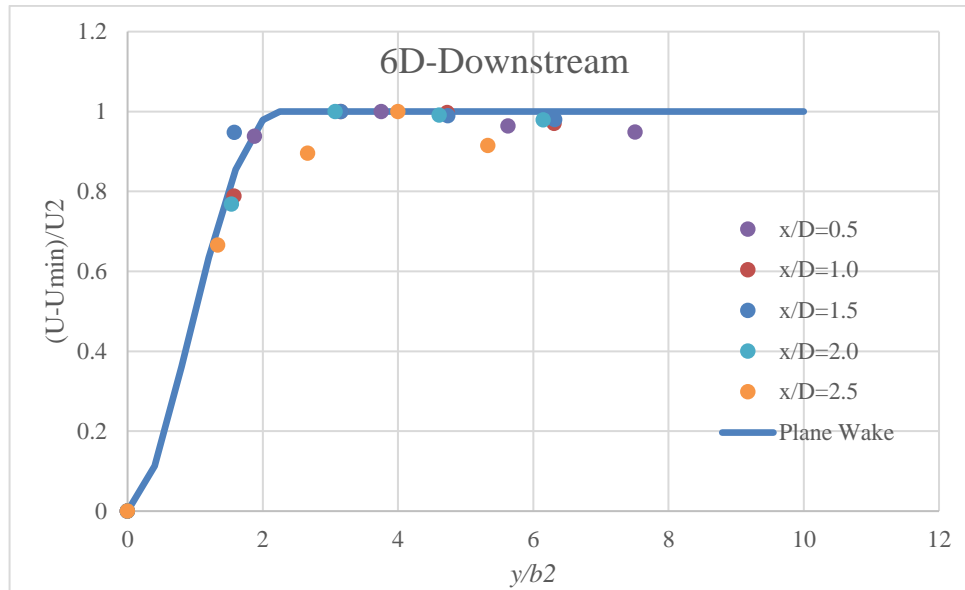


(c)

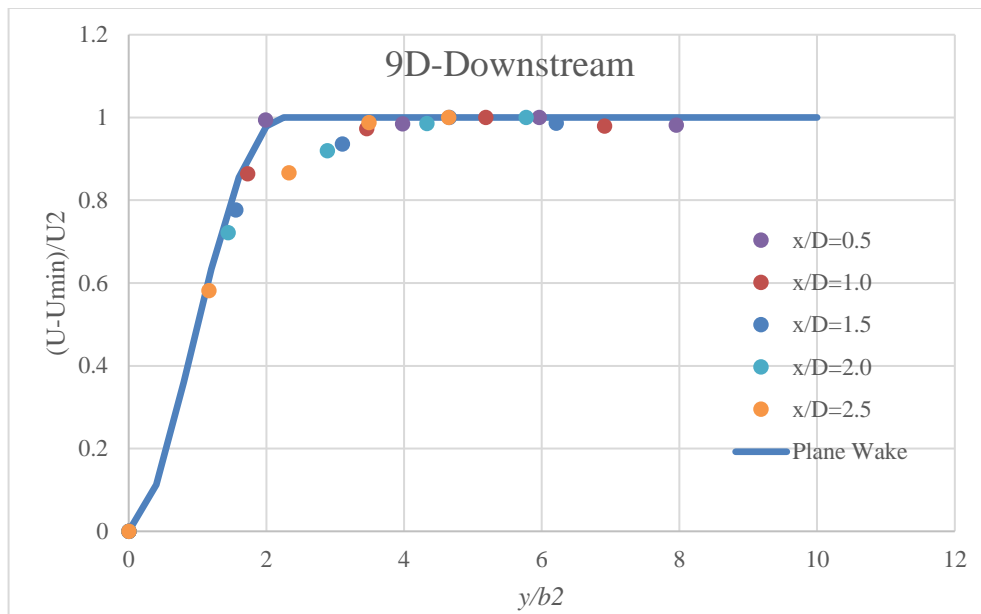
Figure 4.37: Normalized Longitudinal Velocity Variation at Mid Depth in Transverse Direction at Downstream



(a)



(b)



(c)

Figure 4.38: Plane Wake Similarity of longitudinal velocity at Mid-depth in the transverse direction downstream of second cylinder

CHAPTER 5

CONCLUSIONS

5.1 Conclusions

The experimental study examines the details flow fields around a pair of cylinders placed at three different c/c spacings along the plane of symmetry in a rectangular open channel. Mean and turbulent flow fields between two cylinders as well as in the wake of downstream cylinders were investigated using ADV. Measurements were made along the centerline of the flume. Moreover, plane wake similarity of Balachandar has been investigated of variation of longitudinal velocity in the transverse direction at mid-depth. Conclusions from this study can be summarized as follows:

1. Analysis of longitudinal normalized velocity profiles in-between cylinders reveal that the near wake region ($\frac{x}{D}=1.5$) is identical at each scenario. The far wake region ($\frac{x}{D}=1.8-2.5$) is affected by the downstream cylinder in 3D and zero interruption from downstream cylinder in 6D and 9D as in 3D spacing, the cylinders are closely spaced and the flow gets affected by the downstream cylinder which generates relatively more recirculation than other two case studies. However, the flow gets affected as it approaches the d/s cylinder with maximum of $\frac{u_{da}}{U_0}=0.7$ and 0.8 for 6D and 9D respectively. As the recirculation is accompanied by turbulence, that specific zone is more susceptible to transport the sediment particles from the bed.
2. Analysis of longitudinal normalized velocity profiles downstream of the second cylinder states that upstream cylinder has great influence on the both near and far wake of downstream cylinder. The length of the near wake or the recirculation zone increases with the increase in c/c spacing of cylinders. In the far wake region, the rate of flow development to achieve cross sectional mean velocity becomes slower with increasing c/c spacing.
3. In the near wake of midstream, the recirculation is stronger near the surface than the bottom, whereas the reverse is true for the near wake of downstream of second cylinder. However, in overall, the recirculation in the midstream is stronger than the that in the downstream.

4. Wall wake similarity analysis is done in the far wake region for the longitudinal velocity profiles along vertical POS at all sections of three test scenarios and the variations of the profiles compared with the plane wake equation of Schlichting. For the midstream section, no significant similarity was observed with a very weak similarity only at $\frac{x}{D}=2.2$ for 6D and 9D. However, the results at downstream follow wake similarity up to $\frac{x}{D}=1.8$ for all 3 cases. Although the number of sections in which follow wake similarity reduces with increased c/c spacing, since the size of the near wake region is becomes larger with increasing c/c spacing of cylinders.
5. Normalized longitudinal mean velocity profiles are inspected along the POS for all three test scenarios and found that for all flow regimes, there is a zone of jet-like flow behind the cylinders. For midstream, these jet-like high velocity profiles persist up to $\frac{x}{D}=4.5$ for 6D and 9D spacing. For downstream, this length is $\frac{x}{D}=3.8$ for all cases.
6. The range of magnitude and position of peak of turbulent intensity in longitudinal, transverse and vertical directions are similar in three scenarios in midstream. The longitudinal turbulent intensity and vertical turbulent is almost two-third and half respectively of transverse intensity. The maximum of longitudinal and transverse intensity tends to occur at the end of the recirculation zone, whereas maximum vertical intensity occurs before this point. However, in the downstream, all the three intensities occur at the end of the recirculation zone which indicates the scour is more likely to occur in this region.
7. Turbulent kinetic energy variation follows the same variation of longitudinal or transverse intensities. The maximum turbulent KE for all three cases occurs near the end of their respective recirculation zones. For the midstream, the value of the normalized maximum KE is almost 0.52 in the midstream. For the downstream, the maximum value increased from 0.48 for 3D to 0.54 for 6D, then it decreased to 0.44 for 9D. The normalized maximum KE at further downstream locations reduces to 0.2 for all cases.

8. The measurement of turbulent shear stress is relatively chaotic than the turbulent intensities. The maximum of turbulent shear stresses occurs within the recirculation zone for all cases.
9. Wake similarity profile in terms of near wake on a horizontal plane at mid-depth is drawn for test results taken from both upstream pier and downstream pier measurements. The findings confirm Balachandar's equation justifying the validity of this experiment.
10. Based on the length of recirculation zone of upstream and downstream pier and the higher kinetic energy within the recirculation zone, the scour in the upstream pier is expected to be higher than that in the downstream pier, which is also consistent with the findings in literature.
11. The experimental results show the effect of different spacing of a pair of circular cylinders in terms of variation of mean flow, recirculation zone and turbulence parameters in the midstream and downstream sections. Although the mean flow velocity is low in the recirculation zone, turbulence is very high in this zone. A depth averaged model will give a low shear stress and corresponding low sediment transport which is in contrast of a real situation. Therefore, these results will be useful in validation of depth averaged as well as CFD modeling of flow affected by similar obstructions, specially these data will help in simulating flows more precisely around the bridge piers. Moreover, the results can be used in understanding and interpretation of sediment transport, scour and fish habitat assessment in natural rivers with similar structures.

5.2 Recommendation for Future Works

1. Depth averaged and CFD modeling can be performed after validating the models using these results and then different scenarios can be simulated by varying pier diameter, flow depth and rate for different flow.
2. The present study will provide an improved understanding of the complex three-dimensional flow and turbulence in the near and far wake region.

Similar study may be undertaken by positioning the cylinders in oblique angle for different water level and discharge to observe the flow behavior.

References

1. Choi, H., Jeon, W. P., and Kim, J., "Control of Flow over a Bluff Body," *Annu. Rev. Fluid Mech.*, vol. 40, pp. 113-139, 2008.
2. Schewe, G., "Reynolds-Number Effects in Flow around More-or-Less Bluff Bodies," *J. Wind. Eng. Ind. Aerodyn.*, vol. 89, pp. 1267-1289, 2001.
3. Aiba, S., and Watanabe, H., "Flow Characteristics of a Bluff Body Cut from a Circular Cylinder," *J. Fluids Eng.*, vol. 119(2), pp. 453-454, 1997.
4. Kumar, P., and Singh, S. K., "Flow Past a Bluff Body Subjected to Lower Subcritical Reynolds Number," *J Ocean Eng. Sci.*, vol. 5(2), pp. 173-179, 2020.
5. Board, Naval Studies, and National Research Council. *Twenty-Fourth Symposium on Naval Hydrodynamics 2003*. National Academies Press.
6. Liu, R., *Flow around Bluff Bodies with Corner Modifications on Cross-sections*, Ph.D. Thesis, Department of Geology, University of New Hampshire, 2019.
7. Ramamurthy, A. S., and Lee, P. M., "Wall Effects on Flow Past Bluff Bodies," *J. Sound Vib.*, vol. 31(4), pp. 443-451, 1973.
8. Matsumoto, M., "Vortex Shedding of Bluff Bodies: a Review," *J Fluids Struct.*, vol. 13(8), pp. 791-811, 1999.
9. Thakur, V., Yadav, T., and Rajiv, B., "Drag Optimization of Bluff Bodies Using CFD for Aerodynamic Applications," *Int. J. Comput. Eng. Sci.*, vol. 7(4), pp. 25-32, 2017.
10. Rodi, W., "Comparison of LES and RANS Calculations of the Flow around Bluff Bodies," *J. Wind. Eng. Ind. Aerodyn.*, vol. 69, pp. 55-75, 1997.
11. Abikan, A., Lu, Y., and Yang, Z., "Numerical Study of Flow over a Bluff Body with Drag Reduction Devices," in *2nd International Conference on Fluid Dynamics & Aerodynamics*, Vol. VI(5), October 2017.
12. Dey, S., Rajkumar, Raikar, V., and Roy, A., "Scour at Submerged Cylindrical Obstacles under Steady Flow." *J Hydraul Eng.*, vol. 134(1), pp. 105-109, 2008.
13. Dey S, Swargiary, D., Sarkar, S., Fang, H., and Gaudio, R., "Self-Similarity in Turbulent Wall-Wake Flow Downstream of a Wall-Mounted Vertical Cylinder," *J Hydraul Eng.*, vol. 144(6), pp. 04018023. 2018.

14. Kumar, M., "Study of the Impact of Inclination on Scouring around the Bridge Pier," *Int J Adv. Tech. Eng. Sci.*, vol. 8, pp. 1164-1170, 2018.
15. Camussi, R., Guj, G., Marco, A. D., and Ragni, A., "Characterization of a Separated Turbulent Boundary Layer by Time-Frequency Analyses of Wall Pressure Fluctuations," *Eng. Turbulence Model. Exp.*, vol. 6, pp. 719-728, 2005.
16. https://www.princeton.edu/~asmits/Bicycle_web/separation.html
17. Sparrow, E.M., Abraham, J. P., and Minkowycz, W. J., "Flow Separation in a Diverging Conical Duct: Effect of Reynolds number and Divergence Angle," *Int J Heat Mass Tran.*, vol. 52(13), pp. 3079-3083, 2009.
18. Schlichting, H. (1968) *Boundary-layer theory*, McGraw-Hill, New York.
19. Rajaratnam, N., and Rai, S.P., "Plane Turbulent Wall Wakes", *Trans. of the ASCE, Journal of Engineering Mechanics Division*, Vol. 105, pp. 779-794, 1979.
20. Balachandar, R., Ramachandran, S., and Tachie, M.F., "Characteristics of Shallow Turbulent Near Wakes at Low Reynolds Numbers," *J. Fluids Eng.*, vol. 122, pp. 302-308, 2000.
21. Lloyd, P.M., and Stansby, P. K., "Shallow-water flow around model conical islands of small side slope I: Surface piercing," *J Hydraul Eng.*, vol. 123(12), pp. 1057-1067, 1997.
22. Ingram, R.G., and Chu, V.H., "Flow around Islands in Rupert Bay: An Investigation of the Bottom Friction Effect," *J. Geophysical Res.*, vol. 92, pp. 14521-14533, 1987.
23. Chen, D., and Jirka, G. H., "Experimental Study of Plane Turbulent Wakes in a Shallow Water Layer," *Fluid Dynamics Res.*, vol. 16, pp. 11-41, 1995.
24. Sforza, P.M., and Mons, R. F., "Wall-wake: Flow Behind a Leading Edge Obstacle," *AIAA Journal*, vol. 8(2), pp. 2162-2167, 1970.
25. Shamloo, H., Rajaratnam, N., and Katopodis, C., "Hydraulics of simple habitat structures," *J Hydr. Res.*, vol. 39(4), pp. 351-366, 2001.
26. Roshko, A. (1961). Experiments on the Flow Past a Circular Cylinder at Very High Reynolds Number," *J. Fluid Mech.*, vol. 10(3), pp. 345-356, 1961.

27. Antonia, R.A., "Organization in a Turbulent Near Wake," *Fluid Dynamics Res.*, vol. 7, pp. 139–149, 1991.
28. Akilli, H., and Rockwell, D. (2002). Vortex Formation from a Cylinder in Shallow Water," *Phys. Fluids*, vol. 14(9), pp. 2957–2967, 2002.
29. Perrin, R., Braza, M., Cid, E., Cazin, S., Moradei, F., Barthet, A., Sevrain, A., and Hoarau, Y., "Near-Wake Turbulence Properties in the High Reynolds Number Incompressible Flow around a Circular Cylinder Measured by Two and Three Component PIV," *Flow Turbulence Combust*, vol. 77, pp. 185–204, 2006.
30. Ozturk, N.A., Akkoca, A., and Sahin, B. "Flow Details of a Circular Cylinder Mounted on a Flat Plate," *J. Hydr. Res.*, vol. 46(3), pp. 344–355, 2008.
31. Paul, S. S., and Tachie, M. F., "Near Wake Structure of Finite Cylinders in an Open Channel Flows," in *7th International Symposium on Turbulence and Shear Flow Phenomena*, July 2011.
32. Ahmed N. A., and Wagner, D. J., "Vortex Shedding and Transition Frequencies Associated with Flow around a Circular Cylinder," *AIAA Journal*, vol. 41 (3), pp. 542-544, 2003.
33. Smith, H.D., and Foster, D.L., "Three-dimensional flow around a bottom-mounted short cylinder," *J. Hydr. Eng.*, vol. 133(5), pp. 534–544, 2007.
34. Arya, S.P.S., and Gadiyaram, P.S., "An Experimental Study of Flow and Dispersion in the Wakes of Three-Dimensional Low Hills," *Atmos. Environ.*, vol. 20(4), pp. 729–740, 1986.
35. Jirka, G. H., "Large Scale Flow Structures and Mixing Processes in Shallow Flows," *J. Hydr. Res.*, vol. 39(6), pp. 567–573, 2001.
36. Katopodis, C., "Developing a Toolkit for Fish Passage, Ecological Flow Management and Fish Habitat Works," *J. Hydr. Res.*, vol. 43(5), pp. 451–467, 2005.
37. Sadeque, M.A.F., Rajaratnam, N., and Loewen, M.R., "Flow around Cylinders in Open Channels," *J. Eng. Mech.*, vol. 134(1), pp. 60–71, 2008.
38. Sadeque, M.A.F., Rajaratnam, N., and Loewen, M. R., "Shallow turbulent wakes behind bed-mounted cylinder in open channels," *J. Eng. Mech.*, vol. 135(2), pp. 100–110, 2009.

39. Sadeque M. A. F, and Zobeyer, H., "2D Modeling of Shallow Wakes in Open Channel Flows," in *33rd IAHR Congress: Water Engineering for a Sustainable Environment. Vancouver*, Vol. 33, 2009, pp. 5182-5189.
40. Merrick, R., and Bitsuamlak, G., "Control of Flow around a Circular Cylinder by the Use of Surface Roughness: A Computational and Experimental Approach." in *4th International Conference Advances on Wind and Structures*, 2008.
41. Zhang, X., Li, Z., and Fu, S., "Study of the flow around a cylinder from the subcritical to supercritical regimes." *Ocean Syst. Eng.*, vol. 4, 2014.
42. Yuce, M. I., and Kareem, D. A., "A Numerical Analysis of Fluid Flow around Circular and Square Cylinders." *J Am Water Works Assoc*, vol. 108(10), pp. 546-554, 2016.
43. Khaple, S., Hanmaiahgari, P.R., and Gaudio, R., "Interference of an Upstream Pier on Local Scour at Downstream Piers," *Acta Geophys.*, vol. 65, pp. 29–46, 2017.
44. Gao, Y. Y., Yin, C. S., Zhang, H. Q., Yang, K., Zhao, X. Z., and Sun, Z., "Numerical Study on Flow around Four Square-Arranged Cylinders at Low Reynolds Numbers," *Math. Probl. Eng*, vol. 4, pp. 1-18, 2017.
45. Bose, S. K. and Dey, S. "Far-Wake Flows Downstream of Cylinders: A Novel Generalized Similarity Method," *Eur. J. Mech. B/Fluids*, 67, pp. 65–69, 2018.
46. Dey, S., Swargiary, D., Sarkar, S., Fang, H., and Gaudio. R., "Turbulence Features in a Wall-Wake Flow Downstream of a Wall-Mounted Vertical Cylinder," *Eur. J. Mech. B/Fluids*, vol. 69, pp. 46–61, 2018.